Effective models for seismic wave propagation in porous media

PROEFSCHRIFT

ter verkrijging van de graad van doctor
aan de Technische Universiteit Delft,
op gezag van de Rector Magnificus prof.ir. K.C.A.M. Luyben,
voorzitter van het College voor Promoties,
in het openbaar te verdedigen op maandag 2 mei 2016 om 10:00 uur

door

Asiya KUDAROVA

Master of Science in Mechanics
Saint Petersburg State Polytechnic University, Russia
geboren te Leningrad, Sovjet Unie.

Dit proefschrift is goedgekeurd door de promotor:

Prof. dr. ir. C.P.A. Wapenaar

Copromotors:

Dr. ir. G.G. Drijkoningen

Dr. ir. K.N. van Dalen

Samenstelling promotiecommissie:

Rector Magnificus,	Technische Universiteit Delft, voorzitter
Prof. dr. ir. C.P.A. Wapenaar,	Technische Universiteit Delft, promotor
Dr. ir. G.G. Drijkoningen,	Technische Universiteit Delft, copromotor
Dr. ir. K.N. van Dalen,	Technische Universiteit Delft, copromotor
Onafhankelijke leden	
Prof. dr. ir. D.M.J. Smeulders,	Technische Universiteit Eindhoven
Prof. dr. ir. E. Slob,	Technische Universiteit Delft
Prof. dr. ing. H. Steeb,	Universität Stuttgart, Germany
Prof. dr. J. Bruining,	Technische Universiteit Delft
Prof. dr. W.A. Mulder,	Technische Universiteit Delft, reservelid

This work is financially supported by the CATO-2-program. CATO-2 is the Dutch national research program on CO_2 Capture and Storage technology (CCS). The program is financially supported by the Dutch government and the CATO-2 consortium parties.

Printed by: Gildeprint - The Netherlands, `www.gildeprint.nl`.

Cover design by: Alexia's Writings and Designs.

ISBN 978 − 94 − 6233 − 279 − 9

An electronic version of this dissertation is available at

`http://repository.tudelft.nl`.

Contents

Chapter 1

Introduction

1.1 Background

A mechanical wave is an oscillatory motion of a continuum accompanied by a transfer of energy that travels through space. Measurable characteristics of waves are linked to the physical properties of the medium where waves propagate. This is used, for example, in nondestructive testing of materials and structures. In geophysics, seismic waves are used to study Earth's interior. Seismic motion is often associated with earthquakes. An earthquake is one of the natural sources of seismic waves. On the one hand earthquakes can severely damage structures, but on the other hand they are very useful for studying the Earth's interior. Among others, seismic waves excited by earthquakes are used to define locations of natural seismic sources. Movements in the Earth generating seismic waves happen not only naturally, but are also induced by humans, and it is very important to monitor this seismic activity; e.g. from mining, hydraulic fracturing, enhanced oil recovery, geothermal operations or underground gas storage. Passive seismic monitoring of natural wave motions cannot provide all the information about the subsurface we are interested in. That is why active seismic acquisition is used, seismic signals are generated in the vicinity of an object of interest to get some information about it. This can be offshore, on land, and even on another planet. Even some animals, like mole rats, for example, actively generate seismic waves, they use them for communication and orientation.

In geophysics, a seismic survey is an important and powerful tool for exploration and production of resources. It helps to find potential locations of new oil and gas reservoirs, and to monitor existing reservoirs. It is very important,

for example, to predict possible leakage which can happen due to injection and production-induced fracturing and other processes in the subsurface. In order to interpret data collected from a survey, researchers study, among other things, the dependencies between the attributes of seismic signals and the properties of the reservoir. One of the challenges in the interpretation is the presence of transition zones in the reservoir, where oil and gas are mixed with water. Such zones are often called partially or patchy saturated. They represent highly heterogeneous porous media. It was observed that such heterogeneities cause significant attenuation of seismic waves which is also frequency-dependent (Müller et al., 2010). Attenuation can severely impact the quality of seismic data and cause errors in interpretation, but at the same time seismic attenuation is an attribute for characterization of the subsurface. Studying the dependence between inhomogeneities in reservoir properties and seismic attributes can provide an insight into the complexity of the subsurface. To this end, various models are being developed to obtain quantitative relationships between rock and fluid properties and seismic attributes (e.g., velocity, attenuation). The ultimate goal of using models is to reduce uncertainty in predictions. Studying the sensitivities of the model predictions to the change of parameters gives insight into the possible cause of observed phenomena. For example, changes in velocities can be related to changes in fluid saturations, etc.

One of the reasons of growing attention to models for predicting sensitivity of observed wave-propagation attributes to changes in fluid saturations and other subsurface properties is the injection of gas in reservoirs for enhanced oil recovery. In the second half of the last century, when the first gas injections took place, it was not known what consequences this could have. Observations over many years showed that different fields respond differently to gas injection. High-rate injections were linked with the increase of small earthquakes in the vicinity of many fields. Oil and gas fields are extensively monitored and available data are used to study effects of gas injection and predict possible scenarios for processes happening in the field, such as fluid movements, changes in the pressure conditions, etc.

Carbon dioxide (CO_2) is widely injected in fields; one of the first projects was initiated in 1972 in the Kelly-Snider oil field in Texas. Until recently, the CO_2 used for injection originated from naturally occurring CO_2, but technologies have been developed to deliver CO_2 produced from industrial processes to nearby fields. At the moment, the possibilities are discussed to inject CO_2 as captured from industrial activities into abandoned gas fields to control CO_2 emissions worldwide. This

is related to the fact that more and more CO_2 is released into the atmosphere, especially in developing countries, where the energy demand is getting higher every year and industrial activity expands rapidly. The long-term consequence is a global climate change that can drastically change life on our planet if no measures are taken. Governments of the developed countries support many research projects on carbon capture and storage (CCS). In particular, the research in this thesis was carried out in the context of the Dutch national research program on CCS technology (CATO-2) supported by the Dutch government and consortium partners. Many questions have to be answered before large-scale CCS can be implemented. Research is being carried out not only in physics, chemistry and other technical disciplines, but also in economy, public perception, policy making and other non-technical disciplines. The main challenges for research in geophysics are the long-term consequences of storing large amounts of gas underground, developing cost-effective but accurate techniques to monitor the storage site and predicting possible leakages of CO_2. It is important to reduce uncertainty in predictions to ensure safety. This thesis contributes to the development of models for predicting quantitative relations between wave-propagation characteristics and reservoir properties, which are important for monitoring CO_2 storage sites, but not limited to application in CCS.

One of the challenges for practical application of quantitative models is a lack of input data. In practice, we do not have all the details about the structure of the subsurface. Although modern computational techniques allow to carry out simulations with very complicated models, it is often advantageous to use simpler ones with less parameters. Complicated models with many parameters provide more accurate estimates from a theoretical point of view, but in practice increase uncertainty since it is often hard to determine input parameters required to run the model because of lack of available measurements. Therefore, a compromise has to be found between the desired accuracy of predictions and the introduced assumptions.

1.2 Models for wave propagation in porous media

Seismic waves contain important information on subsurface properties. In this thesis, we propose models to quantify the dependence between wave-propagation

characteristics and subsurface properties related to a porous medium, specifically a poroelastic solid. The commonly used equations for wave propagation in poroelastic solids are Biot's equations (Biot, 1956a,b, 1962). Biot's theory is a linear theory of two-phase media: one phase corresponds to an elastic solid, and the second phase corresponds to a fluid moving through the pores of the solid. The assumptions in Biot's theory are:

- The solid frame is homogeneous and isotropic with constant porosity ϕ, bulk modulus K_m, permeability k_0 and shear modulus μ. The solid grains have constant density ρ_s and bulk modulus K_g.
- The medium is fully saturated by one type of fluid with viscosity η, bulk modulus K_f and density ρ_f.
- Darcy's law governs the relative motion between solid and fluid phases.
- The wavelength of the passing wave is much larger than the characteristic size of the pores and grains.

It is widely accepted that Biot's theory underestimates observed attenuation and dispersion of elastic waves (Johnston et al., 1979; Winkler, 1985; Gist, 1994). One of the reasons is a violation of the assumption of uniform saturation with a single fluid. Inhomogeneities in solid-frame properties also cause attenuation. Many models for wave propagation in heterogeneous porous media were developed to address this effect. Each model proposes an attenuation mechanism which is based on certain assumptions. These assumptions are related, among other things, to the scale of the heterogeneities and their distributions, and the frequency range of interest. Seismic waves used to probe the subsurface usually have a frequency range 1 – 100 Hz. Well-logging tools use the frequency range extended up to 100 kHz, and ultrasonic measurements (up to MHz) are used in the laboratory. The wavelengths vary from meters to kilometers in field studies to millimeters in laboratory studies. Depending on the scale of observations, different models are used to study wave attenuation and dispersion. Attenuation due to dissipation at the pore scale is described by a squirt-flow mechanism (O'Connell and Budiansky, 1977; Mavko and Nur, 1979; Palmer and Traviola, 1980; Dvorkin and Nur, 1993). Differences in fluid saturation between thin compliant pores and larger stiffer ones, the presence of thin cracks, different shape and orientation of the pores, as well as distribution of immiscible fluids in a pore cause attenuation and dispersion due to local or squirt flow. This mechanism usually plays a role at ultrasonic frequencies.

In this thesis, we consider a frequency range between 1 Hz and several kHz, where the wavelengths are much larger than the typical pore and grain size. In this case, the wavelength is not sensitive to the geometry of the pores and other local pore-scale effects, and Biot's theory can be used to predict wave attenuation and dispersion. The attenuation mechanism in Biot's theory is driven by the wavelength-scale fluid-pressure gradients created by a passing wave, which results in relative fluid-to-solid movement accompanied by internal friction due to the viscous forces between the solid and fluid phases. For many typical rocks, this mechanism is significant for frequencies of the order of kHz and higher, well outside the seismic frequency range. However, significant attenuation and dispersion at seismic frequencies can be observed in heterogeneous porous media when the heterogeneities are much larger than the pore and grain sizes but smaller than the wavelength. Spatial variations in solid-frame and fluid properties at this scale, which is called the mesoscopic scale, cause fluid-pressure gradients that drive the so-called mesoscopic fluid flow. It results in attenuation and dispersion which is not captured by Biot's theory.

One possible solution to account for the mesoscopic-scale effects when modeling wave propagation in heterogeneous media is to solve the equations of motion with spatially varying parameters. However, this approach can be inefficient in practice. First, it can require a lot of computation time, but it can also be counterproductive because it will require introduction of assumptions on the distribution of heterogeneities and introduction of additional parameters, thus increasing uncertainty in the analysis.

Another solution is to use an effective-medium approach. This approach, as mainly discussed in this thesis, allows to describe the macroscopic properties of the heterogeneous medium using equations of motion with spatially invariant coefficients. These coefficients can be derived analytically or numerically using different homogenization techniques. Then, a medium containing heterogeneities is replaced by an equivalent homogeneous medium. Equivalence means that all wave propagation characteristics in the initially heterogeneous medium and the corresponding homogenized one are the same, provided that the assumptions used in the derivation of the effective coefficients are met. For example, one common assumption for modeling mesoscopic-scale heterogeneities is that the wavelength is much larger than the characteristic size of heterogeneities. This assumption is also assumed in the models presented in this thesis. Such models are mostly used in the seismic frequency range (i.e., at relatively low frequencies), since the wavelength decreases

with frequency. However, they can be used to compare numerical results and observations in the laboratory at higher frequencies provided that heterogeneities in a sample are small enough and the wavelength assumption is met.

Another assumption used in the derivation of an effective medium is the one on the distribution of heterogeneities. A choice is often made between periodic and random or non-periodic configurations. In reality, there are no strictly periodically distributed properties, and a non-periodic distribution is more realistic. However, models with periodic configurations can be advantageous in different applications. First, they require less parameters, which helps to reduce uncertainty. Second, many methods and theories have been developed to deal with periodic configurations, including exact solutions that can be used to validate effective models. The solutions for periodic media can be used as benchmark for models that deal with more complicated geometries. In some cases, analytical expressions for effective coefficients can be obtained for a periodic geometry. This is why many models for seismic wave propagation in porous media with mesoscopic-scale heterogeneities assume a periodic distribution of inclusions.

One of the first models to account for mesoscopic-scale inclusions in porous media are the ones of White et al. (1975) and White (1975) for periodically layered media and porous media with periodically distributed spherical patches, respectively. In that work, it was emphasized that the presence of different fluids in mesoscopic-scale patches causes significant dispersion and attenuation at seismic frequencies. Each model provides an analytical expression for a frequency-dependent P-wave modulus, which is being used in numerous studies (e.g., Carcione et al., 2003, Carcione and Picotti, 2006, Krzikalla and Müller, 2011, Deng et al., 2012, Nakagawa et al., 2013, Zhang et al., 2014, Quintal et al., 2009, 2011, Quintal, 2012, Morgan et al., 2012, Wang et al., 2013, Lee and Collett, 2009, Amalokwu et al., 2014, Qi et al., 2014, Sidler et al., 2013). The improvements of the models of White were discussed by Dutta and Seriff (1979), Dutta and Ode (1979a,b), Vogelaar and Smeulders (2007) and Vogelaar et al. (2010). Arbitrary geometries of patches were considered by Johnson (2001), but this model requires more parameters. Arbitrary shape and distribution of inclusions is also assumed in the approach of Rubino et al. (2009), and is extensively used in numerous studies (Rubino et al., 2011, Rubino and Velis, 2011, Rubino and Holliger, 2012, Rubino et al., 2013). A comprehensive review on different models for mesoscopic-scale heterogeneities in porous media can be found in Toms et al. (2006) and Müller et al. (2010).

The models of White and many other models dealing with seismic wave propagation in heterogeneous porous media provide a frequency-dependent plane-wave modulus that can be used to describe an initially heterogeneous porous medium with fluid and solid phases by an equivalent homogeneous effective viscoelastic one-phase medium. In many cases, it is advantageous to deal with the equations of viscoelasticity, because they simplify the analysis and computations, compared to the equations of poroelasticity. However, the macroscopic attenuation mechanism due to viscous interaction of the solid and fluid phases is not captured in the effective viscoelastic medium, since it represents a one-phase medium. In this thesis, effective poroelastic models are proposed and their performance is compared to the performance of effective viscoelastic models.

1.3 Objective and outline of this thesis

The objectives of this thesis are to propose new effective models for wave propagation in porous media with mesoscopic-scale heterogeneities and to evaluate their applicability compared to some of the currently used effective models. The thesis is structured as follows. Chapter 2 is an introductory chapter on Biot's theory, which is extensively used throughout the thesis. In Chapter 3, a new effective model is introduced for one-dimensional wave propagation in periodically layered media. The exact analytical solution is obtained to validate the new model and to compare its performance with the model of Vogelaar and Smeulders (2007), which provided an extension of the original model of White et al. (1975). In Chapter 4 another widely used model of White is considered (White, 1975), where heterogeneities are modelled as spherical inclusions, and an extension is proposed. Models proposed in Chapters 3 and 4 account for Biot's global-flow attenuation mechanism, which extends their applicability compared to the previous models. In Chapters 3 and 4 effective models with frequency-dependent coefficients are considered, while in Chapter 5 the analytical result of White et al. (1975) is used to derive an effective model with coefficients that do not depend on frequency. Such models are advantageous in some situations, as discussed in Chapter 5. In Chapter 6, the method of asymptotic homogenization with multiple scales is applied to a periodically layered poroelastic medium to evaluate applicablity of the method. Finally, in Chapter 7, an effective model is proposed for periodically layered media to describe angle-dependent attenuation and dispersion. Discussion of the presented results and conclusions are given in Chapter 8.

Chapter 2

Elastic wave propagation in fluid-saturated porous media: Biot's theory and extensions

In this chapter, we review the theory of wave propagation in fluid-saturated porous media, first developed by Maurice Biot, and its extensions. This theory is extensively used in this thesis. We touch upon historical background, introduce main equations, discuss some aspects of the theory important within the scope of this thesis and briefly review other works on dynamic equations of poroelasticity.

2.1 Introduction

Biot's theory (Biot, 1956a,b, 1962) is a linear theory of a two-phase medium consisting of a porous solid frame filled with a fluid moving through the pores of the solid. Biot laid the foundation for the linear elasticity of porous media which plays a tremendously important role in the field of poromechanics. Earlier works in this field that stipulated the development of Biot's theory are the works of Karl von Terzaghi (see, e.g., von Terzaghi, 1943) who was deservedly called the father of soil mechanics. A comparison of Biot's equations with the theory of consolidation by von Terzaghi was presented by Cryer (1963). A set of equations governing the acoustic wave propagation in isotropic porous media was also developed by Frenkel (1944), before Biot's publications, but his work did not receive as much attention as the work of Biot. The comparison of Frenkel's and Biot's equations was presented by Pride and Garambois (2005). A very interesting historic overview on the

development of the theory of poromechanics can be found in the book by de Boer (2000).

2.2 Constitutive equations

In Biot's theory the medium is assumed macroscopically isotropic, with a constant porosity ϕ, bulk modulus K_m, permeability k_0 and shear modulus μ. The solid grains are assumed to have constant density ρ_s and bulk modulus K_g. The solid frame contains connected pores fully saturated by one type of Newtonian fluid with viscosity η, bulk modulus K_f and density ρ_f. Sealed void pores are considered part of the solid. The wavelength of a passing wave is assumed to be much larger than the characteristic size of grains and pores. A representative volume element is introduced, which is small compared to the wavelength but large compared to the grain and pore sizes. The deformation of the poroelastic medium is described by two displacement fields averaged over the representative volume. They are the solid particle displacement vector $u_i(x, y, z, t)$ and vector $U_i(x, y, z, t)$ for the fluid particle displacement, or, instead, vector $w_i = \phi(U_i - u_i)$ for the relative fluid-to-solid displacement. The equations of motion can be expressed in terms of (u_i, U_i), (u_i, w_i) or (u_i, p), where p is the fluid pressure. It can be more convenient to work with (u_i, p) formulation since the geophones and hydrophones measure the components of the solid particle velocity and fluid pressure p, whereas the fluid particle velocity cannot be measured directly, but it is related to the measured quantities mathematically via the equations of motion.

The porosity in Biot's theory is defined as a volume fraction

$$\phi = V_f/V, \quad V = V_f + V_s, \tag{2.1}$$

where V is a volume of a representative element, V_f and V_s are the volumes occupied by the pores and the solid grains within the volume V, respectively.

Since linear elasticity is considered, the deformations are small and the strain tensors e_{ij} for the solid phase and ϵ_{ij} for the fluid phase read

$$\begin{aligned} e_{ij} &= \tfrac{1}{2}\left(u_{j,i} + u_{i,j}\right), \\ \epsilon_{ij} &= \tfrac{1}{2}\left(U_{j,i} + U_{i,j}\right), \end{aligned} \tag{2.2}$$

where a comma in the subscript denotes a spatial derivative with respect to the index following it. The total stress tensor τ_{ij} is defined as

$$\tau_{ij} = \tilde{\tau}_{ij} + \tau\delta_{ij}, \tag{2.3}$$

where $\tilde{\tau}_{ij}$ and τ are the components of the stress tensor corresponding to the solid and fluid parts, respectively, and δ_{ij} is the Kronecker delta. The stress components are defined as

$$\begin{aligned} \tilde{\tau}_{ij} &= -\sigma_{ij} - (1-\phi)p\delta_{ij}, \\ \tau &= -\phi p, \end{aligned} \tag{2.4}$$

where σ_{ij} are the intergranular stresses and p is the fluid pressure. The stress-strain relations read

$$\begin{aligned} \tilde{\tau}_{ij} &= 2\mu e_{ij} + (Ae_{kk} + Q\epsilon_{kk})\,\delta_{ij}, \\ \tau &= Qe_{kk} + R\epsilon_{kk}. \end{aligned} \tag{2.5}$$

Throughout the thesis, Einstein's summation convention is used, i.e., repeated indices are summed over, unless otherwise specified. In equations (2.5), μ and A correspond to the Lamé parameters in the equations of elasticity, where μ is a shear modulus of the drained frame. The conventional Lamé coefficient of the drained frame $\lambda = K_m - (2/3)\mu$ is equal to $A - Q^2/R$, which follows from the expressions given below (equation (2.6)). Coefficient R is a measure of pressure required on the fluid to force a certain volume of fluid into the porous aggregate while the total volume remains constant. Q is a coupling coefficient between the volume changes of the solid and fluid.

Four independent measurements are required to define these four elastic parameters (A, Q, R, μ). The shear modulus μ is obtained directly using a shear test on a drained sample. The so-called drained (jacketed) and undrained (unjacketed) experiments are used to define the remaining coefficients. In the jacketed test, a porous sample is enclosed in a thin impermeable jacket and put into a watertank subject to an external fluid pressure p. The internal fluid pressure is kept constant. This test is used to study volumetric effects caused by the intergranular stress, since there are no changes in pore fluid pressure. In the unjacketed test, the fluid can move freely. Then, there are no changes in intergranular stresses across the boundaries of the sample, and the effect of fluid pressure on volumetric response is studied. More details about the derivation of the relations between the elastic coefficients and the physical properties of the solid and fluid can be found

in Biot and Willis (1957) and van Dalen (2013). The expressions of the parameters A, Q and R in terms of the measurable physical properties of the medium read

$$\begin{aligned} A &= \frac{\phi K_m + (1-\phi) K_f \left(1 - \phi - K_m/K_s\right)}{\phi + K_f \left(1 - \phi - K_m/K_s\right)/K_s} - \frac{2}{3}\mu, \\ Q &= \frac{\phi K_f \left(1 - \phi - K_m/K_s\right)}{\phi + K_f \left(1 - \phi - K_m/K_s\right)/K_s}, \\ R &= \frac{\phi^2 K_f}{\phi + K_f \left(1 - \phi - K_m/K_s\right)/K_s}. \end{aligned} \tag{2.6}$$

2.3 Equations of motion

The equations defining the elastic wave propagation in a poroelastic medium according to Biot's theory consist of stress-strain relations and momentum equations, similar to the equations for the elastic medium. An important mechanism incorporated in Biot's equations is a dissipation mechanism due to viscous friction between the solid and fluid phases in motion. No other dissipation mechanisms are taken into account.

We do not reproduce the detailed derivation of Biot's equations of motion; it is well described in Biot's papers and reviewed in many publications by other authors (e.g., van Dalen, 2013). In general, there are seven field variables, namely, three components of the solid (u_i) and the fluid (U_i) particle displacements, and the pore fluid pressure (p); alternative to U_i, the relative fluid-to-solid particle displacement w_i can be used. Bonnet (1987) showed that only four of the variables are independent. Biot (1956a) formulated the equations of motion for a statistically isotropic (the directions x, y and z are equivalent and uncoupled dynamically) poroelastic solid in terms of solid and fluid particle displacements:

$$\begin{aligned} \rho_{11}\ddot{u}_i + \rho_{12}\ddot{U}_i + b_0(\dot{u}_i - \dot{U}_i) &= \tilde{\tau}_{ij,j} \\ \rho_{12}\ddot{u}_i + \rho_{22}\ddot{U}_i - b_0(\dot{u}_i - \dot{U}_i) &= -\phi p_{,i}. \end{aligned} \tag{2.7}$$

He introduced mass coefficients ρ_{11}, ρ_{12} and ρ_{22} which take into account non-uniformity of the relative fluid flow. Coefficient ρ_{12} is a mass coupling parameter between fluid and solid which must be negative. Coefficients ρ_{11} and ρ_{22} must be positive, and $\rho_{11}\rho_{22} - \rho_{12}^2 > 0$, in order to ensure positive definition of the quadratic

form of kinetic energy (Biot, 1956a). The expressions for these coefficients read

$$\begin{aligned} \rho_{11} &= (1-\phi)\rho_s - \rho_{12}, \\ \rho_{22} &= \phi\rho_f - \rho_{12}, \\ \rho_{12} &= -(\alpha_\infty - 1)\phi\rho_f, \end{aligned} \tag{2.8}$$

where α_∞ is the high-frequency limit of the tortuosity factor α, a measure for the shape of the pores. The frequency dependence of this factor is discussed in Section 2.5. Tortuosity is one of the key parameters defining the behaviour of Biot's slow wave (discussed in Section 2.6). It is real-valued for a non-viscous fluid, and can be defined for a specific pore geometry. It can be measured using slow-wave arrival times and derived from electrical measurements (Brown, 1980, Johnson, 1980, Berryman, 1980). Biot also introduced the viscous factor b_0 which is related to Darcy's permeability k_0:

$$b_0 = \frac{\eta\phi^2}{k_0}. \tag{2.9}$$

Note that this frequency-independent formulation of the viscous factor is valid at low frequencies, where the fluid flow is of the Poiseuille type. High-frequency corrections were proposed; they are discussed in Section 2.5.

In this thesis, we also use equations of motion formulated in terms of (u_i, w_i). In the general case of an anisotropic tortuosity α_{ij} and permeability k_{ij}, they read (Biot, 1962)

$$\begin{aligned} \rho\ddot{u}_i + \rho_f\ddot{w}_i &= \tau_{ij,j}, \\ \rho_f\ddot{u}_i + m_{ij}\ddot{w}_j + \eta r_{ij}\dot{w}_j &= -p_{,i}, \end{aligned} \tag{2.10}$$

where $\rho = \phi\rho_s + (1-\phi)\rho_f$, $m_{ij} = \alpha_{ij}\rho_f/\phi$ and tensor r_{ij} is an inverse of the permeability tensor $\mathbf{r} = \mathbf{k_0^{-1}}$. In the isotropic case $k_{0ij} = k_0\delta_{ij}$ and $\alpha_{ij} = \alpha_\infty\delta_{ij}$. As has been mentioned above, this formulation with frequency-independent coefficient m_{ij} and r_{ij} is only valid at low frequencies. An alternative formulation valid at higher frequencies is discussed in Section 2.5.

2.4 Biot's critical frequency

Biot's critical frequency is defined as

$$\omega_B = \frac{\eta\phi}{\alpha_\infty k_0 \rho_f}. \tag{2.11}$$

It separates two different regimes. For frequencies below ω_B, the relative fluid-solid motion is governed by viscous forces, and only a fast P-wave can propagate in the porous medium. Above ω_B, inertial coupling dominates, both a fast and a slow P-wave can propagate, and the tortuosity factor becomes important. Many natural rocks have a relatively high Biot's critical frequency, of the order of MHz, well outside the seismic frequency range. But the critical frequency is decreasing with increasing permeability, and for high-permeable sandstones and sands it can become of the order of kHz and even lower, and it thus enters the seismic frequency band. In this case, Biot's attenuation mechanism due to relative motion of fluid and solid phases described by (2.10) is not negligible and should be accounted for in models for seismic attenuation, which is discussed in this thesis.

2.5 Dynamic permeability

The time-independent viscous factor b_0 in (2.9) is valid in the low-frequency range. For corrections at higher frequencies, models of frequency-dependent permeability were developed (Biot, 1956b, Auriault et al., 1985, Johnson et al., 1987). For formulations of the equations of motion in the time domain, the frequency-dependent viscous factor has to be transformed to the time domain, which yields replacing frequency-dependence by a convolution operator.

In this thesis, we solve the equations of motion in the frequency domain. The Fourier transform is applied for transforming to the frequency-domain:

$$\hat{f}(x, y, z, \omega) = \int_{-\infty}^{\infty} \exp(-\mathrm{i}\omega t) f(x, y, z, t) dt. \tag{2.12}$$

Since the time signal is real-valued, the inverse Fourier transform is formulated in the following way:

$$f(x,y,z,t) = \frac{1}{\pi}\int_0^\infty \mathrm{Re}\left(\hat{f}(x,y,z,\omega)\exp(\mathrm{i}\omega t)\right) d\omega. \tag{2.13}$$

We therefore only need to consider positive frequencies $\omega \geq 0$.

In this thesis, we adopt the formulation of Johnson et al. (1987) of dynamic permeability $\hat{k}$ which describes transition from the viscous- to the inertia-dominated regime. Throughout the thesis, a hat above a quantity stands for frequency-dependence. The expression for $\hat{k}$ reads

$$\hat{k}(\omega) = k_0\left(\sqrt{1+\mathrm{i}M\frac{\omega}{2\omega_B}}+\mathrm{i}\frac{\omega}{\omega_B}\right)^{-1}, \tag{2.14}$$

where parameter $M = 8\alpha_\infty k_0/(\phi\Lambda^2)$ is a pore-shape factor, and Λ is the characteristic length scale of the pores. It was mentioned by Johnson et al. (1987) that M is often close to 1. In this thesis, we assume $M = 1$; furthermore, $\mathrm{Re}(\sqrt{1+\mathrm{i}M\omega/\omega_B}) \geq 0$. Incorporation of dynamic permeability (2.14) results in the following formulation of the second equation in (2.10) in the frequency domain (for the isotropic case):

$$-\omega^2\rho_f\hat{u}_i + \frac{\eta}{\hat{k}(\omega)}\mathrm{i}\omega\hat{w}_i = -\hat{p}_{,i}. \tag{2.15}$$

An alternative to the formulation of frequency-dependent permeability, frequency-dependent tortuosity can be used:

$$\hat{\alpha}(\omega) = \alpha_\infty\left(1-\mathrm{i}\frac{\omega_B}{\omega}\sqrt{1+\mathrm{i}M\frac{\omega}{2\omega_B}}\right). \tag{2.16}$$

In this case, the second equation in (2.10) is formulated as follows (for the isotropic case):

$$-\omega^2\left(\rho_f\hat{u}_i + \frac{\rho_f\hat{\alpha}(\omega)}{\phi}\hat{w}_i\right) = -\hat{p}_{,i}. \tag{2.17}$$

Formulations (2.15) and (2.17) are equivalent. We define the frequency-dependent viscous factor $\hat{b}$ as

$$\hat{b}(\omega) = b_0\sqrt{1+\mathrm{i}M\frac{\omega}{2\omega_B}}. \tag{2.18}$$

It replaces the factor b_0 in equations (2.7), when the high-frequency correction is adopted. With this definition, equation (2.15) (or (2.17)) reads

$$-\omega^2\left(\rho_f\hat{u}_i+\frac{\alpha_\infty\rho_f}{\phi}\hat{w}_i\right)+\mathrm{i}\omega\frac{\hat{b}(\omega)}{\phi^2}\hat{w}_i=-\hat{p}_{,i}. \tag{2.19}$$

2.6 Biot's slow wave

One of the significant findings in Biot's theory is the prediction of three types of waves. Together with the shear wave, Biot's theory predicts two compressional waves, a slow and a fast one. The existence of the slow wave was first experimentally observed by Plona (1980), using a synthetic rock. It was a very important observation which confirmed the validity of the equations of poromechanics. Further discussion of laboratory experiments and the possibility to observe the slow wave in real rocks can be found in Kliments and McCann (1988). The authors mentioned that it is not likely to observe the slow wave in real rocks. The slow wave is highly attenuated, and it cannot be observed in seismic data. However, it was observed in real sandstones in laboratory experiments (Nagy et al., 1990, Kelder and Smeulders, 1997). An overview of different experiments is given by Smeulders (2005). Despite the fact that Biot's slow wave is not visible at seismic data, it still affects the observations (Allard et al., 1986, Rasolofosaon, 1988, Rubino et al., 2006). Slow waves generated at an interface can significantly affect the predicted amplitudes and phases of the fast compressional wave (Pride et al., 2002). This is why it is important to take into account mode conversions at the interface properly.

Biot's theory does not predict any slow S-waves. Sahay (2008) proposed a correction to Biot's constitutive equations and predicted a slow S-wave mode that is generated at interfaces and other inhomogeneities and influences attenuation of fast P- and S-waves. In this theory, an attenuation mechanism due to viscous loss within the fluid is taken into account, in addition to Biot's attenuation due to viscous forces between the solid and fluid phases.

2.7 Boundary conditions

Boundary conditions have to be defined to solve equations of motion in a poroelastic medium. In an infinite medium, Sommerfeld's radiation condition is used

implying that there is no incoming energy flux from infinity (Sommerfeld, 1949). The boundary conditions at an interface of a poroelastic medium are not uniquely defined. They depend on the surface flow impedance (Deresiewicz and Skalak, 1963) which defines the connection of the pores at both sides of the interface. The two limiting cases are the open and closed-pore boundary conditions. The open-pore conditions assume full connection between the pores in contact, while the closed-pore ones do not assume any direct connections between the pores. The situation when the pores are partially connected is in between these two limiting cases. The choice of the boundary conditions strongly affects predicted reflection and transmission coefficients. Open-pore boundary conditions give a better agreement between predicted reflection coefficients and the ones measured in a laboratory (Rasolofosaon, 1988, Wu et al., 1990, Jocker and Smeulders, 2009). Experimental results showed that it is hard to generate the slow wave with closed-pore boundary conditions (Rasolofosaon, 1988), which do not allow a fluid flow across the interface. Sidler et al. (2013) showed that there is a discrepancy in predictions of poroelastic and equivalent viscoelastic solutions at a fluid/porous-solid interface, where the poroelastic solution with the open-pore boundary conditions predicts an energy loss related to the generation of a slow wave at the interface. The viscoelatic solution does not account for this energy loss. With closed-pore boundary conditions, the agreement between the solutions is much better. This example clearly shows the importance of choosing the correct boundary conditions depending on the problem and the desired accuracy in capturing physical effects. While most algorithms used in exploration geophysics are based on the viscoelastic modeling, the poroelastic modeling with open-pore boundary conditions can be advantageous for fitting the model with observed data.

Interface conditions consistent with Biot's equations were derived by Gurevich and Schoenberg (1999). They showed that they correspond to the limiting case of the open-pore boundary conditions proposed by Deresiewicz and Skalak (1963). These are the only boundary conditions derived from the macroscopic Biot equations, without taking into account microscopic details of the interface. Gurevich and Schoenberg (1999) also found that the realistic scenario of a partially permeable contact between two porous media can be modelled within the scope of Biot's theory by introducing a transition layer with an infinitely small thickness and a small interface permeability coefficient, provided the open-pore boundary conditions hold at both sides of this layer.

The influence of fully or partially impermeable interface assumptions is a matter of many studies since it is not yet fully resolved. The correspondence between experimental and numerical studies with poroelastic materials is severely influenced by the boundary conditions. The properties of an effective homogeneous medium, which is equivalent to some heterogeneous medium, are significantly influenced by the choice of the boundary conditions at the internal interfaces related to heterogeneities. This is confirmed in this thesis by comparing the predictions of effective models derived from the same heterogeneous medium, but with different boundary conditions used (Chapters 3, 4 and 7). In our models, we use Biot's theory with the open-pore boundary conditions (Deresiewicz and Skalak, 1963), which imply the continuity of the following field variables at interfaces:

- solid-particle displacements;
- relative fluid-to-solid particle displacement normal to the interface;
- normal and tangential intergranular stresses;
- pore fluid pressure.

2.8 Other formulations of dynamic equations of poroelasticity

Apart from the works of Biot, equations of dynamic poroelasticity were reported in other publications. As has been mentioned in the beginning of this chapter, Frenkel (1944) was the first one to develop the theory of dynamic poroelasticity. A thorough review on further developments and generalizations of Biot-Frenkel theory made by Russian scientists was carried out by Nikolaevskiy (2005). Biot's theory was compared to the linear theory of porous media for wave propagation problems in case of incompressible constituents and zero apparent mass density (Bowen, 1982, Ehlers and Kubik, 1994, Schanz and Diebels, 2003). The theory of porous media is based on the theory of mixtures (Truesdell and Toupin, 1960, Bowen, 1976), and extended by the concept of volume fractions (Bowen, 1980, 1982). The dynamic formulation of this theory is published by de Boer et al. (1993), Diebels and Ehlers (1996) and Liu et al. (1998).

In Biot's theory, a fully saturated porous medium is assumed. The extension to a partially saturated poroelastic medium (three-phase medium) was presented

by Vardoulakis and Beskos (1986). A different approach to derive the governing equations of a fully saturated poroelastic medium was used by Burridge and Keller (1981). It is a micromechanical approach based on a two-scale asymptotic homogenization. The obtained equations coincide with Biot's equations in case the viscosity of the fluid is relatively small. The two-scale homogenization method applied to a porous solid, which results in the equations similar to Biot's equations, was also used by Auriault (1980a). In Chapter 6 of this thesis we use the same homogenization approach, but we apply it to a mesoscopic-scale structure, to derive macroscopic equations for porous media with mesoscopic-scale heterogeneities. Pride et al. (1992) derived equations of poroelasticity in the form of Biot's equations using a volume-averaging method. More on these studies can be found in the review by Berryman (2005). A comprehensive review of different formulations of equations of poroelasticity and their numerical and analytical solutions is given by Schanz (2009).

2.9 Concluding remarks

Different formulations of equations of poroelasticity and extensions to Biot's theory have been discussed. However, classical Biot's theory remains a common approach to describe wave propagation in linear poroelasticity. As also mentioned in the previous chapter, Biot's theory underestimates attenuation as observed in real data. It does not account for the presence of inhomogeneities in solid and fluid properties. In this thesis, we study wave propagation in heterogeneous porous media with layered or spherical inclusions. Both host media and inclusions are assumed macroscopically homogeneous and Biot's theory is used to describe wave propagation in each of these domains.

Chapter 3

Effective poroelastic model for one-dimensional wave propagation in periodically layered porous media

In this chapter, an effective poroelastic model is proposed that describes seismic attenuation and dispersion in periodically layered media. In this model, the layers represent mesoscopic-scale heterogeneities (larger than the grain and pore sizes but smaller than the wavelength) that can occur both in fluid and solid properties. The proposed effective medium is poroelastic, contrary to previously introduced models that lead to effective viscoelastic media. The novelty lies in the application of the pressure continuity boundary conditions instead of no-flow conditions at the outer edges of the elementary cell. The approach results in effective Biot elastic moduli and effective porosity that can be used to obtain responses of heterogeneous media in a computationally fast manner. The model is validated by the exact solution obtained with the use of Floquet's theory. Predictions of the new effective poroelastic model are more accurate than the predictions of the corresponding effective viscoelastic model when the Biot critical frequency is of the same order as the frequency of excitation, and for materials with weak frame. This is the case for media such as weak sandstones, weakly consolidated and unconsolidated

This chapter was published as a journal paper in *Geoph. J. Int.* **195**, 1337–1350 (Kudarova et al., 2013). Note that minor changes have been introduced to make the text consistent with the other chapters of this thesis.

sandy sediments. The reason for the improved accuracy for materials with low Biot critical frequency is the inclusion of the Biot global flow mechanism which is not accounted for in the effective viscoelastic media. At frequencies significantly below the Biot critical frequency and for well consolidated porous rocks, the predictions of the new model are in agreement with previous solutions.

3.1 Introduction

A lot of attention has been paid to the proper description of seismic wave attenuation in porous media over the last decades. Currently, it is widely accepted that attenuation in porous materials is associated with the presence of pore fluids and caused by a mechanism often referred to as wave-induced fluid flow. Flow of the pore fluid can occur at different spatial scales, i.e., on the microscopic, mesoscopic and macroscopic scales. Generally, flow is caused by pressure gradients created by passing waves. The flow dissipates energy of the passing wave as it implies a motion of the viscous fluid relative to the solid frame of the porous material.

Wave-induced fluid flow resulting from wavelength-scale pressure gradients between peaks and troughs of a passing seismic wave is often called macroscopic or global flow as the flow takes place on the length scale of the seismic wave. In many practical situations, this mechanism is not the dominant attenuation mechanism of a seismic wave, though it is not always negligible since it depends on parameters such as permeability and porosity. For a medium containing inhomogeneities smaller than the wavelength but much larger than the typical pore size, a passing wave induces a pressure gradient on the sub-wavelength scale that drives a so-called mesoscopic flow. It is widely believed that it is this mechanism, the wave-induced fluid flow between mesoscopic inhomogeneities, that is the main cause of wave attenuation in the seismic frequency band (e.g., Müller and Gurevich, 2005; Müller et al., 2010). Inhomogeneities can also be present on the scale of the pore size. In that case, passing waves induce local or microscopic flow, but its effect is often rather small for seismic waves as the mechanism becomes active only at relatively high frequencies (Pride et al., 2004).

In this thesis, media that have mesoscopic inhomogeneities are considered. In such media the inhomogeneities can occur both in fluid (partial or patchy saturation) and in frame (e.g., double porosity) properties. The direct method to account for the presence of such inhomogeneities and its effect on attenuation is

to solve the equations of poroelasticity (Biot, 1956a; Schanz, 2009; Carcione et al., 2010) with spatially varying coefficients. However, this can be computationally cumbersome and time consuming, thus motivating the development of effective-medium approaches where frequency-dependent coefficients are derived and used as input for the equations of a homogeneous effective medium. The simplest example of this approach is the homogenization of a periodically layered medium in which each layer is homogeneous and waves propagate normal to the layering. White et al. (1975) derived a low-frequency approximation of an effective compressional (P) wave modulus for such a medium by applying an oscillatory compressional test to the representative element that consists of half of the periodic cell and has undrained boundaries (i.e., no-flow conditions). This analysis showed that attenuation is quite significant when the fluid content in each of the layers is considerably different, like for the combination of water and much more compressible gas. White's result has been confirmed by other authors who came to the same effective modulus in a slightly different way. Norris (1993) derived the asymptotic approximation of the fast P-wave Floquet wavenumber in the context of quasistatic Biot's theory and defined the effective modulus based on that. Brajanovski and Gurevich (2005) also based the effective modulus on a wavenumber but used a low-frequency approximation of the matrix propagator method. The low-frequency approximations were overcome by Vogelaar and Smeulders (2007), who solved the White's model in the context of full Biot's equations.

Dutta and Seriff (1979) showed that the geometry of heterogeneities plays a minor role on the behavior of the media as long as the heterogeneities are much smaller than the wavelength. This justifies studies with periodic stratification, the great advantage of which is the availability of analytical expressions for the effective moduli that provide insight and that are easy to apply. Based on White's periodic model, Carcione and Picotti (2006) focused on the analysis of different heterogeneities in rock properties that led to high attenuation. They found that changes in porosity and fluid properties cause the most attenuation compared to inhomogeneities in the grain and frame moduli. Wave propagation in fractured porous media is studied by taking a limit case of White's model in which the thickness of one of the layers goes to zero and its porosity goes to one (Brajanovski and Gurevich, 2005; Deng et al., 2012). Krzikalla and Müller (2011) made an extension of the periodic model to arbitrary angles of incidence, thus accounting for shear-wave attenuation as well. Carcione et al. (2011) used this analytical extension to

validate their numerical oscillatory tests on a stack of layers from which they determined the complex stiffnesses of an effective transversely isotropic medium. They refer to this extension as Backus/White model, because it is based on White's result and the extension of the O'Doherty-Anstey formalism, and on Backus averaging applied to poroelasticity by Gelinsky and Shapiro (1997). Apparently, the periodic model of White is the starting point of many other studies on partially saturated media. Rubino et al. (2009) proposed an equivalent medium for a more realistic geometry of heterogeneities than in White's model, also using oscillatory compressibility (and shear) tests in the space-frequency domain. This approach is used, in particular, in studies on CO_2 monitoring (Rubino et al., 2011; Picotti et al., 2012).

The above-discussed effective media that capture the mesoscopic attenuation mechanism are in fact viscoelastic media. In all 1-D models, only one frequency-dependent elastic modulus is obtained for the considered representative element. This is a result of employing the no-flow boundary condition (undrained boundary), which implies that there is no relative fluid-to-solid motion at the outer edges of the representative element. Consequently, there is only one degree of freedom in the effective medium, which is the displacement of the frame; the effective medium thus allows for the existence of only one P-wave mode. Though the derivation of the effective modulus is based on the equations of poroelasticity, the obtained effective models can therefore be referred to as viscoelastic, as it was explicitly done for the 2D case by Rubino et al. (2009). A viscoelastic model is after all characterized by a single complex-valued frequency-dependent bulk modulus, being the counterpart of a temporal convolution operator in the time-domain stress-strain relation (e.g., Carcione, 2007); a poroelastic model would require more effective parameters. Reduction of parameters and degrees of freedom in the effective medium facilitates its application and increases efficiency of computations, thus making the application of the equivalent viscoelastic media popular for studies of mesoscopic loss in porous media. Dutta and Ode (1979a) noted, however, that the choice of boundary conditions at the outer edges of the representative element, as originally made by White et al. (1975), is not unique. Instead of the no-flow condition, the pressure continuity condition may be applied, as commonly used at the interface of two porous layers (Deresiewicz and Skalak, 1963).

In this chapter, we derive an effective model for the same periodic configuration as considered by White, but using the pressure continuity boundary condition that allows relative fluid-to-solid motion at the outer edges of the representative

element (for which we take the full periodic cell). We show that this leads to an effective poroelastic model that has two degrees of freedom, the frame and fluid displacements, and that allows the existence of both the fast and the slow compressional waves. The choice of boundary conditions implies that flow on the wavelength scale is permitted and the effective poroelastic model thus also captures the macroscopic attenuation mechanism (next to the mesoscopic mechanism). The effect of both global and mesoscopic flow on wave propagation in layered media normal to the layering was also captured by Gelinsky et al. (1998), who proposed a statistical model for small fluctuations of the medium parameters and introduced an approximate solution for frequencies well below the Biot critical frequency. We derive frequency-dependent effective poroelastic parameters valid for any contrast in medium parameters and for all frequencies where the effective model approach is valid. We also derive low-frequency approximations of the effective parameters. The frequency-dependent (fast) P-wave attenuation and transient point-source responses are compared to those predicted by the full-frequency range version of White's model (Vogelaar and Smeulders, 2007) and to the analytical solution as obtained using Floquet's theory (Floquet, 1883). It appears that the effective poroelastic model yields the proper P-wave attenuation even in situations where the macroscopic attenuation mechanism plays a significant role.

The chapter is structured as follows. First, the basic equations of Biot's theory are introduced in Section 3.2. Then, the derivation of the effective porous medium is given (Section 3.3, supported by Appendices 3.A and 3.B). Expressions for point-source responses are derived in Section 3.4 (and Appendix 3.C), and numerical results are presented in Section 3.5. Limitations of the effective poroelastic model are discussed in Section 6.4 and conclusions are given in Section 3.7.

3.2 Biot theory overview

In this section, the basic equations of Biot's theory (Biot, 1956a) expressed for the displacement fields in porous media are introduced. The one-dimensional form of the stress-strain relations read

$$\begin{aligned} -\phi p &= Q u_{,z} + R U_{,z}, \\ -\sigma - (1-\phi) p &= P u_{,z} + Q U_{,z}. \end{aligned} \tag{3.1}$$

Here ϕ is the porosity, p is the pore fluid pressure, σ is intergranular stress, u is the solid and U is the fluid displacements with respect to an absolute frame of reference. The comma stands for the spatial derivative. The poroelastic coefficients P, Q, R are related to the porosity, the bulk moduli of the grains (K_s), fluid phase (K_f) and the drained matrix (K_m), as well as to the shear modulus (μ), via the following expressions:

$$\begin{aligned} P &= \frac{\phi K_m + (1-\phi)K_f\left(1-\phi-K_m/K_s\right)}{\phi + K_f\left(1-\phi-K_m/K_s\right)/K_s} + \frac{4}{3}\mu, \\ Q &= \frac{\phi K_f\left(1-\phi-K_m/K_s\right)}{\phi + K_f\left(1-\phi-K_m/K_s\right)/K_s}, \\ R &= \frac{\phi^2 K_f}{\phi + K_f\left(1-\phi-K_m/K_s\right)/K_s}. \end{aligned} \tag{3.2}$$

The momentum equations read

$$\begin{aligned} -\sigma_{,z} - (1-\phi)p_{,z} &= \rho_{11}\ddot{u} + \rho_{12}\ddot{U} + b * (\dot{u} - \dot{U}), \\ -\phi p_{,z} &= \rho_{12}\ddot{u} + \rho_{22}\ddot{U} - b * (\dot{u} - \dot{U}), \end{aligned} \tag{3.3}$$

where a dot stands for a time-derivative, $*$ for temporal convolution, ρ_{11}, ρ_{12} and ρ_{22} are the real-valued density terms related to the porosity, the fluid density ρ_f, the solid density ρ_s and to the tortuosity α_∞:

$$\begin{aligned} \rho_{11} &= (1-\phi)\rho_s - \rho_{12}, \\ \rho_{12} &= -(\alpha_\infty - 1)\phi\rho_f, \\ \rho_{22} &= \phi\rho_f - \rho_{12}. \end{aligned} \tag{3.4}$$

In the original low-frequency Biot's theory Biot (1956a) the damping operator $b = b(t)$ is a time-independent viscous factor $b_0 = \eta\phi^2/k_0$, where η is the viscosity of the fluid, and k_0 is permeability. With the adoption of the correction to this factor to account for dynamic effects (Johnson et al., 1987) the visco-dynamic operator $\hat{b}$ in the frequency domain reads:

$$\hat{b} = b_0\sqrt{1 + \mathrm{i}\frac{\omega}{2\omega_B}M}, \quad \mathrm{Re}(\hat{b}) > 0 \quad \text{for all} \quad \omega. \tag{3.5}$$

Here M is the parameter that depends on the geometry of the pores, permeability and porosity. Following Johnson et al. (1987), we will assume $M = 1$ throughout

the chapter. $\omega_B = \phi\eta/(k_0\alpha_\infty\rho_f)$ is the Biot critical frequency. A hat above a quantity stands for frequency dependence. The transition to the frequency domain is carried out by a Fourier transform defined as

$$\hat{f}(\omega) = \int_{-\infty}^{\infty} \exp(-\mathrm{i}\omega t) f(t) dt. \tag{3.6}$$

The transition back to the time domain is carried out by applying the inverse Fourier transform

$$f(t) = \frac{1}{2\pi} \int_{-\infty}^{\infty} \exp(\mathrm{i}\omega t) \hat{f}(\omega) d\omega. \tag{3.7}$$

The combination of the stress-strain relations (3.1) and the equations of motion (3.3) leads to a set of equations in terms of the fluid (U) and solid (u) particle displacements. These equations are solved in the frequency domain via seeking a solution in the form $\hat{u} = \hat{A}\exp(\mathrm{i}kz)$, $\hat{U} = \hat{B}\exp(\mathrm{i}kz)$. Substitution of these expressions leads to a system of linear homogeneous equations for the amplitudes $\hat{A}$, $\hat{B}$, which has a non-trivial solution when the determinant of the system is zero:

$$(PR - Q^2) - (P\hat{\rho}_{22} + R\hat{\rho}_{11} - 2Q\hat{\rho}_{12})\frac{k^2}{\omega^2} + (\hat{\rho}_{11}\hat{\rho}_{22} - \hat{\rho}_{12}^2)\frac{k^4}{\omega^4} = 0. \tag{3.8}$$

Here frequency-dependent density terms are defined as:

$$\begin{aligned} \hat{\rho}_{11} &= \rho_{11} - \mathrm{i}\hat{b}/\omega, \\ \hat{\rho}_{12} &= \rho_{12} + \mathrm{i}\hat{b}/\omega, \\ \hat{\rho}_{22} &= \rho_{22} - \mathrm{i}\hat{b}/\omega. \end{aligned} \tag{3.9}$$

The dispersion equation (3.8) has four roots $\pm k_{P1}$, $\pm k_{P2}$ that correspond to the wavenumbers of the up- and down-going fast and slow P-waves. The fluid-to-solid amplitude ratios for both waves are:

$$\hat{\beta}_{P1,P2} = -\frac{Pk_{P1,P2}^2 - \hat{\rho}_{11}\omega^2}{Qk_{P1,P2}^2 - \hat{\rho}_{12}\omega^2}. \tag{3.10}$$

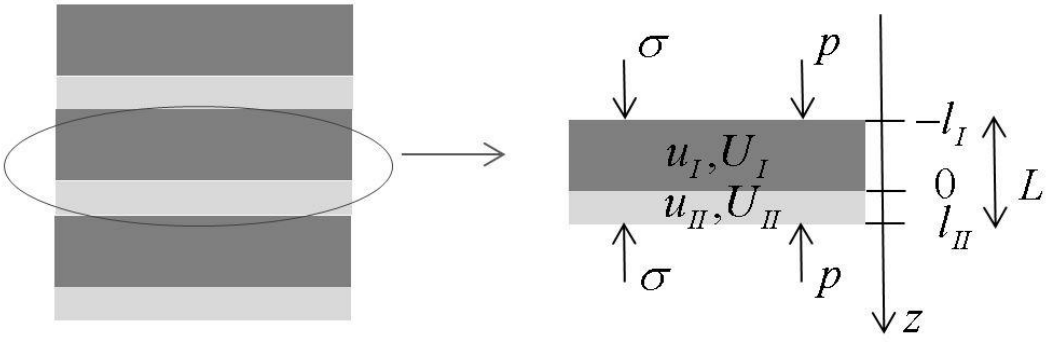

FIGURE 3.1: Left: periodically layered medium; right: its elementary cell.

Thus, for arbitrary excitation the displacement fields read

$$\begin{aligned}\hat{u}(z) &= \hat{A}_1 \mathrm{e}^{\mathrm{i}k_{P1}z} + \hat{A}_2 \mathrm{e}^{\mathrm{i}k_{P2}z} + \hat{A}_3 \mathrm{e}^{-\mathrm{i}k_{P1}z} + \hat{A}_4 \mathrm{e}^{-\mathrm{i}k_{P2}z},\\ \hat{U}(z) &= \hat{\beta}_{P1}(\hat{A}_1 \mathrm{e}^{\mathrm{i}k_{P1}z} + \hat{A}_3 \mathrm{e}^{-\mathrm{i}k_{P1}z}) + \hat{\beta}_{P2}(\hat{A}_2 \mathrm{e}^{\mathrm{i}k_{P2}z} + \hat{A}_4 \mathrm{e}^{-\mathrm{i}k_{P2}z}).\end{aligned} \tag{3.11}$$

The amplitudes $\hat{A}_1$ to $\hat{A}_4$ are determined by the excitation and boundary conditions. These expressions will be used in further derivations.

3.3 Effective poroelastic model for periodic layering

In this section, effective frequency-dependent poroelastic parameters are derived to describe wave propagation in periodically stratified media normal to the stratification. The periodic medium and its elementary cell are depicted in Fig. 3.1. The thicknesses of the layers are denoted by l_I and l_{II}, and $L = l_I + l_{II}$ is the period of the system. Each of the layers I and II is homogeneous and is described by Biot's equations introduced in the previous section, and has its own set of material properties contained in the coefficients of equations (3.2), (3.4) and (3.5).

Since we consider the period L much smaller than the wavelength, it is reasonable to regard some elementary cell as a representative volume of the homogeneous effective medium. Then the elastic moduli can be determined from oscillatory compressional-stress tests. A similar approach has been used by White et al. (1975), but with a different choice of boundary conditions; they chose a representative elementary cell that consists of the halves of the layers and applied the

total stress continuity and no-flow conditions at the outer edges of the elementary cell. Here, the full periodic cell is chosen and an oscillatory pressure p is applied together with an oscillatory intergranular stress σ at the outer edges of the elementary cell, as depicted in Fig. 3.1 (right panel). We emphasize that, with this choice (suggested by Dutta and Ode, 1979a), no kinematic condition restricting the flow across the outer edges of the cell is applied; two phases, solid and fluid displacements, remain in the effective medium, while the no-flow condition allows for only one phase in the effective medium.

The solutions of Biot's equations in each of the layers consist of up- and down-going plane waves [as in eq. (3.11)]:

$$\begin{aligned} \hat{u}_{I,II} &= \sum_{i=1}^{4} \hat{A}_i^{I,II} \exp(\mathrm{i}k_i^{I,II} z), \\ \hat{U}_{I,II} &= \sum_{i=1}^{4} \hat{\beta}_i^{I,II} A_i^{I,II} \exp(\mathrm{i}k_i^{I,II} z). \end{aligned} \tag{3.12}$$

Throughout the chapter the indices and superscripts I and II refer to the properties of the layers I and II, respectively. The wavenumbers $k_i^{I,II}$ for each of the layers are found as the roots of the corresponding dispersion equations (3.8) and the fluid-to-solid amplitude ratios $\hat{\beta}_i^{I,II}$ are found according to relations (3.10). In order to find the unknown amplitudes $\hat{A}_i^{I,II}$ a system of eight linear algebraic equations has to be solved that follow from the eight boundary conditions:

$$\begin{aligned} &\{\hat{u}_I, \hat{w}_I, \hat{\sigma}_I, \hat{p}_I\}|_{z=0} = \{\hat{u}_{II}, \hat{w}_{II}, \hat{\sigma}_{II}, \hat{p}_{II}\}|_{z=0}\,, \\ &\hat{p}_I(-l_I) = \hat{p}, \qquad \hat{p}_{II}(l_{II}) = \hat{p}, \\ &\hat{\sigma}_I(-l_I) = \hat{\sigma}, \qquad \hat{\sigma}_{II}(l_{II}) = \hat{\sigma}. \end{aligned} \tag{3.13}$$

Here, the first four boundary conditions assume the continuity of intergranular stress, pore pressure, solid particle displacement and fluid displacement relative to the matrix $\hat{w} = \phi(\hat{U} - \hat{u})$ at the interface between the layers I and II (following Deresiewicz and Skalak, 1963). The latter four conditions express the excitation at the outer edges; they are thus different from those applied by White et al. (1975) and Vogelaar and Smeulders (2007). The coefficients of the linear system of equations are written out explicitly in Appendix 3.A.

As mentioned before, the elementary cell is regarded as a representative volume of the homogenized effective medium. Thus, the strains of the elementary cell

$$\hat{u}_{,z} = \frac{\hat{u}_{II}(l_{II}) - \hat{u}_I(-l_I)}{L}, \quad \hat{U}_{,z} = \frac{\hat{U}_{II}(l_{II}) - \hat{U}_I(-l_I)}{L} \tag{3.14}$$

can be regarded as the strains of the effective medium. They are related to the intergranular stress and pore pressure according to Biot's stress-strain relations (3.1)

$$\begin{bmatrix} \hat{u}^e_{,z} \\ \\ \hat{U}^e_{,z} \end{bmatrix} = \mathbf{E}_e^{-1} \begin{bmatrix} \hat{\sigma} \\ \\ \hat{p} \end{bmatrix}, \quad \mathbf{E}_e = \frac{1}{\phi_e} \begin{bmatrix} \hat{Q}_e(1-\hat{\phi}_e) - \hat{\phi}_e\hat{P}_e & \hat{R}_e - \hat{\phi}_e(\hat{Q}_e + \hat{R}_e) \\ \\ -\hat{Q}_e & -\hat{R}_e \end{bmatrix}. \tag{3.15}$$

Substitution of the amplitudes $\hat{A}_i^{I,II}$, which are found after solving the system of equations from Appendix 3.A, into equations (3.12), and then substitution of the result into (3.14), provides the following relations:

$$\begin{aligned} \hat{u}_{,z} &= \alpha_1\hat{\sigma} + \alpha_2\hat{p}, \\ \hat{U}_{,z} &= \alpha_3\hat{\sigma} + \alpha_4\hat{p}. \end{aligned} \tag{3.16}$$

Here α_1 to α_4 are frequency-dependent complex-valued coefficients. In order to derive the effective Biot coefficients, equations (3.15) and (3.16) should be compared. This leads to a system of four nonlinear algebraic equations, the solution of which is

$$\begin{aligned} \hat{P}_e &= -\frac{-\alpha_3\alpha_2 - \alpha_4\alpha_3 + \alpha_4\alpha_1 + {\alpha_3}^2}{{\alpha_3}^2\alpha_2 - \alpha_3\alpha_1\alpha_2 - \alpha_4\alpha_1\alpha_3 + \alpha_4{\alpha_1}^2}, \\ \hat{Q}_e &= \frac{\alpha_3(\alpha_1 - \alpha_2)}{{\alpha_3}^2\alpha_2 - \alpha_3\alpha_1\alpha_2 - \alpha_4\alpha_1\alpha_3 + \alpha_4{\alpha_1}^2}, \\ \hat{R}_e &= -\frac{\alpha_1(\alpha_1 - \alpha_2)}{{\alpha_3}^2\alpha_2 - \alpha_3\alpha_1\alpha_2 - \alpha_4\alpha_1\alpha_3 + \alpha_4{\alpha_1}^2}, \\ \hat{\phi}_e &= \frac{\alpha_1 - \alpha_2}{\alpha_1 - \alpha_3}. \end{aligned} \tag{3.17}$$

These coefficients are the effective complex-valued frequency-dependent elastic moduli and porosity of the effective poroelastic medium.

In the low-frequency regime, all effective models that capture the mesoscopic attenuation mechanism predict similar behaviour of the inverse quality factor Q^{-1} of the fast compressional wave (Pride et al., 2003). In order to validate the effective coefficients (that are combined in Q^{-1}) in the current effective poroelastic

model, we derive low-frequency analytical expressions using a perturbation method described in Appendix 3.C. The terms of the expansion

$$\hat{\Phi}_e = \Phi_0 + \omega\Phi_1 + \omega^2\Phi_2 + \mathcal{O}(\omega^3) \tag{3.18}$$

can be found for each of the effective coefficients (3.17). The matrix $\mathbf{E}$ [eq. (3.15)] containing the zeroth-order terms turns out to be a harmonic average of the matrices for each of the layers, exactly like a single Young's modulus for an elastic solid (also known as Wood's law):

$$\mathbf{E}_0^{-1} = \frac{l_I}{L}\mathbf{E}_I^{-1} + \frac{l_{II}}{L}\mathbf{E}_{II}^{-1}. \tag{3.19}$$

The analytical expressions for the first-order terms are quite big; they depend on the properties of both layers, including the viscous terms. Rather simple expressions can be obtained in the specific case of small inclusions, i.e., when $l_{II} << l_I$, using Taylor series in l_{II}. An expansion of the Gassmann modulus $\hat{H}_e = \hat{P}_e + 2\hat{Q}_e + \hat{R}_e$ around $\omega = 0$ reads:

$$\hat{H}_e = H_0 + \mathrm{i}\chi b_0^I l_{II}\omega. \tag{3.20}$$

Here, $H_0 = P_0 + 2Q_0 + R_0$, $b_0^I = (\eta\phi^2/k_0)^I$ is the Biot damping factor of the first layer, and the coefficient χ depends on elastic moduli and porosities of the layers and is not presented here explicitly because of its size.

The theory of Biot predicts the low-frequency attenuation of the fast compressional wave Q^{-1} to be proportional to permeability k_0 (Berryman, 1986). However, in media with mesoscopic heterogeneities the situation is different: the attenuation is inversely proportional to the permeability (Pride et al., 2003); this is confirmed for the current effective poroelastic model:

$$Q^{-1} = 2\left|\frac{\mathrm{Im}(\hat{H}_e)}{\mathrm{Re}(\hat{H}_e)}\right| = \frac{2\chi\omega\eta\phi^2 l_{II}}{H_0 k_0}. \tag{3.21}$$

Here, for reasons of comparison Q^{-1} is defined as in Pride et al. (2004) for their patchy saturation model; in the remainder of this chapter, a slightly different definition of Q^{-1} is adopted.

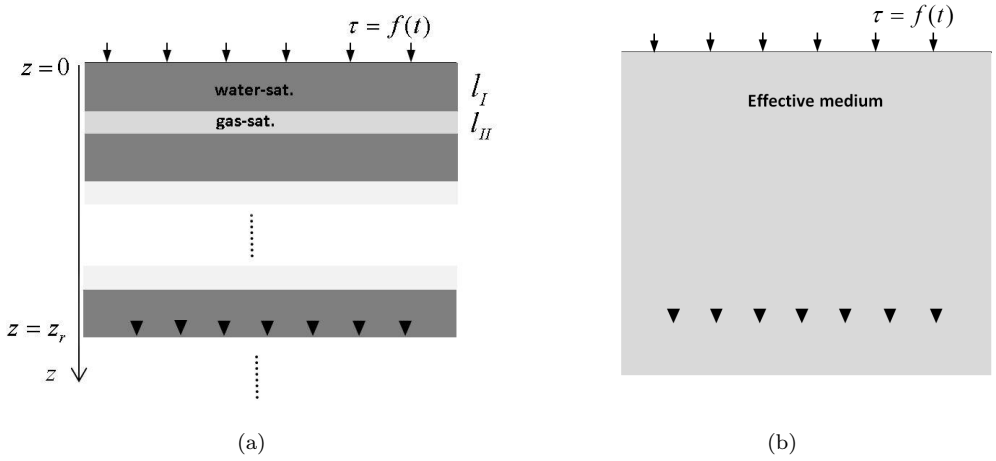

FIGURE 3.2: Geometry of a periodically stratified poroelastic solid (a) and its homogenized analogue (b)

3.4 Configuration and dynamic responses

The dynamic response predicted by the current effective poroelastic model is validated by an exact solution (Floquet's theory, Appendix 3.C) and compared with the response predicted by the effective viscoelastic model proposed by Vogelaar and Smeulders (2007); see next section. In this section, the specific configuration and excitation are given, as well as the derivation of the dynamic responses for different models.

3.4.1 Configuration

The configuration chosen for the simulations of wave propagation in different models is the typical case of partial saturation; it has been used in numerous studies, starting from White et al. (1975). Two different fluids fully saturate the poroelastic solid with the periodic zones in $z-$ direction, as depicted in Fig. 3.2(a). Fig. 3.2(b) depicts the effective homogenized medium that is described either with one single viscoelastic equation, or with the single set of Biot's poroelastic equations, both with the effective coefficients. The saturations of the fluids are $s_I = l_I/L$, $s_{II} = l_{II}/L$. The dry rock properties are the same for both layers, and they do not depend on depth z. This simple configuration allows to account for the effects of fluid flow specifically.

At the top interface $z = 0$ a stress as a function of time is applied. The pore pressure is assumed to be zero at $z = 0$ (free surface). Then, the boundary conditions at the top interface for the exact solution and for the effective poroelastic

model read

$$-\sigma|_{z=0} = f(t), \quad p|_{z=0} = 0. \tag{3.22}$$

For the viscoelastic model, there is only one boundary condition at the top interface, namely, the continuity of the solid stress τ:

$$\tau|_{z=0} = f(t). \tag{3.23}$$

As source function, the Ricker wavelet is chosen:

$$f(t) = f_0 \left(1 - 2\pi^2 f_R^2 (t - t_0)^2\right) \exp\left(-\pi^2 f_R^2 (t - t_0)^2\right). \tag{3.24}$$

Here, f_0 is a constant scaling coefficient with the dimension of stress (Pa), f_R is the central frequency of the wavelet and t_0 is an arbitrary time shift chosen such that the non-zero part of the wavelet lies within the positive domain $t > 0$; only the components that are very small are left in the domain $t < 0$. The dynamic responses of the media are compared far away from the source (in terms of wavelengths) in order to capture the attenuation effects, at a distance z_r below the source.

3.4.2 Exact solution

The exact solution for the periodically layered half-space is obtained with the use of Floquet's theory (Floquet, 1883). For elastic composites, the procedure has been implemented by Braga and Hermann (1992). For periodic poroelastic layering, Floquet's theory has been applied by Norris (1993), but the full solution is not present in that paper, as the author worked with low frequencies and only with the fast P-wave mode. In most cases of interest, the low-frequency solution suffices within the seismic frequency band. However, this is not always the case. In particular, when the Biot critical frequency is relatively small so that the assumption $\omega << \omega_B$ is violated in the seismic frequency band, the full solution is required. Examples are shown in the next section. The procedure of obtaining the exact solution, which contains two modes, in the frequency domain is given in Appendix 3.C. In the examples provided in the next section, this solution is used for validating the effective media at frequencies well below the stop and pass bands typical for periodic structures, because the effective media cannot be applied at higher frequencies where the assumption of the wavelength being much larger than the period is violated. Nevertheless, the exact solution is valid for any frequency.

3.4.3 Effective poroelastic model solution

The system of linear equations from Appendix 3.A is solved numerically (with the application of the standard function of IMSL library for Fortran) for each frequency. Then, the effective coefficients (3.17) are obtained. In order to find the response of the effective poroelastic model Biot's equations of motion are solved first in the frequency domain using the derived effective coefficients. Then the response in time domain is found by applying the inverse Fourier transform (3.7). The effective density of the fluid is taken as an arithmetic average: $\rho_f^e = s_I \rho_f^I + s_{II} \rho_f^{II}$. The effective frequency-dependent density terms (3.9) are also determined from arithmetic averages:

$$\hat{\rho}_{ij} = s_I \hat{\rho}_{ij}^I + s_{II} \hat{\rho}_{ij}^{II}. \tag{3.25}$$

This is consistent with taking $(\eta/\hat{k}_0)_e = s_I(\eta/\hat{k}_0)_I + s_{II}(\eta/\hat{k}_0)_{II}$ as the effective inverse fluid mobility that can be derived from Darcy's law applied to the elementary cell in Fig. 3.1; cf. Schoemaker (2011). Here, for the individual layers, the dynamic permeability $\hat{k}_0$ is defined as (Johnson et al., 1987):

$$\hat{k}_0 = k_0 \left(\sqrt{1 + \mathrm{i}\frac{\omega}{2\omega_B} M} + \mathrm{i}\frac{\omega}{\omega_B} \right)^{-1}. \tag{3.26}$$

We note that, in the limiting case of a homogeneous medium, this dynamic permeability results in the frequency-dependent damping term $\hat{b}$ given in (3.5), and thus in the density terms $\hat{\rho}_{ij}$ specified in (3.9).

The solution of Biot's equations with the effective coefficients is thus found in the form (3.11). The amplitudes of the up-going waves are zero due to the fact that there are no sources at infinity, and all the field variables should go to zero at infinity for a system with viscous damping (on account of the radiation condition). Thus, only two amplitudes of the exponential terms $\exp(-\mathrm{i}k_{P1}^e z)$ and $\exp(-\mathrm{i}k_{P2}^e z)$, where $k_{P1,P2}^e$ are the effective fast and slow compressional wavenumbers, respectively, and $\mathrm{Im}(k_{P1,P2}^e) < 0$, are to be found. The two boundary conditions (3.22) determine the system of linear equations with the unknown amplitudes $\hat{A}_3$ and $\hat{A}_4$:

$$\begin{aligned} &(\hat{Q}_e + \hat{R}_e \hat{\beta}_{P1}^e) k_{P1}^e \hat{A}_3 + (\hat{Q}_e + \hat{R}_e \hat{\beta}_{P2}^e) k_{P2}^e \hat{A}_4 = 0, \\ &\mathrm{i}(\hat{P}_e + \hat{Q}_e \hat{\beta}_{P1}^e) k_{P1}^e \hat{A}_3 + \mathrm{i}(\hat{P}_e + \hat{Q}_e \hat{\beta}_{P2}^e) k_{P2}^e \hat{A}_4 = \hat{f}(\omega), \end{aligned} \tag{3.27}$$

where $\hat{f}(\omega)$ is the Fourier transform of the wavelet (3.24). $\hat{A}_3$ and $\hat{A}_4$ are easily found from this system of equations:

$$\begin{aligned}\hat{A}_3 &= \frac{\mathrm{i}(\hat{Q}_e + \hat{R}_e\hat{\beta}^e_{P2})\hat{f}}{k^e_{P1}(\hat{P}_e\hat{R}_e - \hat{Q}^2_e)(\hat{\beta}^e_{P1} - \hat{\beta}^e_{P2})} \\ \hat{A}_4 &= -\frac{\mathrm{i}(\hat{Q}_e + \hat{R}_e\hat{\beta}^e_{P1})\hat{f}}{k^e_{P2}(\hat{P}_e\hat{R}_e - \hat{Q}^2_e)(\hat{\beta}^e_{P1} - \hat{\beta}^e_{P2})}.\end{aligned} \tag{3.28}$$

3.4.4 Effective viscoelastic model solution

Following Vogelaar and Smeulders (2007), the effective viscoelastic model defines the effective frequency-dependent bulk modulus $\hat{H}$. The wave propagation in the effective medium is described with the viscoelastic wave equation

$$-\rho\omega^2\hat{u} - \hat{H}\hat{u}_{,zz} = 0, \tag{3.29}$$

where the effective density ρ is an arithmetic average of the fluid and solid densities $\rho_f^{I,II}$ and $\rho_s^{I,II}$ in each of the layers, defined as

$$\rho = s_I\left((1-\phi)\rho_s^I + \phi\rho_f^I\right) + s_{II}\left((1-\phi)\rho_s^{II} + \phi\rho_f^{II}\right). \tag{3.30}$$

The solution of the equation (3.29) in the frequency domain can be found in the same way as for the poroelastic model. Only a down-going wave is allowed due to the same radiation condition:

$$\hat{u} = \hat{A}\exp(-\mathrm{i}kz), \qquad k = \omega\sqrt{\rho/\hat{H}}, \quad \mathrm{Im}(k) < 0. \tag{3.31}$$

The excitation is the same as in the poroelastic model. The amplitude $\hat{A}$ is found from the boundary condition (3.23) in the frequency domain:

$$\hat{\tau}|_{z=0} = \hat{f}(\omega) = \hat{H}\hat{u}_{,z}|_{z=0} = -\hat{H}\hat{A}\mathrm{i}k \qquad \Rightarrow \qquad \hat{A} = \frac{\mathrm{i}\hat{f}(\omega)}{\hat{H}k}. \tag{3.32}$$

3.5 Results

In this section, the results of simulations and comparison of the dynamic responses are presented. The sets of chosen material properties for the solid phase are given in Table 3.1. They represent a typical porous rock with stiff frame and high Biot

Parameter	Notation	Units	Rock	Sand 1	Sand 2	Sand 3	Sand 4
Density of solid grains	ρ_s	kg/m^3	2650	2650	2650	2690	2650
Bulk modulus of solid grains	K_s	GPa	40	36	36	32	40
Bulk modulus of frame	K_m	GPa	12.7	0.22	0.044	0.044	0.2
Porosity	ϕ	–	0.15	0.35	0.4	0.38	0.38
Permeability	k_0	m^2	10^{-13}	10^{-10}	10^{-10}	$2.5{\cdot}10^{-11}$	$6.49{\cdot}10^{-12}$
Shear modulus	μ	GPa	20.3	0.1	0.026	0.03	0.12
Tortuosity	α_∞	–	1	1.25	1.25	1.35	1.25
Biot critical frequency (100% water saturation)	$\frac{\omega_B}{2\pi}$	Hz	$2.4 \cdot 10^5$	446	509	1792	7514

TABLE 3.1: Sets of material properties chosen for simulations.

Parameter	Notation	Units	Water	Gas
Density	ρ_f	kg/m^3	1000	140
Bulk modulus	K_f	GPa	2.25	0.056
Viscosity	η	Pa $\cdot$ s	0.001	0.00022

TABLE 3.2: Mechanical properties of the sample pore fluids: water and gas.

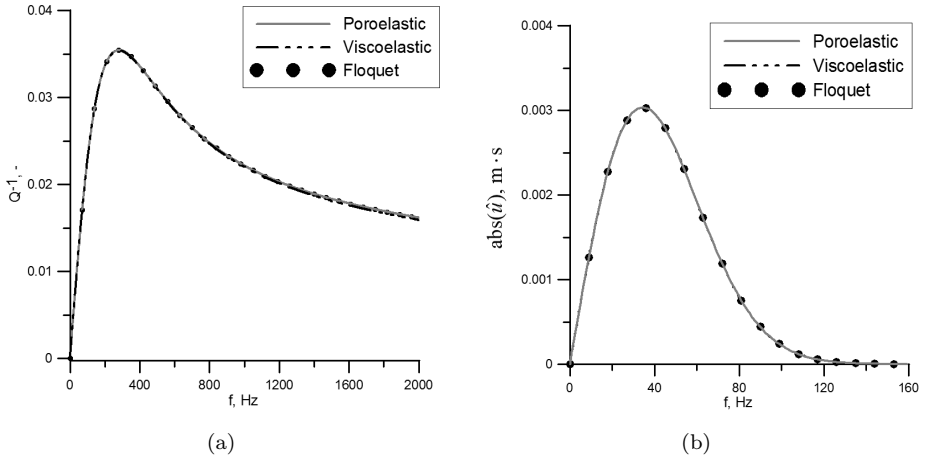

(a) (b)

FIGURE 3.3: Inverse quality factor Q^{-1} (a) and frequency spectrum of the transmission response $|\hat{u}|$ (b). Rock, L=0.1m, gas saturation 10%. On both plots all three lines coincide.

critical frequency (Rock), and a number of sands ranging from unconsolidated to weakly consolidated with much lower Biot critical frequency for which we expect different behavior of the effective poroelastic and viscoelastic models. The references for each of the sets are given in the text below. Pore fluid and gas properties are listed in Table 3.2. They are taken from Gelinsky and Shapiro (1997). The following parameters are chosen for the Ricker wavelet [eq. (3.24)]: $t_0 = 0.022$ s, $f_R = 50$ Hz, $f_0 = 1$ GPa. The position of the receiver is chosen at a distance $z_r = 10^3 \cdot L$ below the source.

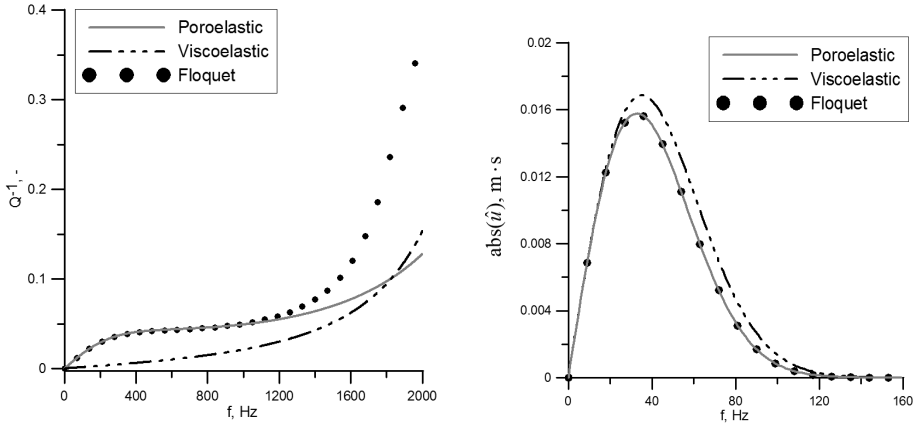

(a) (b)

FIGURE 3.4: Inverse quality factor Q^{-1} (a) and frequency spectrum of the transmission response $|\hat{u}|$ (b). Sand 1, L=0.1m, gas saturation 10%.

The first set of material properties from Table 3.1 (Rock) is taken from Gelinsky and Shapiro (1997). It is a porous rock with high Biot critical frequency (well outside the seismic range) and well consolidated. For a gas saturation of 10%, the inverse quality factor $Q^{-1} = 2\,|\mathrm{Im}(k^e_{P1})/\mathrm{Re}(k^e_{P1})|$ (where k^e_{P1} is the fast P-wave wavenumber) versus frequency $f = \omega/(2\pi)$ is depicted in Fig. 3.3(a). As one can see from the plot, the responses of the effective poro- and viscoelastic models (gray solid line and black dotted line, respectively) and the exact solution (black circles) almost coincide. In agreement with this prediction, we find that the magnitudes of the responses in the frequency domain (the absolute values of the solid particle displacement) of all three models coincide (see Fig. 3.3(b)).

Sand 1 from Table 3.1 is an example of coarse sand. It has much higher permeability than Rock and, as a consequence, much lower value of the Biot critical frequency that is of the same order as the frequency of excitation. The set of physical properties is taken from Turgut and Yamamoto (1990). Because of the lack of data of tortuosity for this sand, it is assumed to be the same as for Sand 2. As one can see in Fig. 3.4, the agreement between the attenuations and responses predicted by the models is violated for Sand 1. There is a large difference between the models in the predicted attenuations [Fig. 3.4(a)]. The poroelastic model predicts practically the same attenuation as the exact solution over a broad frequency range; deviations occur with increasing frequency, but that is expected because the associated wavelengths get smaller so that the effective model becomes inappropriate. However, the viscoelastic model significantly underestimates the attenuation at all frequencies where the effective-model approach is supposed to

be valid. As a result, the magnitude of the response of the viscoelastic model differs from that of the exact solution and the poroelastic model [Fig. 3.4(b)], while the latter two coincide. The low value of Biot critical frequency in case of Sand 1 implies that the frequency dependence of the visco-dynamic operator $\hat{b}$ that is contained in the effective densities (3.25) [cf. (3.9) for a homogeneous medium] starts to play a role, and that the macroscopic attenuation mechanism gives a non-negligible contribution to the damping of the propagating wave, which is not captured by the effective viscoelastic model. The latter model only captures the mesoscopic mechanism and does not allow fluid flow on the macroscopic scale due to the no-flow boundary conditions at the outer edges of the representative elementary cell.

One can notice that different frequency ranges are shown in the plots of the attenuations and responses. The frequency range in the plots of the responses corresponds to the width of the frequency spectrum of the excitation wavelet. Relatively low frequencies have been chosen for the excitation wavelet to demonstrate realistic responses of the different models at a certain depth (100 m). In principle, the difference between the predictions of the models varies with frequency, ratio of inhomogeneities (gas saturation) and distance from the source. The attenuation plots show the difference between the models at a broader frequency range and provide an insight into possible deviations in the magnitudes of the responses at higher frequencies. In most of the plots [Figs. 3.4(a), 3.5(a), 3.7(a), 3.8(a), 3.9(b)] the predictions of attenuations by the effective poroelastic model start to deviate from the predictions of the exact solution at higher frequencies. This is due to the violation of the effective medium approach: the wavelength of a propagating wave becomes shorter (compared to the period of the system).

The next example (Sand 2 from Table 3.1) is also a high-permeable material with low Biot critical frequency which has weaker frame than Sand 1. It is an unconsolidated sand sediment. This set of material properties is taken from Williams (2001) keeping only real parts of the bulk moduli. The inverse quality factor for gas saturation 10% is depicted in Fig. 3.5(a). The poroelastic model predicts the same attenuation as the exact solution at all frequencies of interest for the current configuration (where the effective medium approach is valid). The magnitudes of the responses for different saturations are depicted in Figs. 3.5(b), 3.6(a)–3.6(d). As one can notice, the difference in the magnitudes of the responses increases with the increase of gas saturation. Again, the viscoelastic model underestimates attenuation for all gas saturations, while the poroelastic model is in agreement

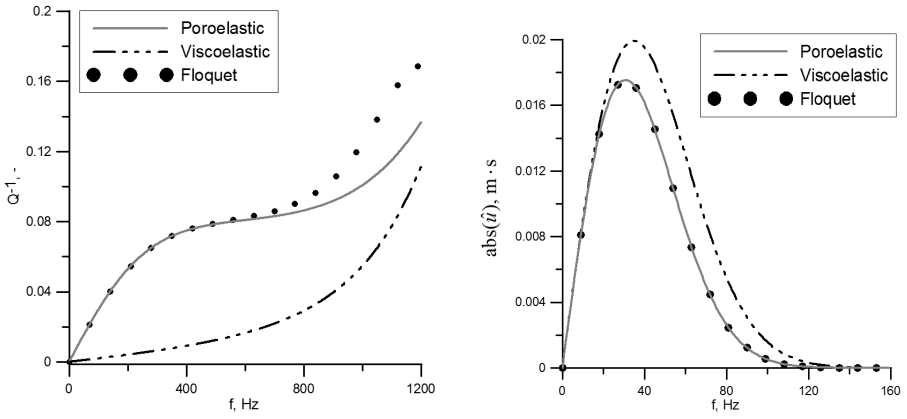

(a) (b)

FIGURE 3.5: Inverse quality factor Q^{-1} (a) and frequency spectrum of the transmission response $|\hat{u}|$ (b). Sand 2, L=0.1m, gas saturation 10%.

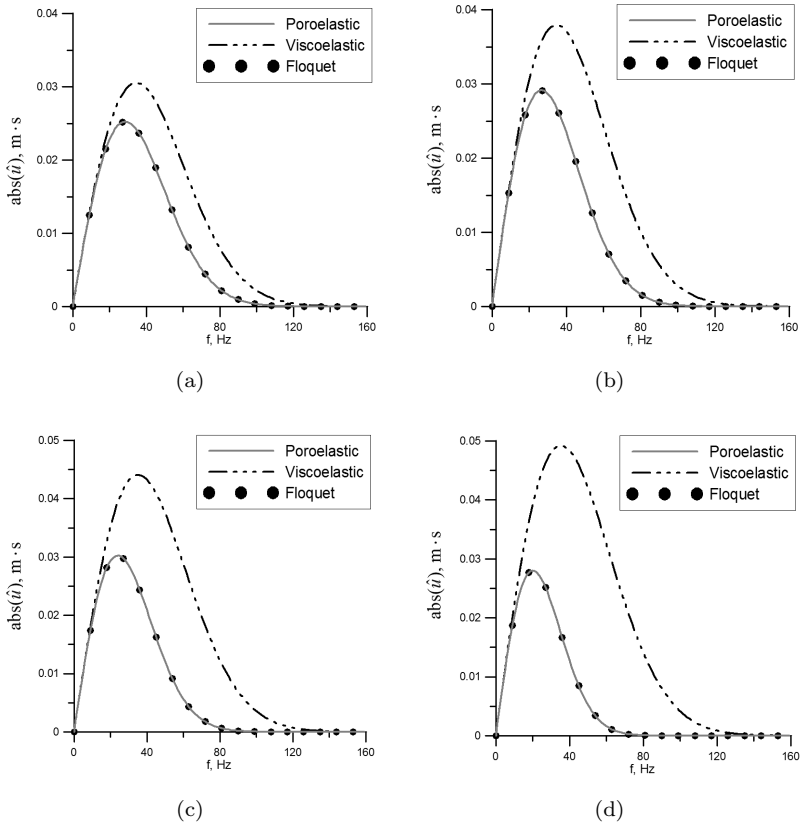

(a) (b)

(c) (d)

FIGURE 3.6: Frequency spectrum of the transmission response $|\hat{u}|$ for gas saturations (a) 30%; (b) 50%; (c) 70%; (d) 90%. Sand 2, L=0.1m.

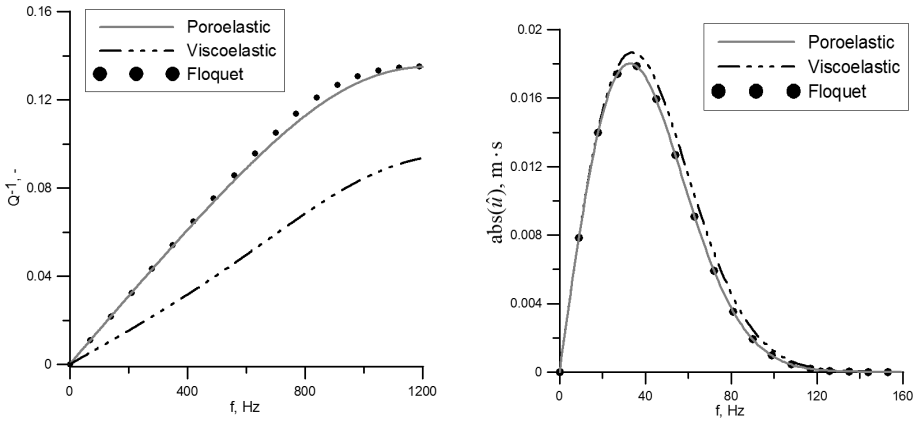

FIGURE 3.7: Inverse quality factor Q^{-1} (a) and frequency spectrum of the transmission response $|\hat{u}|$ (b). Sand 3, L=0.1m, gas saturation 10%.

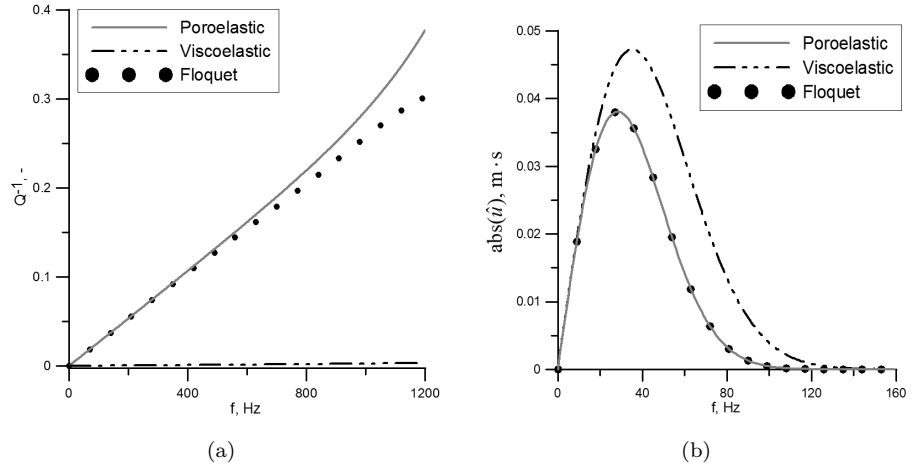

FIGURE 3.8: Inverse quality factor Q^{-1} (a) and frequency spectrum (b). Sand 3, L=0.1m, gas saturation 90%.

with the exact solution. The viscoelastic model underestimates the attenuation by almost a factor two for high gas saturation [Fig. 3.6(d)].

Sand 3 has been chosen as an example of a weakly consolidated material with lower permeability and higher Biot critical frequency than in the previous examples of sands. This set of material properties has been taken from Hefner and Jackson (2010). The parameters of this sand are referred to as SAX99 in the mentioned paper; they were obtained during the sediment acoustics experiment in 1999. The predicted attenuations for gas saturations of 10% and 90% are depicted in Figs. 3.7(a) and 3.8(a), respectively. As in the previous examples, the poroelastic model predicts practically the same attenuation as the exact solution, and the

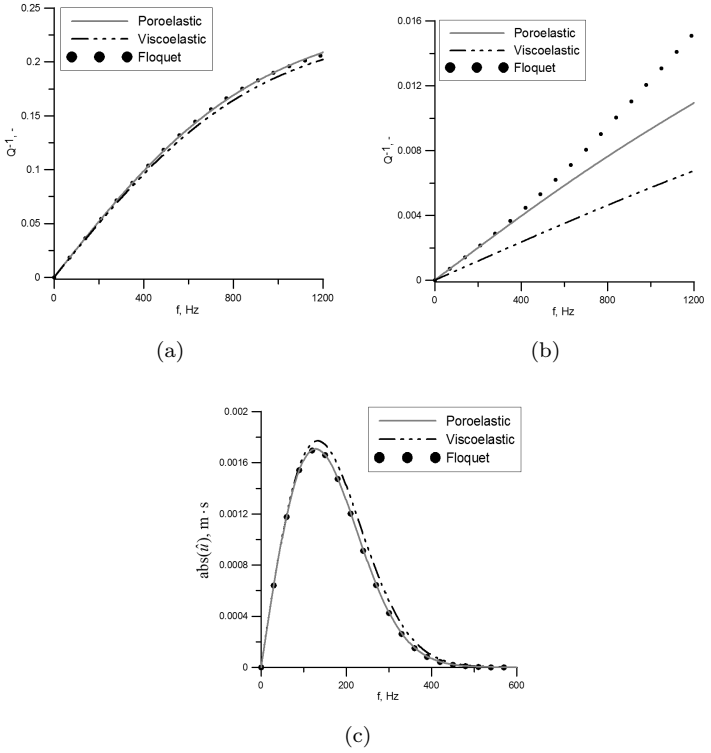

FIGURE 3.9: Inverse quality factor Q^{-1} for gas saturation 10% (a) and for gas saturation 90% (b); frequency spectrum for gas saturation 90% (c). Sand 4, L=0.1m,

viscoelastic model significantly underestimates the attenuation. The difference in the magnitude of the responses for gas saturation 10% [Fig. 3.7(b)] is not as large as for Sand 2 [Fig. 3.5(b)], but it also increases with the increase of gas saturation [Fig. 3.8(b)].

As can be concluded based on the examples shown above, the differences in predictions of the models become less pronounced with the decrease of permeability (increase of Biot critical frequency; cf. Sands 2 and 3) and increase of bulk and shear moduli of the frame (for materials with equal permeability, cf. examples Sand 1 and Sand 2). This observation is confirmed by the results for Sand 4 (see Fig. 3.9) that has even lower permeability than Sand 3 and stiffer frame. This set of material properties has been taken from Chotiros (1995), where it is referred to as Ottawa sand. As in the previous examples, the difference between the models is more pronounced for higher gas saturations. The inverse quality factor for saturation 10% is depicted in Fig. 3.9(a). The poroelastic model and the exact solution are in agreement; the viscoelastic model slightly underestimates the attenuation with increasing frequency. However, this would hardly affect the magnitude of the

responses for the chosen configuration (the corresponding plot is left out). The difference between all three models is significant for a gas saturation of 90% [Fig. 3.9(b)]. At low frequencies the poroelastic model still gives the same result as the exact solution, while the viscoelastic model predicts less attenuation. At higher frequencies, where the effective medium approach is violated, all solutions give different results. Still, the prediction of the poroelastic model is closer to the exact solution than that of the viscoelastic model. The response in the frequency domain for a gas saturation of 90% is depicted in Fig. 3.9(c). A higher central frequency (200 Hz) of the Ricker wavelet is taken for this example in order to distinguish differences between the responses. As can be expected based on the attenuation plot, the viscoelastic model overestimates the magnitude of the response. The results for Sand 4 show that the viscoelastic model can still be less accurate for materials with Biot critical frequency much higher than the frequency of excitation, but this inaccuracy has a much less pronounced effect on the magnitude of the responses in the frequency range of interest for seismic applications. For materials with much higher Biot critical frequency and stiffer frame, like Rock from the first example, both effective viscoelastic and poroelastic models are in agreement with each other and the exact solution.

3.6 Discussion

The use of an effective medium requires that the involved wavelengths are much larger than the period L of the medium. The weak point of the current effective poroelastic model is that the wavelength of the slow P-wave can be very small (i.e., of the order of the period of the system or even smaller), which thus violates the requirement. However, this inconsistency hardly affects the response of the effective poroelastic medium as the contribution of the slow P-wave to the total response is generally very small at seismic frequencies. Possibly superior approaches of homogenization that circumvent the inconsistency exist, but the present analysis shows that the choice of the pressure continuity condition in (3.13) at the edge of the representative elementary cell, rather than the no-flow condition, can be important for the behavior of the effective model. The no-flow boundary condition is in fact quite restrictive as it excludes the macroscopic attenuation mechanism from the effective model (see also Sections 3.1 and 3.5). This restriction is thus circumvented by applying the pressure continuity condition suggested by Dutta and Ode (1979a), and this is particularly important when dealing with high permeable

materials such as weak sandstones, unconsolidated and weakly consolidated sandy sediments. The effective poroelastic model, or the exact solution, should be used when the signal frequency is of the same order as the Biot critical frequency. The predictions of the effective viscoelastic model are also less accurate for materials with weak frame.

3.7 Conclusions

The effective viscoelastic model of White, which consists of a homogeneous porous frame saturated by gas and fluid layers that are organized in a periodic way, has been the starting point of many studies in the research on wave attenuation in partially saturated media (i.e., media having gas inclusions). The model describes wave propagation in the direction normal to the layering and employs the so-called no-flow boundary condition at the outer edges of the representative elementary cell of the effective medium. In this chapter we derived an effective medium for the same configuration, but employed the pressure continuity condition rather than the no-flow condition, as suggested by Dutta and Ode (1979a). This choice leads to an effective poroelastic model that has two degrees of freedom, the frame and fluid displacements, and that allows the existence of both the fast and slow compressional waves. We derived frequency-dependent effective poroelastic parameters as well as their low-frequency approximations. The numerical results show that the frequency-dependent attenuation of the fast compressional wave and the transient point-source response are in agreement with the exact solution obtained using Floquet's theory, both for materials with stiff and weak frames, and for materials with high and low Biot critical frequency. For materials with weak frame, the predictions of White's model are less accurate. In the case of low Biot critical frequency, White's effective viscoelastic model fails as it does not incorporate Biot's wavelength-scale attenuation mechanism. This mechanism is, however, captured by the current effective poroelastic model due to the application of the pressure continuity condition that allows relative fluid-to-solid motion at the outer edges of the representative element, and consequently on the wavelength scale. We expect that the analysis in this chapter has consequences for the applicability of the other models that employ the no-flow boundary conditions, particularly for wave propagation through relatively high permeable (low Biot critical frequency) materials and materials with weak frame. For well-consolidated materials with stiff frame and with Biot critical frequency much higher than the signal frequency, the

newly introduced model is in agreement with the previously introduced viscoelastic model and the exact solution.

3.A Matrix of coefficients

In this appendix the coefficients of the system of linear algebraic equations $\mathbf{Ax} = \mathbf{B}$ that follow from the boundary conditions (3.13) are written out. $\mathbf{A}$ is the 8×8 matrix of the coefficients, $\mathbf{x}$ is a vector of unknown amplitudes $\hat{A}_i^{I,II}$:

$$\mathbf{x} = [\hat{A}_1^I \quad \hat{A}_2^I \quad \hat{A}_3^I \quad \hat{A}_4^I \quad \hat{A}_1^{II} \quad \hat{A}_2^{II} \quad \hat{A}_3^{II} \quad \hat{A}_4^{II}]^{\mathrm{T}}. \tag{3.33}$$

The amplitudes $\hat{A}_i^{I,II}$ are the amplitudes of the displacements $\hat{u}_{I,II}$, $\hat{U}_{I,II}$:

$$\begin{aligned}
\hat{u}_{I,II} &= \hat{A}_1^{I,II} \mathrm{e}^{\mathrm{i}k_{P1}^{I,II} z} + \hat{A}_2^{I,II} \mathrm{e}^{\mathrm{i}k_{P2}^{I,II} z} + \hat{A}_3^{I,II} \mathrm{e}^{-\mathrm{i}k_{P1}^{I,II} z} + \hat{A}_4^{I,II} \mathrm{e}^{-\mathrm{i}k_{P2}^{I,II} z}, \\
\hat{U}_{I,II} &= \hat{\beta}_{P1}^{I,II} \hat{A}_1^{I,II} \mathrm{e}^{\mathrm{i}k_{P1}^{I,II} z} + \hat{\beta}_{P1}^{I,II} \hat{A}_2^{I,II} \mathrm{e}^{\mathrm{i}k_{P2}^{I,II} z} + \hat{\beta}_{P2}^{I,II} \hat{A}_3^{I,II} \mathrm{e}^{-\mathrm{i}k_{P1}^{I,II} z} + \hat{\beta}_{P2}^{I,II} \hat{A}_4^{I,II} \mathrm{e}^{-\mathrm{i}k_{P2}^{I,II} z}.
\end{aligned} \tag{3.34}$$

$\mathbf{B}$ is a vector containing the right-hand side of the system:

$$\mathbf{B} = [\hat{\sigma} \quad \hat{p} \quad \hat{\sigma} \quad \hat{p} \quad 0 \quad 0 \quad 0 \quad 0]^{\mathrm{T}}. \tag{3.35}$$

The coefficients A_{ij} of the matrix $\mathbf{A}$ read:

$$\begin{aligned}
A_{11} &= \mathrm{i}k_{P1}^I (Q_I - \phi_I (P_I + Q_I) + (R_I - \phi_I (Q_I + R_I)) \hat{\beta}_{P1}^I) \exp(-\mathrm{i}k_{P1}^I l_I)/\phi_I, \\
A_{12} &= \mathrm{i}k_{P2}^I (Q_I - \phi_I (P_I + Q_I) + (R_I - \phi_I (Q_I + R_I)) \hat{\beta}_{P2}^I) \exp(-\mathrm{i}k_{P2}^I l_I)/\phi_I, \\
A_{13} &= -\mathrm{i}k_{P1}^I (Q_I - \phi_I (P_I + Q_I) + (R_I - \phi_I (Q_I + R_I)) \hat{\beta}_{P1}^I) \exp(\mathrm{i}k_{P1}^I l_I)/\phi_I, \\
A_{14} &= -\mathrm{i}k_{P2}^I (Q_I - \phi_I (P_I + Q_I) + (R_I - \phi_I (Q_I + R_I)) \hat{\beta}_{P2}^I) \exp(\mathrm{i}k_{P2}^I l_I)/\phi_I, \\
A_{15} &= A_{16} = A_{17} = A_{18} = 0.
\end{aligned} \tag{3.36}$$

$$
\begin{aligned}
A_{21} &= -\mathrm{i}k^I_{P1}(Q_I + R_I\hat{\beta}^I_{P1})\exp(-\mathrm{i}k^I_{P1}l_I)/\phi_I,\\
A_{22} &= -\mathrm{i}k^I_{P2}(Q_I + R_I\hat{\beta}^I_{P2})\exp(-\mathrm{i}k^I_{P2}l_I)/\phi_I,\\
A_{23} &= \mathrm{i}k^I_{P1}(Q_I + R_I\hat{\beta}^I_{P1})\exp(\mathrm{i}k^I_{P1}l_I)/\phi_I,\\
A_{24} &= \mathrm{i}k^I_{P2}(Q_I + R_I\hat{\beta}^I_{P2})\exp(\mathrm{i}k^I_{P2}l_I)/\phi_I,\\
A_{25} &= A_{26} = A_{27} = A_{28} = 0.
\end{aligned}
\tag{3.37}
$$

$$
\begin{aligned}
&A_{31} = A_{32} = A_{33} = A_{34} = 0,\\
&A_{35} = \mathrm{i}k^{II}_{P1}(Q_{II} - \phi_{II}(P_{II} + Q_{II}) + (R_{II} - \phi_{II}(Q_{II} + R_{II}))\hat{\beta}^{II}_{P1})\exp(\mathrm{i}k^{II}_{P1}l_{II})/\phi_{II},\\
&A_{36} = \mathrm{i}k^{II}_{P2}(Q_{II} - \phi_{II}(P_{II} + Q_{II}) + (R_{II} - \phi_{II}(Q_{II} + R_{II}))\hat{\beta}^{II}_{P2})\exp(\mathrm{i}k^{II}_{P2}l_{II})/\phi_{II},\\
&A_{37} = -\mathrm{i}k^{II}_{P1}(Q_{II} - \phi_{II}(P_{II} + Q_{II}) + (R_{II} - \phi_{II}(Q_{II} + R_{II}))\hat{\beta}^{II}_{P1})\exp(-\mathrm{i}k^{II}_{P1}l_{II})/\phi_{II},\\
&A_{38} = -\mathrm{i}k^{II}_{P2}(Q_{II} - \phi_{II}(P_{II} + Q_{II}) + (R_{II} - \phi_{II}(Q_{II} + R_{II}))\hat{\beta}^{II}_{P2})\exp(-\mathrm{i}k^{II}_{P2}l_{II})/\phi_{II}.
\end{aligned}
\tag{3.38}
$$

$$
\begin{aligned}
A_{41} &= A_{42} = A_{43} = A_{44} = 0,\\
A_{45} &= -\mathrm{i}k^{II}_{P1}(Q_{II} + R_{II}\hat{\beta}^{II}_{P1})\exp(\mathrm{i}k^{II}_{P1}l_{II})/\phi_{II},\\
A_{46} &= -\mathrm{i}k^{II}_{P2}(Q_{II} + R_{II}\hat{\beta}^{II}_{P2})\exp(\mathrm{i}k^{II}_{P2}l_{II})/\phi_{II},\\
A_{47} &= \mathrm{i}k^{II}_{P1}(Q_{II} + R_{II}\hat{\beta}^{II}_{P1})\exp(-\mathrm{i}k^{II}_{P1}l_{II})/\phi_{II},\\
A_{48} &= \mathrm{i}k^{II}_{P2}(Q_{II} + R_{II}\hat{\beta}^{II}_{P2})\exp(-\mathrm{i}k^{II}_{P2}l_{II})/\phi_{II}.
\end{aligned}
\tag{3.39}
$$

$$
\begin{aligned}
A_{51} &= A_{53} = \phi_I(1 - \hat{\beta}^I_{P1}),\\
A_{52} &= A_{54} = \phi_I(1 - \hat{\beta}^I_{P2}),\\
A_{55} &= A_{57} = -\phi_{II}(1 - \hat{\beta}^{II}_{P1}),\\
A_{56} &= A_{58} = -\phi_{II}(1 - \hat{\beta}^{II}_{P2}).
\end{aligned}
\tag{3.40}
$$

$$
\begin{aligned}
A_{61} &= A_{62} = A_{63} = A_{64} = 1,\\
A_{65} &= A_{66} = A_{67} = A_{68} = -1.
\end{aligned}
\tag{3.41}
$$

$$
\begin{aligned}
A_{71} &= -A_{73} = -\mathrm{i}k^I_{P1}(Q_I + R_I\hat{\beta}^I_{P1})/\phi_I,\\
A_{72} &= -A_{74} = -\mathrm{i}k^I_{P2}(Q_I + R_I\hat{\beta}^I_{P2})/\phi_I,\\
A_{75} &= -A_{77} = \mathrm{i}k^{II}_{P1}(Q_{II} + R_{II}\hat{\beta}^{II}_{P1})/\phi_{II},\\
A_{76} &= -A_{78} = \mathrm{i}k^{II}_{P2}(Q_{II} + R_{II}\hat{\beta}^{II}_{P2})/\phi_{II}.
\end{aligned}
\tag{3.42}
$$

$$
\begin{aligned}
A_{81} &= -A_{83} = \mathrm{i}k^I_{P1}(Q_I - \phi_I(P_I + Q_I) + (R_I - \phi_I(Q_I + R_I))\hat{\beta}^I_{P1}),\\
A_{82} &= -A_{84} = \mathrm{i}k^I_{P2}(Q_I - \phi_I(P_I + Q_I) + (R_I - \phi_I(Q_I + R_I))\hat{\beta}^I_{P2}),\\
A_{85} &= -A_{87} = -\mathrm{i}k^{II}_{P1}(Q_{II} - \phi_{II}(P_{II} + Q_{II}) + (R_{II} - \phi_{II}(Q_{II} + R_{II}))\hat{\beta}^{II}_{P1}),\\
A_{86} &= -A_{88} = -\mathrm{i}k^{II}_{P2}(Q_{II} - \phi_{II}(P_{II} + Q_{II}) + (R_{II} - \phi_{II}(Q_{II} + R_{II}))\hat{\beta}^{II}_{P2}).
\end{aligned}
\tag{3.43}
$$

3.B Low-frequency approximation of the effective coefficients

In this appendix a perturbation approach is presented which is used to derive the low-frequency approximations (3.18) of the effective coefficients (3.17). For this purpose, the displacement fields are expanded in the Taylor series:

$$
\begin{aligned}
\hat{u} &= u_0 + \omega u_1 + \omega^2 u_2 + \mathcal{O}(\omega^3),\\
\hat{U} &= U_0 + \omega U_1 + \omega^2 U_2 + \mathcal{O}(\omega^3).
\end{aligned}
\tag{3.44}
$$

The visco-dynamic operator $\hat{b}$ contained in the density terms $\hat{\rho}_{ij}$ is also expanded in a series of ω:

$$
\hat{b} = b_0\sqrt{1 + \mathrm{i}\frac{\omega}{2\omega_B}} = b_0\left(1 + \frac{\mathrm{i}\omega}{4\omega_B} + \frac{\omega^2}{32\omega_B^2} + \mathcal{O}(\omega^3)\right). \tag{3.45}
$$

These expansions are substituted into Biot's equations in the frequency domain. Then the equations are solved for each power of ω with the boundary conditions (3.13). The strains of the elementary cell are found as linear combinations of $\hat{\sigma}$ and $\hat{p}$, as before [eq. (3.16)], but now the analytical expressions for the low-frequency

terms of the coefficients α_1 to α_4 can be obtained:

$$\begin{aligned}\frac{\hat{u}(l_{II}) - \hat{u}(-l_I)}{L} &= (a_{10} + \omega a_{11} + \omega^2 a_{12} + ...)\hat{\sigma} + (a_{20} + \omega a_{21} + \omega^2 a_{22} + ...)\hat{p},\\ \frac{\hat{U}(l_{II}) - \hat{U}(-l_I)}{L} &= (a_{20} + \omega a_{21} + \omega^2 a_{22} + ...)\hat{\sigma} + (a_{40} + \omega a_{41} + \omega^2 a_{42} + ...)\hat{p}.\end{aligned} \tag{3.46}$$

All the coefficients a_{ij} are independent of frequency, but do depend on the properties of both layers, and can be found analytically. Then the terms of the expansions of the effective coefficients [eq. (3.18)] can be obtained analytically as combinations of the coefficients a_{ij}. The explicit expressions are not presented here for reasons of brevity. They can be derived with the use of any symbolic software.

3.C Floquet solution

In this appendix the exact solution for a periodically layered porous half-space with excitation at the top (see Fig. 2a) is derived by the use of Floquet's theory (Floquet, 1883). The derivation is similar to that given in Braga and Hermann (1992) for an elastic layered composite.

The equations of motion and stress-strain relations (3.1) – (3.3) can be rewritten in the space-frequency domain into a linear differential equation of the first order in the following matrix form:

$$\frac{\partial \hat{\mathbf{f}}(z)}{\partial z} = \mathrm{i}\hat{\mathbf{N}}(z)\hat{\mathbf{f}}(z), \tag{3.47}$$

where $\hat{\mathbf{f}} = [\mathrm{i}\omega\hat{u}, \mathrm{i}\omega\hat{w}, \hat{\sigma}, \hat{p}]$ is a vector containing field variables, namely, solid particle velocity, relative velocity, intergranular stress and pore pressure. All the elements of this vector are continuous at the interfaces between the layers (Deresiewicz and Skalak, 1963). $\hat{\mathbf{N}}$ is a 4×4 matrix of coefficients that describe the

material properties:

$$\hat{\mathbf{N}} = \begin{bmatrix} \mathbf{0} & \mathbf{N}^a \\ \hat{\mathbf{N}}^b & \mathbf{0} \end{bmatrix},$$
$$\mathbf{N}^a = \frac{1}{PR - Q^2} \begin{bmatrix} -R & \phi(R+Q) - R \\ \phi(Q+R) & \phi(Q+R) - \phi^2(P+2Q+R) \end{bmatrix}, \tag{3.48}$$
$$\hat{\mathbf{N}}^b = \frac{\omega^2}{\phi} \begin{bmatrix} \hat{\rho}_{12}(1-2\phi) + \hat{\rho}_{22}(1-\phi) - \phi\hat{\rho}_{11} & (\hat{\rho}_{22}(1-\phi) - \phi\hat{\rho}_{12})/\phi \\ -(\hat{\rho}_{12} + \hat{\rho}_{22}) & -\hat{\rho}_{22}/\phi \end{bmatrix}.$$

The elements of the matrix $\hat{\mathbf{N}}$ are piecewise constant functions of the coordinate z, they are constant inside each layer and periodic with the period $L = l_I + l_{II}$. Thus, equation (3.47) is a system of four linear differential equations with a periodic matrix of coefficients. Its solution can be expressed via the fundamental matrix of solutions $\hat{\mathbf{X}}$:

$$\hat{\mathbf{f}}(z) = \hat{\mathbf{X}}(z)\mathbf{c}, \tag{3.49}$$

where $\mathbf{c}$ is a column of constants to be found from the boundary conditions. According to Floquet's theory, the matrix $\hat{\mathbf{X}}(z)$ can be found in the form

$$\hat{\mathbf{X}}(z) = \hat{\mathbf{F}}(z)\exp(\mathrm{i}\hat{\mathbf{A}}z), \tag{3.50}$$

where $\hat{\mathbf{F}}(z+L) = \hat{\mathbf{F}}(z)$ is a yet unknown periodic matrix and matrix $\hat{\mathbf{A}}$ is constant (with respect to z).

First, the matrix $\hat{\mathbf{A}}$ has to be found. In each of the layers $k = 1, 2$ the solution of equation (3.47) is

$$\hat{\mathbf{f}}_k(z) = \hat{\mathbf{M}}_k(z)\hat{\mathbf{f}}_k(0), \tag{3.51}$$

where $\hat{\mathbf{M}}_k(z) = \exp(\mathrm{i}\hat{\mathbf{N}}_k z)$ and $\hat{\mathbf{M}}_k(0) = \mathbf{I}$, where $\mathbf{I}$ is the identity matrix. Summation converntion does not apply here. By analogy, the solution of equations (3.47) for the stack of periodic layers can be expressed in the same manner:

$$\hat{\mathbf{f}}(z) = \hat{\mathbf{P}}(z)\hat{\mathbf{f}}(0). \tag{3.52}$$

It follows from (3.52) that $\hat{\mathbf{P}}(0) = \mathbf{I}$. The solution $\hat{\mathbf{f}}(z)$ can be also expressed via the fundamental matrix (3.50) as

$$\hat{\mathbf{f}}(z) = \hat{\mathbf{F}}(z)\exp(\mathrm{i}\hat{\mathbf{A}}z)\hat{\mathbf{f}}(0). \tag{3.53}$$

Then, the periodic matrix $\hat{\mathbf{F}}(L) = \hat{\mathbf{F}}(0) = \mathbf{I}$ and $\hat{\mathbf{P}}(L) = \exp(\mathrm{i}\hat{\mathbf{A}}L)$. On the other hand, using (3.51), the vector $\hat{\mathbf{f}}(L)$ can be expressed as

$$\hat{\mathbf{f}}(L) = \hat{\mathbf{M}}_2(l_{II})\hat{\mathbf{M}}_1(l_I)\hat{\mathbf{f}}(0). \tag{3.54}$$

Thus, the matrix $\mathbf{A}$ can be found from the following exponential relations:

$$\hat{\mathbf{P}}(L) = \exp(\mathrm{i}\hat{\mathbf{A}}L) = \exp(\mathrm{i}\hat{\mathbf{N}}_2 l_{II})\exp(\mathrm{i}\hat{\mathbf{N}}_1 l_I). \tag{3.55}$$

The eigenvalues k_i^F of the matrix $\hat{\mathbf{A}}$ are the so-called Floquet wavenumbers. They are exponentially related to the eigenvalues τ_i of the matrix $\exp(\mathrm{i}\hat{\mathbf{A}}L)$: $\tau_i = \exp(\mathrm{i}k_i^F L)$.

Next, the periodic function $\hat{\mathbf{F}}(z)$ is determined. First, the local coordinate z_n is introduced:

$$z_n = z - (n-1)L, \qquad 0 \le z_n \le L, \qquad n = 1, 2, ... \tag{3.56}$$

The following equalities hold true (cf. (3.52) and (3.53)):

$$\begin{aligned}\hat{\mathbf{P}}(z) = \hat{\mathbf{F}}(z)\exp(\mathrm{i}\hat{\mathbf{A}}z) = \hat{\mathbf{F}}(z_n)\exp(\mathrm{i}\hat{\mathbf{A}}z_n)\exp(\mathrm{i}\hat{\mathbf{A}}L(n-1)) = \\ \hat{\mathbf{P}}(z_n)\exp(\mathrm{i}\hat{\mathbf{A}}L(n-1)).\end{aligned} \tag{3.57}$$

After right-multiplying (3.57) by $\exp(-\mathrm{i}\mathbf{A}z)$ one recognizes

$$\hat{\mathbf{F}}(z) = \hat{\mathbf{P}}(z_n)\exp(-\mathrm{i}\hat{\mathbf{A}}z_n). \tag{3.58}$$

The matrix $\hat{\mathbf{P}}(z_n)$ is the propagator matrix at a distance z_n from the interface between the unit cells $(n-1)$ and n. From (3.51) and (3.52) it can be concluded that

$$\hat{\mathbf{P}}(z_n) = \begin{cases} \hat{\mathbf{M}}_1(z_n), & 0 \le z_n \le l_I; \\ \hat{\mathbf{M}}_2(z_n - l_I)\hat{\mathbf{M}}_1(l_I), & l_I \le z_n \le L. \end{cases} \tag{3.59}$$

Hence, the periodic matrix $\hat{\mathbf{F}}(z)$ is determined.

Finally, the solution for a periodically layered system, with a unit cell consisting of two layers, is found in the space-frequency domain. By combining (3.53), (3.56) and (3.58) the solution $\hat{\mathbf{f}}(z)$ is expressed in the following way:

$$\hat{\mathbf{f}}(z) = \hat{\mathbf{F}}(z)\exp(\mathrm{i}\hat{\mathbf{A}}z)\hat{\mathbf{f}}(0) = \hat{\mathbf{P}}(z_n)\exp(\mathrm{i}\hat{\mathbf{A}}L(n-1))\hat{\mathbf{f}}(0). \tag{3.60}$$

The next step towards the calculation of the field variables contained in $\hat{\mathbf{f}}$ is to find the four unknowns $\hat{\mathbf{f}}(0)$. The displacement field in the first layer $0 \le z \le l_I$ is simply a solution of Biot's equations (3.11). Then the vector $\hat{\mathbf{f}}(0)$ can be expressed as a product of a matrix of coefficients and a column of unknown amplitudes $\hat{A}_1$ to $\hat{A}_4$:

$$\hat{\mathbf{f}}(0) = \begin{bmatrix} \mathrm{i}\omega & \mathrm{i}\omega & \mathrm{i}\omega & \mathrm{i}\omega \\ \mathrm{i}\omega\phi_I(\hat{\beta}^I_{P1}-1) & \mathrm{i}\omega\phi_I(\hat{\beta}^I_{P2}-1) & \mathrm{i}\omega\phi_I(\hat{\beta}^I_{P1}-1) & \mathrm{i}\omega\phi_I(\hat{\beta}^I_{P2}-1) \\ g_{P1} & g_{P2} & -g_{P1} & -g_{P2} \\ h_{P1} & h_{P2} & -h_{P1} & -h_{P2} \end{bmatrix} \begin{bmatrix} \hat{A}_1 \\ \hat{A}_2 \\ \hat{A}_3 \\ \hat{A}_4 \end{bmatrix}, \tag{3.61}$$

where

$$\begin{aligned} g_{P1,P2} &= \frac{-\mathrm{i}k^I_{P1,P2}}{\phi_I}\left(\phi_I P_I - Q_I + \phi_I Q_I + \hat{\beta}^I_{P1,P2}(\phi_I R_I + \phi_I Q_I - R_I)\right), \\ h_{P1,P2} &= \frac{-\mathrm{i}k^I_{P1,P2}}{\phi_I}\left(Q_I + \hat{\beta}^I_{P1,P2} R_I\right). \end{aligned} \tag{3.62}$$

There are four equations to determine the four complex-valued amplitudes $\hat{A}_i$. The first two equations come from the boundary conditions at the top interface (3.22) that assign the values for the third and the fourth components of the vector $\hat{\mathbf{f}}$. The second two come from the elimination of the up-going Floquet waves in the solution (3.60): as there are no sources of energy at any place below the top of the half-space $z = 0$, the field variables (like displacements) should tend to zero when $z \to \infty$ (not to some finite value due to the presence of viscous damping in the system). Thus, the coefficients of the exponential terms in (3.60) that correspond to the up-going Floquet waves (there are two of them, the slow and the fast P waves) should be zeros, and these conditions provide another two equations to solve for the unknown amplitudes.

Chapter 4

Effective model for wave propagation in porous media with spherical inclusions

In this chapter an effective model is proposed to describe dispersion and attenuation in porous media with heterogeneities distributed as periodic spherical inclusions. Both host medium and the inclusion are fully-saturated poroelastic solids, with different physical properties. This model is an extension of White's original model to a two-phase effective poroelastic medium governed by Biot's equations with frequency-dependent coefficients that describe the mesoscopic-scale attenuation mechanism. In addition, Biot's global-flow attenuation is also captured by the proposed effective model, contrary to White's model. The attenuation and dispersion predicted by both models are compared. It is shown that the new model is advantageous for highly permeable and weak-frame media where Biot's global-flow mechanism is not negligible.

4.1 Introduction

Mesoscopic-scale heterogeneities (i.e., those larger than the pore and grain sizes but smaller than the wavelength), cause significant attenuation of seismic waves in porous media. Heterogeneities can occur in fluid or frame properties. It is

The results discussed in this chapter were presented at 74th SEG Annual Meeting, Denver, USA, October 26-31, 2014

widely believed that wave-induced fluid flow is the dominant mechanism of seismic attenuation in these cases; a passing wave induces a pressure gradient on the sub-wavelength scale and drives the so-called mesoscopic flow (Müller and Gurevich, 2005, Müller et al., 2010). Effective-medium approaches are widely used to model mesoscopic-scale effects in heterogeneous systems; it saves computational time. Moreover, the effective moduli can provide insight into the sensitivity of the wave propagation to the changes in medium parameters.

The patchy-saturation models of White et al. (1975) and White (1975) provide low-frequency approximations of the effective P-wave moduli for periodically layered media and media with a periodic distribution of spherical inclusions, respectively. In both cases, the significance of the wave attenuation due to inhomogeneities in the fluid content is emphasized. The models and their variations have been used in numerous studies (Dutta and Ode, 1979a, Johnson, 2001, Carcione et al., 2003, Carcione and Picotti, 2006, Vogelaar and Smeulders, 2007, Vogelaar et al., 2010, Zhang et al., 2014). This class of models describe, in fact, effective one-phase media; they do not account explicitly (i.e., on the macroscale) for the existence of the slow P-wave and relative fluid-solid motion. In addition, they do not take into account Biot's global-flow attenuation mechanism. This mechanism is in many practical situation negligible at seismic frequencies. However, as reported in the previous chapter, its contribution to the seismic attenuation cannot be neglected for materials with high permeability (e.g., sandy sediments with weak frame). In this study, we propose an effective poroelastic model for periodically distributed spherical inclusions that captures both Biot's attenuation mechanism and the attenuation caused by the presence of mesoscopic-scale heterogeneities. It is a generalization of White's model for spherical inclusions.

4.2 Periodic-cell problem

4.2.1 Formulation of the problem

We consider a porous medium with periodically distributed spherical inclusions (Figure 4.1). Each inclusion (blue sphere in Figure 4.1) is located at the center of a cube formed by a host medium. Wave motions in the host medium and the inclusion are described by Biot's equations of poroelasticity (Biot, 1956a, 1962) with different physical properties (differences can occur in solid frame properties, saturating fluid, or both). A cube with the inclusion composes a representative

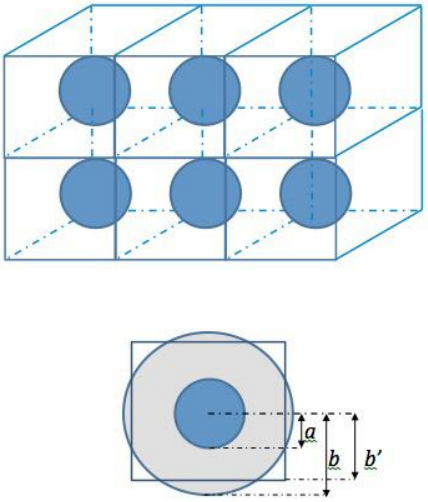

FIGURE 4.1: Geometry of the configuration (top), the periodic cell and its model (bottom).

volume element of such a medium. For the sake of simplicity, the cube is approximated by a sphere, depicted in grey in Figure 4.1 (bottom). This approximation was proposed by White (1975). As a result, the two concentric spheres form a representative volume element, where the volume of the outer sphere is the same as the volume of the initial cube. The radius of the inclusion (inner sphere) is a, and the radius of the outer sphere is b (see Figure 4.1). The ratio of the volume of the inclusion to the volume of the unit cell is defined as $s = a^3/b^3$. The size of the initial cubic volume element is b'. Equality of the volumes of the sphere with radius b and the cube with size $2b'$ provides the relation between these two parameters: $b' \approx 0.8b$. The inclusions are not supposed to have common interfaces. Therefore, there is a limitation on the volume ratio values: $s < 52\%$. For values above 52%, the inclusions from the neighbouring cells will be in contact, while their interaction is not taken into account in the model.

The cell problem is defined as follows. In the first test, an oscillatory harmonic fluid pressure is applied at the outer interface of the cell (Figure 4.2(a)), and in the second test an oscillatory harmonic intergranular stress is applied (Figure 4.2(b)). The boundary conditions used to solve for the response of the cell are the continuity of total stress, pore fluid pressure, solid displacement and relative fluid-to-solid displacement at the inner interface $r = a$, and the continuity of total stress and pore fluid pressure at the outer interface $r = b$. This formulation is different from the one used in White's model (White, 1975), where the total stress

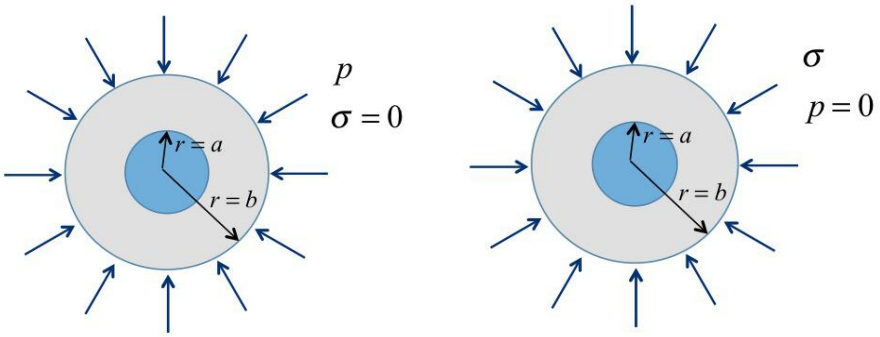

(a) (b)

FIGURE 4.2: Periodic cell of the heterogeneous porous medium subject to an oscillatory fluid pressure 4.2(a) and intergranular stress 4.2(b).

is applied at the interface $r = b$ and a no-flow condition replaces the pressure continuity condition. It was noted by Dutta and Seriff (1979) that the choice of boundary conditions made by White is not unique. Our study thus presents an alternative formulation of the cell problem. This formulation enables us to derive effective poroelastic moduli rather than the effective viscoelastic modulus of White.

4.2.2 Solution to the periodic-cell problem

Biot's theory is used to describe wave motions in the host medium and the inclusion. The equations of motion in the frequency domain (Biot, 1956a, 1962), where the Fourier transform is used as defined in equation (2.12), read:

$$\begin{aligned} \hat{\tau}_{ij,j} &= -\omega^2 \left(\rho \hat{u}_i + \rho_f \hat{w}_i\right), \\ -\hat{p}_{,i} &= -\omega^2 \left(\rho_f \hat{u}_i + \hat{m} \hat{w}_i\right). \end{aligned} \tag{4.1}$$

The stress-strain relations read

$$\begin{aligned} \hat{\tau}_{ij} &= (E_1 - 2\mu)\hat{e}_{kk}\delta_{ij} + E_2 \hat{\varepsilon}_{kk}\delta_{ij} + 2\mu e_{ij}, \\ -\hat{p} &= E_2 \hat{e}_{kk} + E_3 \hat{\varepsilon}_{kk}. \end{aligned} \tag{4.2}$$

In equation (4.2), $\hat{p}$ is the pore fluid pressure, $\hat{\tau}_{ij}$ is the total stress, and the elements of the small-strain tensors $\hat{e}$ and $\hat{\varepsilon}$ are defined as

$$\hat{e}_{ij} = \frac{1}{2}\left(\hat{u}_{j,i} + \hat{u}_{i,j}\right), \qquad \hat{\varepsilon}_{ij} = \frac{1}{2}\left(\hat{w}_{j,i} + \hat{w}_{i,j}\right). \tag{4.3}$$

The visco-dynamic factor $\hat{m}$ in equation (4.1) reads

$$\hat{m} = \frac{\alpha_\infty \rho_f}{\phi} - \frac{\mathrm{i}}{\omega}\frac{\eta}{k_0}\sqrt{1 + \mathrm{i}\frac{\omega}{2\omega_B}}, \tag{4.4}$$

where the high-frequency correction to Biot's viscous factor by Johnson et al. (1987) is adopted. The real part of the square root is chosen positive for all frequencies, and k_0 is Darcy permeability of the medium. Biot's critical frequency $\omega_B = \phi\eta/(k_0\alpha_\infty\rho_f)$ separates the regimes where inertial and viscous forces dominate the fluid flow. The density $\rho = (1-\phi)\rho_f + \phi\rho_s$, where ρ_s and ρ_f are the densities of the solid grains and fluid, respectively, and ϕ denotes the porosity; η is fluid viscosity, α_∞ is the tortuosity; $\hat{u}_i$ is the displacement of the solid phase, and $\hat{w}_i$ is relative fluid-to-solid displacement $\hat{w}_i = \phi(\hat{U}_i - \hat{u}_i)$, where $\hat{U}_i$ is the displacement of the fluid phase. The coefficients E_1, E_2 and E_3 are the elastic parameters as used in Biot's theory:

$$E_1 = P + 2Q + R, \quad E_2 = \frac{Q+R}{\phi}, \quad E_3 = \frac{R}{\phi^2}, \tag{4.5}$$

where

$$\begin{aligned} P &= \frac{\phi K_m + (1-\phi)K_f\left(1-\phi-K_m/K_s\right)}{\phi + K_f\left(1-\phi-K_m/K_s\right)/K_s} + \frac{4}{3}\mu, \\ Q &= \frac{\phi K_f\left(1-\phi-K_m/K_s\right)}{\phi + K_f\left(1-\phi-K_m/K_s\right)/K_s}, \\ R &= \frac{\phi^2 K_f}{\phi + K_f\left(1-\phi-K_m/K_s\right)/K_s}. \end{aligned} \tag{4.6}$$

In equations (4.5) and (4.6) K_s, K_f and K_m are the bulk moduli of the solid grains, fluid and the drained frame matrix, respectively; μ is the shear modulus of the drained frame.

We consider the radial motions $\hat{u}(r,\omega)$ and $\hat{w}(r,\omega)$. The equations of motion (4.1) combined with the stress-strain relations (4.2) in spherical coordinates read

$$\begin{aligned} E_1\frac{\partial}{\partial r}\left(\frac{\partial\hat{u}}{\partial r} + 2\frac{\hat{u}}{r}\right) + E_2\left(\frac{\partial\hat{w}}{\partial r} + 2\frac{\hat{w}}{r}\right) &= -\omega^2\left(\rho\hat{u} + \rho_f\hat{w}\right), \\ E_2\frac{\partial}{\partial r}\left(\frac{\partial\hat{u}}{\partial r} + 2\frac{\hat{u}}{r}\right) + E_3\left(\frac{\partial\hat{w}}{\partial r} + 2\frac{\hat{w}}{r}\right) &= -\omega^2\left(\rho_f\hat{u} + \hat{m}\hat{w}\right). \end{aligned} \tag{4.7}$$

The solution of equations (4.7) can be found in the following form:

$$\begin{aligned}
&\hat{u} = \hat{A} j_1(k_{P1} r) + \hat{B} y_1(k_{P1} r) + \hat{C} j_1(k_{P2} r) + \hat{D} y_1(k_{P2} r), \\
&\hat{w} = \phi(\hat{\beta}_{P1} - 1) \left(\hat{A} j_1(k_{P1} r) + \hat{B} y_1(k_{P1} r) \right) + \phi(\hat{\beta}_{P2} - 1) \left(\hat{C} j_1(k_{P2} r) + \hat{D} y_1(k_{P2} r) \right),
\end{aligned} \tag{4.8}$$

where k_{P1} and k_{P2} are the wavenumbers of the slow and fast P-waves, respectively. They are solutions of the dispersion equation (3.8), and the amplitude ratios $\hat{\beta}_{P1,P2}$ are defined in equation (3.10). The functions j_1 and y_1 are the spherical Bessel functions defined as

$$\begin{aligned}
j_1(x) &= \frac{\sin(x)}{x^2} - \frac{\cos(x)}{x}, \\
y_1(x) &= -\frac{\cos(x)}{x^2} - \frac{\sin(x)}{x}.
\end{aligned} \tag{4.9}$$

There are eight unknown amplitudes $\hat{A}_i$, $\hat{B}_i$, $\hat{C}_i$ and $\hat{D}_i$, where $i = 1, 2$, corresponding to the solutions (4.8) of the inner sphere (blue area in Figure 4.2(a), $i = 1$) and the outer sphere (grey area in Figure 4.2(a), $i = 2$). First, the displacement field should be finite at $r = 0$. It means that $\hat{B}_1$ and $\hat{D}_1$ vanish, because y_1 is singular at $r = 0$. There are six unknown amplitudes left. The cell problem is solved with the use of the remaining six boundary conditions discussed above: continuity of the displacements $\hat{u}$, $\hat{w}$, total stress $\hat{\tau}$ and fluid pressure $\hat{p}$ at the inner interface $r = a$, and continuity of total stress and fluid pressure at the outer interface $r = b$. The unknown amplitudes are found numerically by solving a system of six linear algebraic equations corresponding to the boundary conditions in both tests. The equations read

$$\mathbf{A}\mathbf{x} = \mathbf{B}, \tag{4.10}$$

where matrix $\mathbf{A}$ and vector of unknown amplitudes $\mathbf{x}$ are given in Appendix 4.A. In the first test, vector $\mathbf{B}$ reads

$$\mathbf{B}^{(1)} = (0, \quad 0, \quad 0, \quad 0, \quad \hat{p}, \quad -\hat{p})^{\mathrm{T}}, \tag{4.11}$$

and in the second test, it reads

$$\mathbf{B}^{(2)} = (0, \quad 0, \quad 0, \quad 0, \quad 0 \quad -\hat{\sigma})^{\mathrm{T}}, \tag{4.12}$$

where the fifth component corresponds to the pore fluid pressure, and the sixth one to the total stress (the expressions are given in equations (2.3)–(2.4)); the superscripts 1 and 2 correspond to the first and second test, respectively.

4.3 Effective coefficients

In White's model (White, 1975) one test is used to define the effective frequency-dependent bulk modulus. In the present model, the two tests are used to derive the effective frequency-dependent coefficients $\hat{E}_1$, $\hat{E}_2$ and $\hat{E}_3$, which correspond to the coefficients E_1, E_2 and E_3 introduced in stress-strain relations of a homogeneous medium in equations (4.2). The first test (Figure 4.2(a)) is used to relate the pore fluid pressure applied at the outer interface of the cell to the relative changes in volume of the cell, and the second test (Figure 4.2(b)) relates the intergranular stress at the outer interface to the changes in volume. The relative changes in the volume in both tests can be expressed as

$$\begin{aligned} \hat{e}_{kk}^{(1,2)} &\approx \frac{\Delta V}{V} = \frac{4\pi b^2 \hat{u}^{(1,2)}(b)}{(4/3)\pi b^3} = \frac{3\hat{u}^{(1,2)}(b)}{b}, \\ \hat{\varepsilon}_{kk}^{(1,2)} &\approx \frac{3\hat{w}^{(1,2)}(b)}{b}, \end{aligned} \tag{4.13}$$

where $\hat{u}^{(1,2)}(b)$ and $\hat{w}^{(1,2)}(b)$ are the displacements at the outer interface $r = b$, for the tests 1 and 2. Then, the effective coefficients are found from the following system of effective stress-strain relations:

$$\begin{aligned} \hat{\tau}_0 \quad = \quad -\hat{p} \quad &= \quad \left(\hat{E}_1 - \tfrac{4}{3}\mu\right) \hat{e}_{kk}^{(1)} + \hat{E}_2 \hat{\varepsilon}_{kk}^{(1)}, \\ -\hat{p} \quad &= \quad \hat{E}_2 \hat{e}_{kk}^{(1)} + \hat{E}_3 \hat{\varepsilon}_{kk}^{(1)}, \\ -\hat{\tau}_0 \quad = \quad \hat{\sigma} \quad &= \quad \left(\hat{E}_1 - \tfrac{4}{3}\mu\right) 2\hat{e}_{kk}^{(2)} + \hat{E}_3 \hat{\varepsilon}_{kk}^{(2)}, \\ 0 \quad &= \quad \hat{E}_2 \hat{e}_{kk}^{(2)} + \hat{E}_3 \hat{\varepsilon}_{kk}^{(2)}, \end{aligned} \tag{4.14}$$

where $\hat{\tau}_0$ is the isotropic total stress, the expression of which can be found using equations (4.2). The first two equations in (4.14) correspond to the first test (Figure 4.2(a)), and third and the fourth equations to the second test (Figure 4.2(b)). In fact, these four equations are not independent, and we need to take only three equations from (4.14) to find the unknowns $\hat{E}_1$, $\hat{E}_2$ and $\hat{E}_3$. Solution of equations (4.10) for each of the tests, taking into account (4.13), provides the following relations:

$$\begin{aligned} \hat{e}_{kk}^{(1)} &= \hat{a}_1 \hat{p}, \qquad \hat{\varepsilon}_{kk}^{(1)} = \hat{a}_2 \hat{p}, \\ \hat{e}_{kk}^{(2)} &= -\hat{a}_3 \hat{\sigma}, \quad \hat{\varepsilon}_{kk}^{(2)} = -\hat{a}_4 \hat{\sigma}, \end{aligned} \tag{4.15}$$

where the coefficients of proportionality $\hat{a}_i$ are found numerically. Solution of equations (4.14), taking into account (4.15), provides the expressions for the effective coefficients:

$$\begin{aligned}\hat{E}_1 &= \frac{4}{3}\mu - \frac{\hat{a}_2 + \hat{a}_4}{\hat{a}_1\hat{a}_4 - \hat{a}_2\hat{a}_3},\\ \hat{E}_2 &= \frac{\hat{a}_1 + \hat{a}_3}{\hat{a}_1\hat{a}_4 - \hat{a}_2\hat{a}_3},\\ \hat{E}_3 &= \frac{\hat{a}_3}{\hat{a}_1\hat{a}_4 - \hat{a}_2\hat{a}_3}.\end{aligned} \tag{4.16}$$

Due to the isotropy of the medium, the coefficients $\hat{a}_i$ are not independent: $\hat{a}_1 + \hat{a}_3 + \hat{a}_4 = 0$.

The effective coefficients $\hat{E}_1$, $\hat{E}_2$ and $\hat{E}_3$ defined in (4.16) are substituted into Biot's equations (4.1)–(4.2), together with the effective densities ρ_e, ρ_{fe}, and the effective visco-dynamic factor $\hat{m}_e$ from the right hand-side of the second equation in (4.1):

$$\begin{aligned}&\rho_e = s\rho^I + (1-s)\rho^{II}, \qquad \rho_{fe} = s\rho_f^I + (1-s)\rho_f^{II},\\ &\hat{m}_e = s\left(\frac{\alpha_\infty\rho_f}{\phi} - \frac{\mathrm{i}}{\omega}\frac{\eta}{k_0}\sqrt{1+\mathrm{i}\frac{\omega}{2\omega_B}}\right)_I + (1-s)\left(\frac{\alpha_\infty\rho_f}{\phi} - \frac{\mathrm{i}}{\omega}\frac{\eta}{k_0}\sqrt{1+\mathrm{i}\frac{\omega}{2\omega_B}}\right)_{II}.\end{aligned} \tag{4.17}$$

The sub- and superscripts I and II in refer to the properties of the inner sphere (inclusion), and the host medium, respectively. The definition of the effective parameters in (4.17) is in correspondence with the definition of the effective densities in (3.25).

4.4 Comparison with White's model

Now that the effective coefficients have been defined, the expressions for the wavenumbers of the slow and fast P-waves can be obtained:

$$k_{P1,P2} = \omega\sqrt{\frac{-\hat{d}_1 \pm \sqrt{\hat{d}_1^2 - 4\hat{d}_0\hat{d}_2}}{2\hat{d}_2}}, \tag{4.18}$$

where

$$\begin{aligned}\hat{d}_0 &= \rho_e \hat{m}_e - (\rho_{fe})^2,\\ \hat{d}_1 &= \rho_e \hat{E}_3 - \hat{m}_e \hat{E}_1 + 2\rho_{fe}\hat{E}_2,\\ \hat{d}_2 &= \hat{E}_1 \hat{E}_3 - \hat{E}_2^2.\end{aligned} \tag{4.19}$$

The inverse quality factor, that characterizes the attenuation, and the phase velocity are defined as

$$\begin{aligned}Q^{-1} &= -2\tfrac{\mathrm{Im}(k_{P1})}{\mathrm{Re}(k_{P1})},\\ c &= \left(\tfrac{1}{\mathrm{Re}(\omega/k_{P1})}\right)^{-1}.\end{aligned} \tag{4.20}$$

In the proposed model, the effective medium is described with Biot's equations, as shown above. In White's model, the frequency-dependent bulk modulus $\hat{K}_b$ of the effective medium is derived. It can be used to predict phase velocity and attenuation in the effective medium governed by the equations of viscoelasticity, where the effective wavenumber is related to the bulk modulus $\hat{K}_b$:

$$\begin{aligned}\hat{K}_b &= -\frac{\hat{\tau}}{\Delta V/V} = -\frac{b}{3\hat{u}(b)}\hat{\tau},\\ k &= \omega\frac{\rho_e}{\hat{K}_b + \frac{4}{3}\mu}.\end{aligned} \tag{4.21}$$

To compare predictions of the proposed model and White's model, we obtain White's bulk modulus $\hat{K}_b$ according to its definition in (4.21), where $\hat{u}(b)$ is the solid-phase displacement at $r = b$. It is proportional to the applied total stress $\hat{\tau}$, and the coefficient of proportionality is found by solving the cell problem, similar to the solution presented above. The difference is in the boundary conditions used; in White's model, the pressure continuity condition is replaced with the no-flow condition $\hat{w}(b) = 0$, while the other boundary conditions, namely, the total stress continuity at the outer interface $r = b$ and the conditions at the inner interface $r = a$ remain the same. The system of linear equations is given in Appendix 4.A. A similar solution is presented in Johnson (2001) and Vogelaar et al. (2010).

4.5 Examples and discussion

The sets of material properties chosen for numerical examples are given in Tables 4.1 and 4.2. The properties of Sand 1 are taken from Chotiros (1995), the properties of Rock, Sand 2 and Sand 3 from Turgut and Yamamoto (1990). The chosen

Parameter	Notation	Units	Rock	Sand 1	Sand 2	Sand 3
Density of solid grains	ρ_s	kg/m^3	2650	2650	2650	2650
Bulk modulus of solid grains	K_s	GPa	36	40	36	36
Bulk modulus of frame	K_m	GPa	2.17	0.2	0.1	0.2
Porosity	ϕ	–	0.3	0.38	0.4	0.35
Permeability	k_0	m^2	$5 \cdot 10^{-13}$	$6.49 \cdot 10^{-12}$	10^{-11}	10^{-10}
Shear modulus	μ	GPa	1	0.12	0.05	0.1
Tortuosity	α_∞	–	1.25	1.25	1.25	1.25

TABLE 4.1: Physical properties of solid frames.

Parameter	Notation	Units	Water	Gas
Density	ρ_f	kg/m^3	1000	140
Bulk modulus	K_f	GPa	2.25	0.056
Viscosity	η	Pa $\cdot$ s	0.001	0.00022

TABLE 4.2: Physical properties of sample pore fluids.

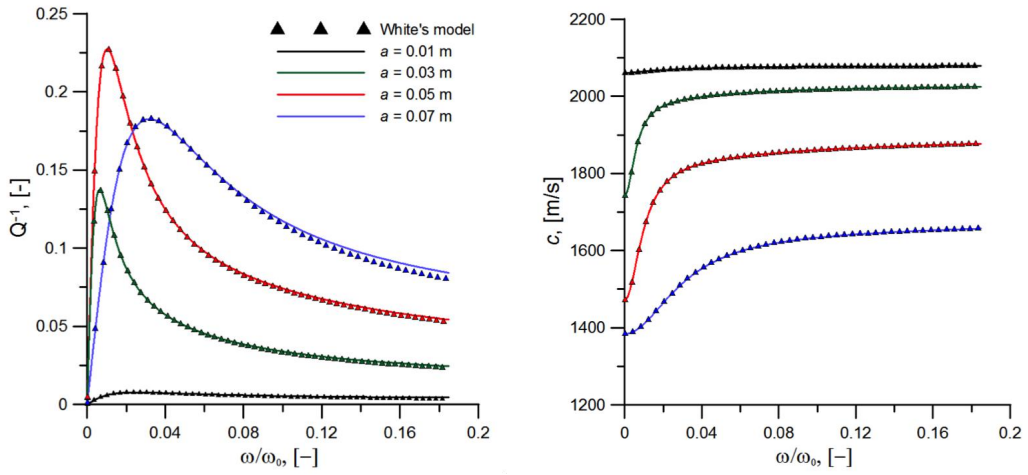

(a) (b)

FIGURE 4.3: Inverse quality factor Q^{-1} (a) and phase velocity (b) versus dimensionless frequency. Rock, b=0.1 m.

outer radius $b = 0.1$ m and remains the same in all examples.

The inner sphere (inclusion) is saturated with gas, and the host medium is saturated with fluid (for properties, see Table 4.2). The solid properties in the examples are the same for both regions in the unit cell. We introduce the dimensionless frequency ω/ω_0, where ω_0 is a frequency at which the wavelength of the fast P-wave is comparable to the size of the periodic cell b: $\omega_0 = 2\pi c_0/b$, where $c_0 = \sqrt{E_0/\rho_e}$ and $E_0^{-1} = (1-s)\,[P+2Q+R]_I^{-1} + s\,[P+2Q+R]_{II}^{-1}$.

It was shown in the previous chapter that the difference between the effective poroelastic and viscoelastic models is pronounced for unconsolidated sandstones,

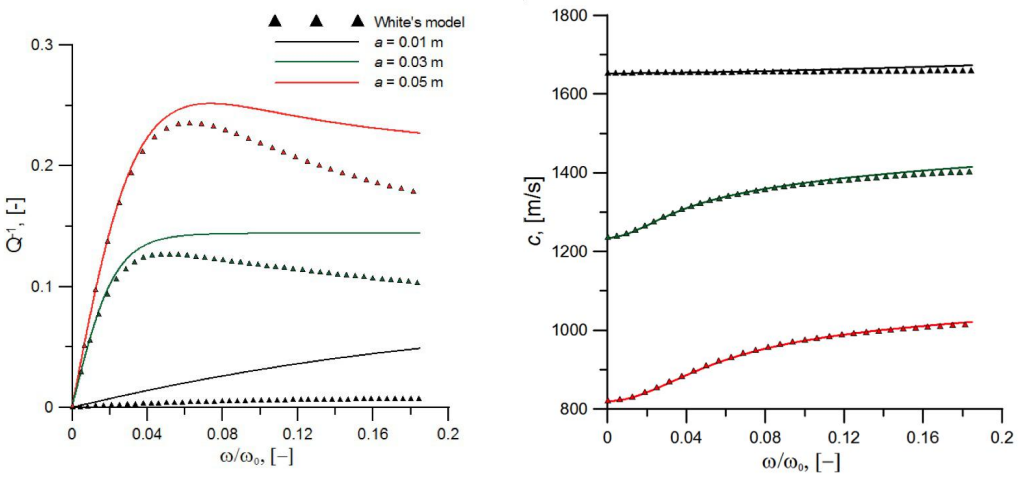

(a) (b)

FIGURE 4.4: Inverse quality factor Q^{-1} (a) and phase velocity (b) versus dimensionless frequency. Sand 1, b=0.1 m.

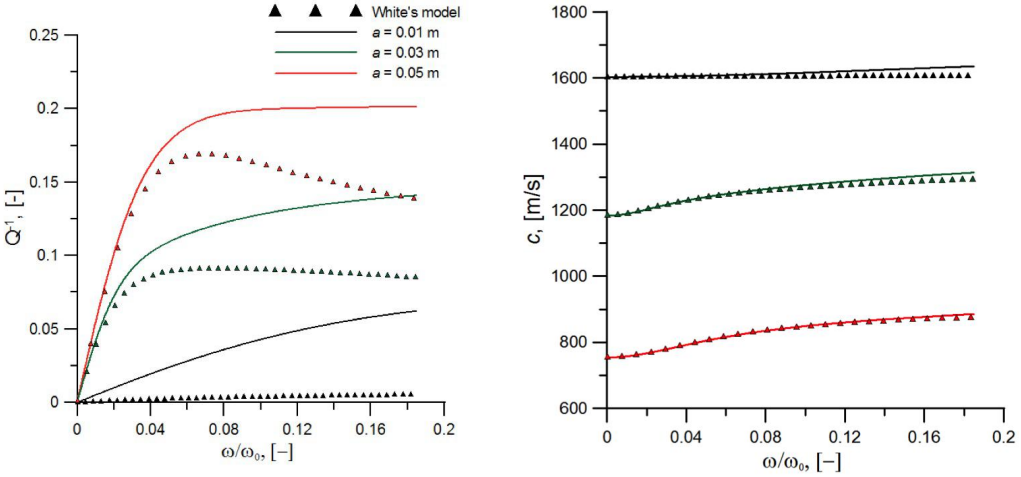

(a) (b)

FIGURE 4.5: Inverse quality factor Q^{-1} (a) and phase velocity (b) versus dimensionless frequency. Sand 2, b=0.1 m.

and the models are in agreement for stiff rocks. In this chapter, we compare attenuation and phase velocity versus frequency for one stiff-frame medium (Rock), and several weaker sands. The results for Rock are shown in Figure 4.3. The attenuation (Figure 4.3(a)) and phase velocity (Figure 4.3(b)) of the fast P-wave predicted by the model proposed in this chapter and by White's model are shown for different sizes of the inclusion a. We see that both models are in good agreement for a wide frequency range.

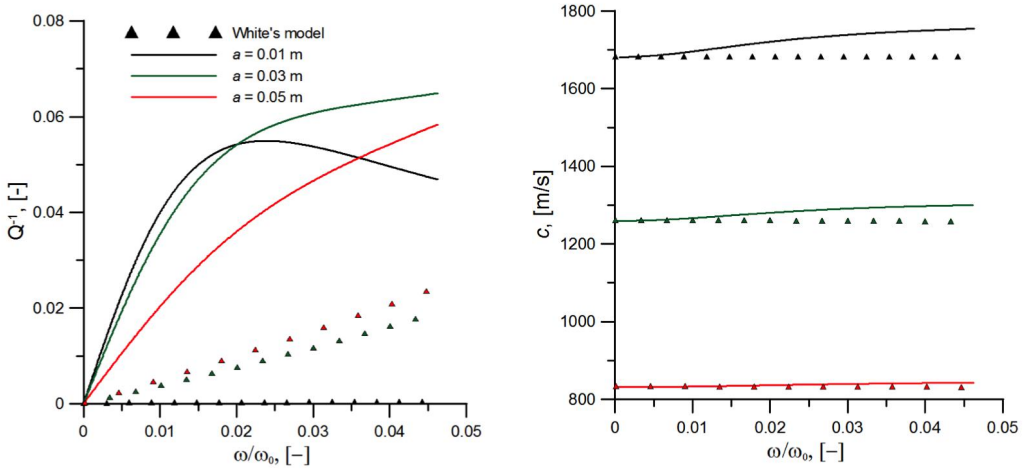

(a) (b)

FIGURE 4.6: Inverse quality factor Q^{-1} (a) and phase velocity (b) versus dimensionless frequency. Sand 3, b=0.1 m.

The results for Sand 1 are depicted in Figures 4.4(a) and 4.4(b), and the results for Sand 2 in Figures 4.5(a) and 4.5(b). Both sands have relatively high permeability. Sand 1 is a weakly consolidated sand, it has a stiffer frame than Sand 2. We observe that White's model predicts significantly lower attenuation and slightly lower velocities than our effective model. This result is consistent with the result obtained in the previous chapter for a periodically-layered medium. For Sand 3, which has higher permeability than the materials in the previous examples, the discrepancy in predictions are even higher, as shown in Figure 4.6. Especially the inverse quality factor shows a very deviating curve for White's model, giving a very different and lower attenuation, also at the lowest frequencies. We conclude that our effective medium is more accurate for a high-permeable material and a material with weak frame, because it allows for a global-flow attenuation mechanism.

4.6 Conclusions

We proposed an extension of White's model for seismic wave propagation in porous media with spherical inclusions. The extended model incorporates Biot's global-flow attenuation mechanism in addition to the mesoscopic-loss mechanism. In this model, the fluid is allowed to flow in and out of the representative volume element. We proposed a semi-analytical derivation of the effective parameters that

can be used as an input to Biot's equations for homogeneous media. The predicted attenuation and phase velocity are in good agreement with predictions by White's model when the global-flow mechanism is negligible. At higher frequencies, the model predicts higher phase velocities than White's model. For sandy sediments, which are characterized by high permeability and a weak frame, White's model predicts significantly smaller attenuation. The result is in agreement with the predictions obtained for periodically layered media (Chapter 3), where an exact analytical solution is used for reference.

The proposed model can serve as a reference theoretical framework for predictions of seismic attenuation in heterogeneous media, when the characteristic size of heterogeneities is much smaller than the wavelength. It can also be used as a benchmark solution for the models with a more complicated geometry, and to calibrate parameters in experimental studies. The model has wider applicability than White's model and other similar models where the no-flow boundary condition is employed.

4.A Coefficients of system of linear equations for cell problems

The systems of linear equations $\mathbf{A}\mathbf{x} = \mathbf{B}^{(1,2)}$ are solved to obtain the coefficients α_i in (4.15). Vectors $\mathbf{B}^{(1,2)}$ contain the amplitudes of the applied total stress and fluid pressure; they are defined in equations (4.11) and (4.12). Vector $\mathbf{x}$ contains the unknown amplitudes:

$$\mathbf{x} = [A_1, \quad C_1, \quad A_2, \quad B_2, \quad C_2, \quad D_2]\,. \tag{4.22}$$

The coefficients of the matrix $\mathbf{A}$ read

$$
\begin{aligned}
&A_{11} = -j_1(\tilde{a}_{II}), \quad A_{12} = -j_1(\tilde{c}_{II}), \quad A_{13} = j_1(\tilde{a}_I)\\
&A_{14} = j_1(\tilde{c}_I), \quad A_{15} = y_1(\tilde{a}_I, \quad A_{16} = y_1(\tilde{c}_I),\\
&A_{21} = \tilde{\phi}^{II}_{P1}A_{11}, \quad A_{22} = \tilde{\phi}^{II}_{P2}A_{12}, \quad A_{23} = \tilde{\phi}^{I}_{P1}A_{13},\\
&A_{24} = \tilde{\phi}^{I}_{P2}A_{14}, \quad A_{25} = \tilde{\phi}^{I}_{P1}A_{15}, \quad A_{26} = \tilde{\phi}^{I}_{P2}A_{16},\\
&A_{31} = -\lambda^{II}_1 j_0(\tilde{a}_{II}) + 2\mu_{II}\left(\left(\tfrac{3}{\tilde{a}^2_{II}} - 1\right) j_0(\tilde{a}_{II} + \tfrac{3}{\tilde{a}_{II}} y_0(\tilde{a}_{II}) - \tfrac{1}{\tilde{a}_{II}} j_1(\tilde{a}_{II})\right),\\
&A_{32} = -\lambda^{II}_2 j_0(\tilde{c}_{II}) + 2\mu_{II}\left(\left(\tfrac{3}{\tilde{c}^2_{II}} - 1\right) j_0(\tilde{c}_{II} + \tfrac{3}{\tilde{c}_{II}} y_0(\tilde{c}_{II}) - \tfrac{1}{\tilde{c}_{II}} j_1(\tilde{c}_{II})\right),\\
&A_{33} = -\left(-\lambda^{I}_1 j_0(\tilde{a}_I) + 2\mu_I\left(\left(\tfrac{3}{\tilde{a}^2_I} - 1\right) j_0(\tilde{a}_I + \tfrac{3}{\tilde{a}_I} y_0(\tilde{a}_I) - \tfrac{1}{\tilde{a}_I} j_1(\tilde{a}_I)\right)\right),\\
&A_{34} = -\left(-\lambda^{I}_1 j_0(\tilde{c}_I) + 2\mu_I\left(\left(\tfrac{3}{\tilde{c}^2_I} - 1\right) j_0(\tilde{c}_I + \tfrac{3}{\tilde{c}_I} y_0(\tilde{c}_I) - \tfrac{1}{\tilde{c}_I} j_1(\tilde{c}_I)\right)\right),\\
&A_{35} = -\left(-\lambda^{I}_1 y_0(\tilde{a}_I) + 2\mu_I\left(\left(\tfrac{3}{\tilde{a}^2_I} - 1\right) y_0(\tilde{a}_I - \tfrac{3}{\tilde{a}_I} j_0(\tilde{a}_I) - \tfrac{1}{\tilde{a}_I} y_1(\tilde{a}_I)\right)\right),\\
&A_{36} = -\left(-\lambda^{I}_1 y_0(\tilde{c}_I) + 2\mu_I\left(\left(\tfrac{3}{\tilde{c}^2_I} - 1\right) y_0(\tilde{c}_I - \tfrac{3}{\tilde{c}_I} j_0(\tilde{c}_I) - \tfrac{1}{\tilde{c}_I} y_1(\tilde{c}_I)\right)\right),\\
&A_{41} = -\left(\tfrac{Q+\hat{\beta}_{P1}R}{\phi}\right)_{II} j_0(\tilde{a}_{II}), \quad A_{42} = -\left(\tfrac{Q+\hat{\beta}_{P2}R}{\phi}\right)_{II} j_0(\tilde{c}_{II}),\\
&A_{44} = -\left(\tfrac{Q+\hat{\beta}_{P2}R}{\phi}\right)_{I} j_0(\tilde{c}_I), \quad A_{45} = -\left(\tfrac{Q+\hat{\beta}_{P1}R}{\phi}\right)_{I} y_0(\tilde{a}_I),\\
&A_{43} = -\left(\tfrac{Q+\hat{\beta}_{P1}R}{\phi}\right)_{I} j_0(\tilde{a}_I), \quad A_{46} = -\left(\tfrac{Q+\hat{\beta}_{P2}R}{\phi}\right)_{I} y_0(\tilde{c}_I),\\
&A_{51} = 0, \quad A_{52} = 0, \quad A_{53} = -\left(\tfrac{Q+\hat{\beta}_{P1}R}{\phi}\right)_{I} j_0(\tilde{b}_I), A_{54} = -\left(\tfrac{Q+\hat{\beta}_{P2}R}{\phi}\right)_{I} y_0(\tilde{d}_I),\\
&A_{55} = -\left(\tfrac{Q+\hat{\beta}_{P1}R}{\phi}\right)_{I} y_0(\tilde{b}_I), \quad A_{56} = -\left(\tfrac{Q+\hat{\beta}_{P2}R}{\phi}\right)_{I} y_0(\tilde{d}_I),\\
&A_{61} = 0, \quad A_{62} = 0,\\
&A_{63} = -\left(-\lambda^{I}_1 j_0(\tilde{a}_I) + 2\mu_I\left(\left(\tfrac{3}{\tilde{b}^2_I} - 1\right) j_0(\tilde{b}_I + \tfrac{3}{\tilde{b}_I} y_0(\tilde{b}_I) - \tfrac{1}{\tilde{b}_I} j_1(\tilde{b}_I)\right)\right),\\
&A_{64} = -\left(-\lambda^{I}_2 j_0(\tilde{d}_I) + 2\mu_I\left(\left(\tfrac{3}{\tilde{d}^2_I} - 1\right) j_0(\tilde{d}_I + \tfrac{3}{\tilde{d}_I} y_0(\tilde{d}_I) - \tfrac{1}{\tilde{d}_I} j_1(\tilde{d}_I)\right)\right),\\
&A_{65} = -\left(-\lambda^{I}_1 y_0(\tilde{b}_I) + 2\mu_I\left(\left(\tfrac{3}{\tilde{b}^2_I} - 1\right) y_0(\tilde{b}_I - \tfrac{3}{\tilde{b}_I} j_0(\tilde{b}_I) - \tfrac{1}{\tilde{b}_I} y_1(\tilde{b}_I)\right)\right),\\
&A_{66} = -\left(-\lambda^{I}_2 y_0(\tilde{d}_I) + 2\mu_I\left(\left(\tfrac{3}{\tilde{d}^2_I} - 1\right) y_0(\tilde{d}_I - \tfrac{3}{\tilde{d}_I} j_0(\tilde{d}_I) - \tfrac{1}{\tilde{d}_I} y_1(\tilde{d}_I)\right)\right),
\end{aligned}
\tag{4.23}
$$

where indices I and II correspond to the properties of the medium I (outer sphere) and II (inner sphere), respectively. The symbols used in (4.23) are defined as

follows:

$$\begin{aligned}
&\lambda_{1,2}^{I,II} = \Big(P + Q + \hat{\beta}_{P1,P2}(Q+R) - 2\mu\Big)_{I,II}\,,\\
&\tilde{a}_{I,II} = k_{P1}^{I,II} a, \quad \tilde{c}_{I,II} = k_{P2}^{I,II} a,\\
&\tilde{b}_I = k_{P1}^{I} b, \quad \tilde{d}_I = k_{P2}^{I} b,\\
&\tilde{\phi}_{P1,P2}^{I,II} = \left(\phi(\beta_{P1,P2} - 1)\right)_{I,II}\,.
\end{aligned} \tag{4.24}$$

The functions y_0 and j_0 are spherical Bessel functions defined as

$$j_0(x) = \frac{\sin(x)}{x}, \quad y_0(x) = -\frac{\cos(x)}{x}. \tag{4.25}$$

A similar system of equations is solved to obtain the effective bulk modulus of White's model. In this system, the fluid pressure is not applied at the outer interface $r = b$. The pressure continuity condition is replaced by the no-flow condition, which assumes the equality of the solid and fluid phase displacements: $\hat{w} = 0$ at $r = b$. The coefficients of matrix $\mathbf{A}$ defined above remain the same, apart from the coefficients A_{53}–A_{56}:

$$\begin{aligned}
&A_{53} = -\tilde{\phi}_{P1}^{I} j_1(\tilde{b}_I), \quad A_{54} = -\tilde{\phi}_{P2}^{I} j_1(\tilde{d}_I),\\
&A_{55} = -\tilde{\phi}_{P1}^{I} y_1(\tilde{b}_I), \quad A_{56} = -\tilde{\phi}_{P2}^{I} y_1(\tilde{d}_I).
\end{aligned} \tag{4.26}$$

Vector $\mathbf{B}$ (one vector in this case, because only one test is used to derive the effective bulk modulus) reads

$$\mathbf{B} = (0, \quad 0, \quad 0, \quad 0, \quad 0, \quad -\hat{\sigma})^{\mathrm{T}}. \tag{4.27}$$

4.B Alternative approach to derive effective coefficients

Effective coefficients can be also derived by comparing the dynamic compliance matrices of the periodic unit cell of the same size, corresponding to the equivalent homogeneous medium. We consider the low-frequency solution of equations (4.1), neglecting the inertia terms and taking the steady-state value k_0 of the dynamic permeability $\hat{k}$. The solution of equations (4.7) with the inertial terms neglected

can be found in the following form:

$$\begin{aligned} \hat{u} &= \hat{A}r + \frac{\hat{B}}{r^2} + E_2\left(\hat{C}j_1(qr) + \hat{D}y_1(qr)\right), \\ \hat{w} &= -E_1\left(\hat{C}j_1(qr) + \hat{D}y_1(qr)\right), \end{aligned} \tag{4.28}$$

where

$$q = \sqrt{\mathrm{i}\omega\frac{\eta}{k_0}\frac{E_1}{E_2^2 - E_1E_3}}. \tag{4.29}$$

The stress-strain relations (4.2) can be rewritten in terms of the displacements in spherical coordinates:

$$\begin{aligned} \hat{\tau} &= 3\left(E_1 - \frac{4}{3}\mu\right)\hat{A} - 4\frac{\mu}{r}E_2\left(\hat{C}j_1(qr) + \hat{D}y_1(qr)\right), \\ \hat{p} &= -3E_2\hat{A} + (E_1E_3 - E_2^2)\left(\hat{C}\frac{\sin(qr)}{r} - \hat{D}\frac{\cos(qr)}{r}\right). \end{aligned} \tag{4.30}$$

The unknown amplitudes $\hat{A}_i$, $\hat{B}_i$, $\hat{C}_i$ and $\hat{D}_i$, where $i = 1, 2$, correspond to the solutions (4.28) of the inner sphere (blue area in Figure 4.2(a), $i = 1$) and the outer sphere (grey area in Figure 4.2(a), $i = 2$). The displacement field should be finite at $r = 0$, which means that $\hat{B}_1$ and $\hat{D}_1$ vanish. There are six unknown amplitudes left. The cell problem is solved with the use of the same boundary conditions, as discussed in Section 4.2.2. However, here both harmonic pressure and total stress are applied at the outer interface of the cell in a single test. The equations for the unknown amplitudes read $\tilde{\mathbf{A}}\mathbf{x} = \tilde{\mathbf{B}}$, where the structure of matrix $\tilde{\mathbf{A}}$ is similar to matrix $\mathbf{A}$, but the field variables are expressed with the use of equations (4.28)–(4.30). Vector $\tilde{\mathbf{B}}$ reads

$$\tilde{\mathbf{B}} = (0, \quad 0, \quad 0, \quad 0, \quad \hat{p}, \quad \hat{\tau})^{\mathrm{T}}. \tag{4.31}$$

The solution of the periodic-cell problem discussed above provides the frequency-dependent elements of the dynamic compliance matrix (coefficients of proportionality between the displacements and the applied stress $\hat{\tau}$ and pressure $\hat{p}$ at $r = b$):

$$\begin{bmatrix} \hat{u}(b) \\ \\ \hat{w}(b) \end{bmatrix} = \begin{bmatrix} \hat{\alpha}_1 & \hat{\alpha}_2 \\ \\ \hat{\alpha}_2 & \hat{\alpha}_3 \end{bmatrix} \begin{bmatrix} \hat{\tau} \\ \\ -\hat{p} \end{bmatrix}. \tag{4.32}$$

The elements of the compliance matrix α_i in (4.32) depend on frequency and the

physical properties of the medium in the inner and outer spheres in the periodic cell. In order to find the parameters of an equivalent homogeneous medium, we compare the elements of the compliance matrix in (4.32) with the elements of the compliance matrix obtained for a homogeneous periodic cell with the same boundary conditions. For a homogeneous cell, the unknown amplitudes of the displacement fields in (4.28) have to be found, in a similar way as for a non-homogeneous cell. The amplitudes $\hat{B}$ and $\hat{D}$ in (4.28) vanish as $\hat{u}$ and $\hat{w}$ are finite at $r = 0$, and the remaining amplitudes $\hat{A}$ and $\hat{C}$ are linear combinations of applied stress $\hat{\tau}$ and pressure $\hat{p}$ defined in the system of two linear algebraic equations, i.e., the continuity of total stress and fluid pressure (4.30) at $r = b$. The resulting displacements at $r = b$ read

$$\begin{bmatrix} \hat{u}(b) \\ \\ \hat{w}(b) \end{bmatrix} = \begin{bmatrix} \dfrac{bg_{qb}}{\Delta} & \dfrac{3bE_1E_2f_{qb}}{\Delta} \\ \\ \dfrac{3bE_1E_2f_{qb}}{\Delta} & \dfrac{E_1b(3E_1-4\mu)f_{qb}}{\Delta} \end{bmatrix} \begin{bmatrix} \hat{\tau} \\ \\ -\hat{p} \end{bmatrix},$$

where

$$g_{qb} = \left(q^2b^2\sin(qb)\left(E_2^2 - E_1E_3\right) - 3E_2^2f_{qb}\right),$$

$$f_{qb} = \sin(qb) - qb\cos(qb),$$

$$\Delta = \sin(qb)q^2b^2(3E_1 - 4\mu)(E_2^2 - E_1E_3) + 12E_2^2\mu f_{qb}. \tag{4.33}$$

The elements of the compliance matrix in (5.27) are frequency-dependent non-linear transcendental functions of the medium parameters E_1, E_2, E_3, η, μ, ϕ and k_0. We compare the zero-frequency approximation of the derived dynamic compliance matrix in (5.27) with the matrix obtained in (4.32). The zero-frequency approximation of (5.27) gives the following result:

$$\begin{bmatrix} \hat{u}(b) \\ \\ \hat{w}(b) \end{bmatrix} = \begin{bmatrix} -\frac{bE_3}{\tilde{\Delta}} & \frac{bE_2}{\tilde{\Delta}} \\ \\ \frac{bE_2}{\tilde{\Delta}} & \frac{b(4\mu-3E_1)}{3\tilde{\Delta}} \end{bmatrix} \begin{bmatrix} \hat{\tau} \\ \\ -\hat{p} \end{bmatrix}, \tag{4.34}$$

in which $\tilde{\Delta} = 3E_2^2 - 3(E_1 - 4\mu)E_3$.

As in White's model, we assume that the shear modulus remains the same throughout the cell. Equating the compliance matrices in equations (4.32) and (4.34) results in expressions for the frequency-dependent coefficients of the effective

homogenized medium:

$$\begin{aligned}\hat{E}_1 &= \frac{1}{3}\frac{\hat{\alpha}_1 b}{\hat{\alpha}_1\hat{\alpha}_3 - \hat{\alpha}_2^2},\\ \hat{E}_2 &= -\frac{1}{3}\frac{\hat{\alpha}_2 b}{\hat{\alpha}_1\hat{\alpha}_3 - \hat{\alpha}_2^2},\\ \hat{E}_3 &= \frac{1}{3}\frac{\hat{\alpha}_3 b}{\hat{\alpha}_1\hat{\alpha}_3 - \hat{\alpha}_2^2} + \frac{4}{3}\mu.\end{aligned} \tag{4.35}$$

The effective coefficients defined in (5.28) can be used to calculate the wavenumbers in the effective medium according to (5.29) and (5.30). The results obtained with coefficients (5.28) coincide at low frequencies with the results obtained using the coefficients (4.16).

Chapter 5

Higher-order elasticity models for a periodically layered poroelastic composite

In the previous chapters, effective models were derived with frequency-dependent coefficients. The frequency dependence was introduced to account for attenuation and dispersion caused by the presence of mesoscopic-scale heterogeneities. In this chapter, alternative effective models for a periodically layered poroelastic medium are proposed with coefficients that do not depend on frequency. This is advantageous for calculations in the time domain, especially in multi-scale numerical modelling.

5.1 Introduction

The effective homogenized models described in the previous chapters can be used for modeling wave propagation in the domains where linear elasticity is assumed. The frequency-dependent coefficients do not complicate the analysis as the linear problems can be studied in the frequency-domain. However, time-domain analysis is necessary to account for nonlinear effects that arise, for example close to a powerful vibration source, or within a domain in which significant elastic deformations or nonlinear fluid-solid interaction processes take place. As the time domain modeling of large domains is computationally expensive, hybrid simulation approaches are used, based on the application of the boundary element methods. The domain where nonlinear deformations occur is linked to a domain where linear elasticity

models apply using the time-domain Green's functions. To enable efficient coupling, the time-domain Green's functions should be as simple as possible, which is difficult to achieve when working with models that contain frequency-dependent coefficients. This motivates introduction of a sufficiently accurate linear model with coefficients that do not depend on frequency.

Higher-order continuum models are often used when more accurate description of the microstructure of a medium has to be taken into account, not captured by the classical continuum. This is required, for example, to mimic dispersion properties of an inhomogeneous medium for more accurate modeling. Higher-order continuum models are used to account for the influence of the processes on a microscale on a higher scale of observation (macroscale). Such models can be derived by means of homogenization of continua with microstructure. They give more accurate predictions compared to the classical continuum at shorter wavelengths. In this thesis, we are dealing with porous media containing mesoscopic heterogeneities.

For the periodically layered porous media considered in Chapter 3, the microstructure is represented by the periodic cell, and a higher-order continuum can be derived to account for the presence of layered heterogeneities. Higher-order homogenization was extensively studied for periodically layered elastic solids (Chen and Fish, 2001, Fish et al., 2002, Andrianov et al., 2008). In this chapter, it is applied to a poroelastic solid. Prior to that, we derive a higher-order viscoelastic continuum from the dispersion equation obtained from White's model (White et al., 1975), by matching the associated dispersion relation and that of the postulated higher-order continuum model for low frequencies. The resulting equation contains higher-order spatial and temporal derivatives of the displacement. Next, homogenization with multiple spatial scales is applied to a poroelastic composite governed by Biot's equations (Biot, 1956a). A method of asymptotic expansions with multiple spatial scales (Benssousan et al., 1978, Sanchez-Palencia, 1980, Bakhvalov and Panasenko, 1989) is extensively used for homogenization of heterogeneous media. In poroelasticity, the method was applied to derive macroscopic equations of motion from microstructure by Burridge and Keller (1981). Similar work was done by Levy (1979). Studies on higher-order homogenization of periodic elastic composites can be found in Chen and Fish (2001), Fish et al. (2002) and Andrianov et al. (2008). Further extensions to non-periodic cases and multiple dimensions are described in Capdeville et al. (2010a,b). The method and its advantages are comprehensively described by Auriault (1980b, 2002), where

examples are given, including porous-media examples. Homogenization with multiple scales is applied by Mei and Auriault (1989) to problems of flow in porous media and consolidation. Here we apply the method to wave propagation in a periodically layered poroelastic composite.

5.2 White's model for periodically layered porous media

The model of White et al. (1975) has been discussed in Chapter 3, where a solution in terms of the full Biot equations proposed by Dutta and Seriff (1979) and Vogelaar and Smeulders (2007) was used in numerical examples. In this chapter, we use the original solution by White et al. (1975), where an analytical expression for the effective P-wave modulus $\hat{K}(\omega)$ is given:

$$\hat{K}(\omega) = \frac{K^*}{1 + \mathrm{i}\frac{2(R_I - R_{II})^2}{\omega L (Z_I + Z_{II})}}, \tag{5.1}$$

where L is the length of a periodic cell, and other coefficients are defined in terms of properties of the layers I and II:

$$\begin{aligned}
\frac{1}{K^*} &= \frac{1-s}{K_I} + \frac{s}{K_{II}}, \\
K_{I,II} &= \left(K_m + K_a \left(1 - \frac{K_m}{K_s}\right)^2 + \frac{4}{3}\mu \right)_{I,II}, \\
R_{I,II} &= \left(\left(1 - \frac{K_m}{K_s}\right) \frac{K_a}{M} \right)_{I,II}, \\
Z_{I,II} &= \left(Z_0 \cot\left(\frac{1}{2}\alpha_w l\right) \right)_{I,II},
\end{aligned} \tag{5.2}$$

where K_m is a drained frame bulk modulus, μ is a shear modulus, K_s is the solid grains bulk modulus, K_f is the bulk modulus of the pore fluid, ϕ is porosity, l_I and l_{II} are the length of the layers I and II in the periodic cell, respectively, and

$s = l_{II}/L$. For each layer I and II

$$\begin{aligned} K_a &= \left(\frac{1-\phi}{K_s} - \frac{K_m}{K_s^2} + \frac{\phi}{K_f} \right)^{-1}, \\ Z_0 &= \sqrt{\eta K_e \mathrm{i}/(\omega k_0)}, \qquad \alpha_w = \sqrt{-\mathrm{i}\omega\eta/(k_0 K_e)}, \\ K_e &= K_a(K_m + \frac{4}{3}\mu)/K, \end{aligned} \tag{5.3}$$

where η is the fluid viscosity and k_0 denotes permeability of the solid frame. The plane-wave modulus $\hat{K}(\omega)$ defined in (5.1) is used in the description of one-dimensional P-wave propagation in a viscoelastic medium governed by the following equation of motion

$$-\omega^2 \rho \hat{u} - \hat{K}(\omega)\hat{u}_{,zz} = 0, \tag{5.4}$$

where the density term $\rho = (1-s)\left(\phi\rho_s + (1-\phi)\rho_f\right)_I + s\left(\phi\rho_s + (1-\phi)\rho_f\right)_{II}$ and ρ_s and ρ_f are the densities of the solid grains and fluid, respectively. The solution of the equation (5.4) is $\hat{u} = \hat{A}\exp(-\mathrm{i}kz)$, and the corresponding dispersion equation reads

$$k^2 = \omega^2 \frac{\rho}{\hat{K}(\omega)}. \tag{5.5}$$

5.3 Derivation of effective models with frequency-independent coefficients

5.3.1 Viscoleastic model approximating White's model dispersion relation

The equation of motion describing the effective medium is chosen such that it predicts the same frequency dependence of the wavenumber as White's model in the frequency range of interest. The frequency dependence of k in (5.5) is rather complicated. We expand $\omega^2\rho/\hat{K}(\omega)$ in series of ω around $\omega = 0$, up to the order $\mathcal{O}(\omega^5)$:

$$k^2 = f_2\omega^2 - \mathrm{i}f_3\omega^3 - f_4\omega^4 + \mathcal{O}(\omega^5). \tag{5.6}$$

The expansion coefficients f_i read:

$$\begin{aligned} f_2 &= \frac{\rho}{H}, \quad H = \left(\frac{K^*(R_{II} - R_I)^2 + Lg_1}{K^* L g_1} \right)^{-1}, \\ f_3 &= \frac{1}{3}\mathrm{i}\rho \frac{(R_{II} - R_I)^2 g_1 g_2}{L g_1^2}, \\ f_4 &= \frac{1}{45}\rho \frac{(R_{II} - R_I)^2 g_3 g_2}{L g_1^3}, \end{aligned} \tag{5.7}$$

where

$$\begin{aligned} g_1 &= n_I h_{II} + n_{II} h_I, \\ g_2 &= n_I^2 n_{II}^2, \\ g_3 &= h_I h_{II} \left(n_I^4 + 10 g_2 + n_{II}^4 \right) + 6 n_I n_{II} \left(n_I^2 h_I^2 + n_{II}^2 h_{II}^2 \right), \end{aligned} \tag{5.8}$$

in which the following notations were introduced:

$$n_{I,II} = \left(\frac{\eta}{K_e k_0} \right)_{I,II}, \qquad h_{I,II} = \left(\frac{\eta K_e}{k_0} \right)_{I,II}. \tag{5.9}$$

Let us take the approximation $k^2 = f_2 \omega^2$. This dispersion relation corresponds to the classical wave equation, whose frequency domain form reads

$$-\rho \omega^2 \hat{u} - H \hat{u}_{,zz} = 0. \tag{5.10}$$

At the low frequency band, where $f_2 >> f_3 \omega$ and $f_2 >> f_4 \omega^2$, equation (5.6) can be approximated by the following equations, in which ω^2 in the terms proportional to ω^3 and ω^4 is either fully or partially replaced by k^2/f_2:

$$k^2 = f_2 \omega^2 - \mathrm{i} \frac{f_3}{f_2} \omega k^2 - \frac{f_4}{f_2} \omega^2 k^2, \tag{5.11}$$

$$k^2 = f_2 \omega^2 - \mathrm{i} \frac{f_3}{f_2} \omega k^2 - f_4 \omega^4. \tag{5.12}$$

Restricting the expansion order to ω^3, the above equations can be further simplified to

$$k^2 = f_2 \omega^2 - \mathrm{i} \frac{f_3}{f_2} \omega k^2. \tag{5.13}$$

The equations of motion, corresponding to equations (5.11)–(5.13) read

$$\begin{aligned} u_{,zz} &= f_2\ddot{u} - \tfrac{f_3}{f_2}\dot{u}_{,zz} + \tfrac{f_4}{f_2}\ddot{u}_{,zz}, \\ u_{,zz} &= f_2\ddot{u} - \tfrac{f_3}{f_2}\dot{u}_{,zz} + f_4\dddot{u}, \\ u_{,zz} &= f_2\ddot{u} - \tfrac{f_3}{f_2}\dot{u}_{,zz}. \end{aligned} \tag{5.14}$$

These are approximations of White's model. They are also governed by the viscoelastic equations, as White's model, but the effective coefficients do not depend on frequency, and higher-order derivatives are introduced. We will now discuss another approximation, where effective model is governed by the equations of poroelasticity with higher-order terms. The results for all models are discussed in Section 5.4.

5.3.2 Poroelastic model obtained from homogenization with multiple spatial scales

Within the concept of separation of scales in the asymptotic two-scale homogenization method of Sanchez-Palencia (1980), the macroscopic scale is associated with some parameter of length $\tilde{L}$ that is of the same order as the length of the travelling wave, and the microscopic scale is the characteristic size of heterogeneities which is the period of the system, the length of the unit cell L. The following small parameter is introduced: $\varepsilon = L/\tilde{L}$. Two space variables are introduced: x and $y = x/\varepsilon$. These variables are treated as two independent space variables corresponding to the variations along the axis normal to the layering (denoted by z in the previous section) on length scales L and $\tilde{L}$, respectively.

The displacement vector $\mathbf{u} = [u, \quad w]^T$, where u and w are solid and relative fluid-to-solid particle displacements, respectively, is looked for in the form of the expansion

$$\mathbf{u} = \mathbf{u}_0(x, y, t) + \varepsilon\mathbf{u}_1(x, y, t) + \varepsilon^2\mathbf{u}_2(x, y, t) + ..., \tag{5.15}$$

where $\mathbf{u}_i(x, y, t)$ are $\tilde{L}$-periodic with respect to y. Since $y = y(x)$, the full spatial derivative should now be expressed using the chain rule:

$$f_{;x} = f_{,x} + \varepsilon^{-1} f_{,y}, \tag{5.16}$$

where the semicolon in the subscript denotes the full derivative. The stress vector $\boldsymbol{\sigma} = [\tau, -p]^T$, where τ denotes the total stress $\tau = -\sigma - p$, σ is intergranular stress and p is pore fluid pressure. This vector is related to the displacement vector via the stress-strain relations from Biot's theory (Biot, 1956a):

$$\boldsymbol{\sigma} = \mathbf{E}\mathbf{u}_{;x}, \tag{5.17}$$

where matrix $\mathbf{E}$ is given below. Subsituting (5.15) into (5.17) and taking into account (5.16) gives:

$$\boldsymbol{\sigma} = \varepsilon^{-1}\boldsymbol{\sigma}_{-1}(x,y,t) + \boldsymbol{\sigma}_0(x,y,t) + \varepsilon\boldsymbol{\sigma}_1(x,y,t) + \varepsilon^2\boldsymbol{\sigma}_2(x,y,t) + ..., \tag{5.18}$$

where

$$\begin{aligned} &\boldsymbol{\sigma}_i = \mathbf{E}\left(\mathbf{u}_{i,x} + \mathbf{u}_{i+1,y}\right), \quad i = 0,1,2,..., \\ &\boldsymbol{\sigma}_{-1} = \mathbf{E}\mathbf{u}_{0,y}. \end{aligned} \tag{5.19}$$

Each of the layers is governed by Biot's equations of poroelasticity of (Biot, 1956a) reviewed in Chapter 2:

$$\mathbf{P}^{(a,b)}\ddot{\mathbf{u}}^{(a,b)} + \mathbf{B}^{(a,b)}\dot{\mathbf{u}}^{(a,b)} - \mathbf{E}^{(a,b)}\mathbf{u}_{;xx} = \mathbf{0}, \tag{5.20}$$

where superscripts a and b distinguish the regions $0 \le y \le s\tilde{L}$ and $s\tilde{L} \le y \le \tilde{L}$, respectively. In equation (5.20) the elements of the matrices $\mathbf{P}$, $\mathbf{B}$ and $\mathbf{E}$ contain the physical properties of the layers corresponding to the regions a and b:

$$\mathbf{P} = \begin{bmatrix} (1-\phi)\rho_s + \phi\rho_f & \rho_f \\ \rho_f & \frac{\alpha\rho_f}{\phi} \end{bmatrix}, \mathbf{B} = \begin{bmatrix} 0 & 0 \\ 0 & \frac{b_0}{\phi^2} \end{bmatrix}, \mathbf{E} = \begin{bmatrix} P+2Q+R & \frac{Q+R}{\phi} \\ \frac{Q+R}{\phi} & \frac{R}{\phi^2} \end{bmatrix}. \tag{5.21}$$

The following notations are used above: α is tortuosity and b_0 is Biot's viscous factor $b_0 = \eta\phi^2/k_0$. The poroelastic coefficients P, Q, R are given in (3.2).

The expansion of $\mathbf{u}$ (5.15) is substituted into the governing equation (5.20) for each of the layers. Each power of ε in the resulting equation can be equated to zero, thus forming a set of equations that is solved successively with the following boundary conditions (i.e., $\tilde{L}$-periodicity of the displacement and stress vectors,

and continuity of these vectors at the interface between the layers):

$$\begin{aligned}
&\mathbf{u}_i^{(a)}(x,0,t) = \mathbf{u}_i^{(b)}(x,\tilde{L},t),\\
&\boldsymbol{\sigma}_{i-1}^{(a)}(x,0,t) = \boldsymbol{\sigma}_{i-1}^{(b)}(x,\tilde{L},t),\\
&\mathbf{u}_i^{(a)}(x,s\tilde{L},t) = \mathbf{u}_i^{(b)}(x,s\tilde{L},t),\\
&\boldsymbol{\sigma}_{i-1}^{(a)}(x,s\tilde{L},t) = \boldsymbol{\sigma}_{i-1}^{(b)}(x,s\tilde{L},t), \quad i = 0,1,2,... \quad .
\end{aligned} \tag{5.22}$$

In addition, an averaging operator is introduced:

$$\mathbf{U}_i(x,t) = \frac{1}{\tilde{L}}\left(\int_0^{s\tilde{L}} \mathbf{u}_i^{(a)} dy + \int_{s\tilde{L}}^{\tilde{L}} \mathbf{u}_i^{(b)} dy\right), \quad i = 0,1,2,... \quad , \tag{5.23}$$

where $\mathbf{U}_i(x,t)$ denotes the macroscopic displacement vector.

Equating the terms of ε^{-2} to zero, the following part from equation (5.20) remains:

$$\mathbf{E}^{(a,b)}\mathbf{u}_{0,yy}^{(a,b)} = \mathbf{0}. \tag{5.24}$$

Solving this equation for the regions a and b using the boundary conditions (5.22) ($i = 0$) leads to a simple result: $\mathbf{u}_0^{(a)} = \mathbf{u}_0^{(b)} = \mathbf{U}_0(x)$.

Equating the terms of ε^{-1} to zero gives

$$\mathbf{E}^{(a,b)}\left(\mathbf{u}_{0,x}^{(a,b)} + \mathbf{u}_{1,y}^{(a,b)}\right)_{,y} = \mathbf{0}. \tag{5.25}$$

The solution of (5.25) is $\mathbf{u}_1^{(a)} = \mathbf{a}_1 y + \mathbf{b}_1$ and $\mathbf{u}_1^{(b)} = \mathbf{c}_1 y + \mathbf{d}_1$, where $\mathbf{a}_1$, $\mathbf{b}_1$, $\mathbf{c}_1$ and $\mathbf{d}_1$ are the vectors of unknown functions of x and t found from the boundary conditions (5.22) and related to $\mathbf{U}_1$ using (5.23).

Equating the terms of ε^0 to zero results in the following equation:

$$\mathbf{P}^{(a,b)}\ddot{\mathbf{u}}_0^{(a,b)} + \mathbf{B}^{(a,b)}\dot{\mathbf{u}}_0^{(a,b)} - \mathbf{E}^{(a,b)}\left(\mathbf{u}_{0,xx}^{(a,b)} + 2\mathbf{u}_{1,xy}^{(a,b)} + \mathbf{u}_{2,yy}^{(a,b)}\right) = \mathbf{0}. \tag{5.26}$$

Integrating (5.26) over the unit cell $y = [0, \tilde{L}]$ and taking into account periodicity of $\boldsymbol{\sigma}_1$ leads to the macroscopic equation of motion for $\mathbf{U}_0$:

$$\mathbf{P}_0\ddot{\mathbf{U}}_0 + \mathbf{B}_0\dot{\mathbf{U}}_0 - \mathbf{E}_0\mathbf{U}_{0,xx} = \mathbf{0}, \tag{5.27}$$

where the matrices are defined as

$$\mathbf{P}_0 = s\mathbf{P}_1 + (1-s)\mathbf{P}_2, \qquad \mathbf{B}_0 = s\mathbf{B}_1 + (1-s)\mathbf{B}_2,$$

$$\mathbf{E}_0 = s\mathbf{E}_1 + (1-s)\mathbf{E}_2 + s(1-s)(\mathbf{E}_2 - \mathbf{E}_1)(s\mathbf{E}_2 + (1-s)\mathbf{E}_1)^{-1}(\mathbf{E}_1 - \mathbf{E}_2). \tag{5.28}$$

For an elastic composite, the matrices in (5.28) reduce to scalars, and the matrix of the effective moduli $\mathbf{E}_0$ reduces to the well-known harmonic average of the moduli of the layers.

The next-order term $\mathbf{u}_2^{(a,b)}$ is found by solving equation (5.26) in the form of polynomial $\mathbf{u}_2^{(a,b)} = \mathbf{a}_2^{(a,b)} y^2 + \mathbf{b}_2^{(a,b)} y + \mathbf{c}_2^{(a,b)}$, where the vectors $\mathbf{b}_2^{(a,b)}$ and $\mathbf{c}_2^{(a,b)}$ are found from the boundary conditions (5.22) and using the expression (5.23) for $\mathbf{U}_2$, and the vectors $\mathbf{a}_2^{(a,b)}$ are derived from equation (5.26).

Equating the terms of ε^1 to zero gives:

$$\mathbf{P}^{(a,b)}\ddot{\mathbf{u}}_1^{(a,b)} + \mathbf{B}^{(a,b)}\dot{\mathbf{u}}_1^{(a,b)} - \mathbf{E}^{(a,b)}\left(\mathbf{u}_{1,xx}^{(a,b)} + 2\mathbf{u}_{2,xy}^{(a,b)} + \mathbf{u}_{3,yy}^{(a,b)}\right) = \mathbf{0}. \tag{5.29}$$

Integrating (5.29) over the unit cell $y = [0, \tilde{L}]$ and taking into account periodicity of $\boldsymbol{\sigma}_2$ and the equation (5.27) leads to the macroscopic equation of motion for $\mathbf{U}_1$:

$$\mathbf{P}_0\ddot{\mathbf{U}}_1 + \mathbf{B}_0\dot{\mathbf{U}}_1 - \mathbf{E}_0\mathbf{U}_{1,xx} = \mathbf{0}. \tag{5.30}$$

The next-order term $\mathbf{u}_3^{(a,b)}$ is found from the equation (5.29), similar to the previous terms.

Equating the terms of ε^2 to zero gives

$$\mathbf{P}^{(a,b)}\ddot{\mathbf{u}}_2^{(a,b)} + \mathbf{B}^{(a,b)}\dot{\mathbf{u}}_2^{(a,b)} - \mathbf{E}^{(a,b)}\left(\mathbf{u}_{2,xx}^{(a,b)} + 2\mathbf{u}_{3,xy}^{(a,b)} + \mathbf{u}_{4,yy}^{(a,b)}\right) = \mathbf{0}. \tag{5.31}$$

Implementing the same integration as above, and taking into account (5.27) and (5.30), we come to the macroscopic equation for $\mathbf{U}_2$:

$$\mathbf{P}_0\ddot{\mathbf{U}}_2 + \mathbf{B}_0\dot{\mathbf{U}}_2 - \mathbf{E}_0\mathbf{U}_{2,xx} - \tilde{L}^2\left(\boldsymbol{\alpha}_1\mathbf{U}_{0,xxxx} + \boldsymbol{\alpha}_2\dot{\mathbf{U}}_{0,xx} + \boldsymbol{\alpha}_3\ddot{\mathbf{U}}_0\right) = \mathbf{0}. \tag{5.32}$$

The expressions for the matrices $\boldsymbol{\alpha}_{1-3}$ in this equation are given in Appendix 5.A. In the absence of terms $\boldsymbol{\alpha}_2$ and $\boldsymbol{\alpha}_3$ (when there is no damping terms b_0 in each of the layers), (5.32) is canceled out to the equation obtained for the elastic composite (Fish et al., 2002, Andrianov et al., 2008) assuming the matrices from (5.21) are scalars.

Now, we combine the macroscopic equations derived above to come up with a single macroscopic description of the effective medium. The macroscopic displacement, where orders up to ε^2 are kept, reads: $\mathbf{U} = \mathbf{U}_0 + \varepsilon\mathbf{U}_1 + \varepsilon^2\mathbf{U}_2$. Substitution of $\mathbf{U}$ into the summation (5.27) + $\varepsilon\cdot$ (5.30) + $\varepsilon^2\cdot$ (5.32) and keeping the terms up to order ε^0 results in

$$\mathbf{P}_0\ddot{\mathbf{U}} + \mathbf{B}_0\dot{\mathbf{U}} - \mathbf{E}_0\mathbf{U}_{,xx} - L^2\left(\boldsymbol{\alpha}_1\mathbf{U}_{,xxxx} + \boldsymbol{\alpha}_2\dot{\mathbf{U}}_{,xx} + \boldsymbol{\alpha}_3\ddot{\mathbf{U}}\right) = 0. \tag{5.33}$$

Note that only one length scale L, which is the length of the periodic cell, is left in the final equation (5.33). The length scale $\tilde{L}$ is reduced in the multiplication of $\varepsilon = L/\tilde{L}$ to the last three terms in equation (5.32). The first three terms in equation (5.33) are the classical Biot terms for a homogeneous medium with the matrices of density and damping terms determined as the arithmetic averages of the corresponding matrices of each of the layers, and the matrix of elastic moduli determined as the harmonic average of the corresponding matrices of the layers. As discussed above, a similar result is known for elastic composites, where the effective density is the arithmetic average of the densities of the layers, and the effective Young's modulus is the harmonic average of the moduli of the layers. The higher-order terms are corrections that explicitly contain information about the scale of heterogeneities: apart from the properties of the layers and saturations, they also depend on the characteristic size of heterogeneities, which is the length of the periodic unit cell L.

The dispersion equation corresponding to equation (5.33) has four pairs of roots with opposite signs. It predicts four P-waves in each direction: a fast and a slow wave, as predicted by Biot's theory, and two additional highly attenuated waves, which are the results of the scattering of the fast and the slow wave by the inhomogeneities. The corresponding wavenumbers are found as the roots of the polynomial equation:

$$\begin{aligned}
&\omega^4(\tilde{P}_{1,1}\tilde{P}_{2,2} - \tilde{P}_{1,2}\tilde{P}_{2,1}) + \omega^2(\tilde{P}_{1,2}\tilde{H}_{2,1} - \tilde{H}_{1,1}\tilde{P}_{2,2} + \tilde{H}_{1,2}\tilde{P}_{2,1} - \tilde{P}_{1,1}\tilde{H}_{2,2})k^2 + \\
&(\omega^2L^2(\tilde{P}_{1,1}\alpha_1^{2,2} - \tilde{P}_{1,2}\alpha_1^{2,1} + \tilde{P}_{2,2}\alpha_1^{1,1} - \tilde{P}_{2,1}\alpha_1^{1,2}) - \tilde{H}_{2,1}\tilde{H}_{1,2} + \tilde{H}_{1,1}\tilde{H}_{2,2})k^4 + \\
&L^2(\tilde{H}_{1,2}\alpha_1^{2,1} + \alpha_1^{1,2}\tilde{H}_{2,1} - \tilde{H}_{2,2}\alpha_1^{1,1} - \tilde{H}_{1,1}\alpha_1^{2,2})k^6 + L^2(\alpha_1^{1,1}\alpha_1^{2,2} - \alpha_1^{1,2}(\alpha_1^{2,1})k^8 = 0,
\end{aligned} \tag{5.34}$$

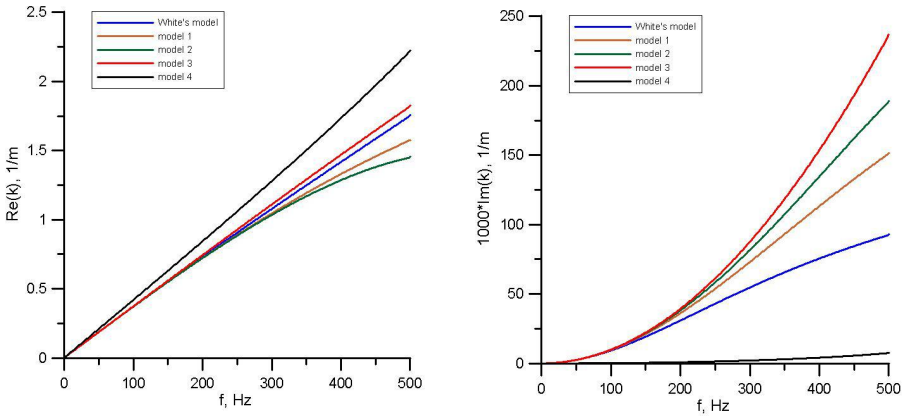

(a) (b)

FIGURE 5.1: Real (a) and imaginary (b) parts of the wavenumber predicted by different models L=0.1 m, gas saturation 10%.

where $\alpha_1^{i,j}$ are the elements of the matrix $\boldsymbol{\alpha}_1$ and $\tilde{P}_{i,j}$ and $\tilde{H}_{i,j}$ are the elements of the matrices

$$\begin{aligned} \tilde{\mathbf{P}} &= \mathbf{P} + \mathbf{B}/(\mathrm{i}\omega) - L^2\boldsymbol{\alpha}_3, \\ \tilde{\mathbf{H}} &= \mathbf{E}_0 + \mathrm{i}\omega\boldsymbol{\alpha}_2. \end{aligned} \tag{5.35}$$

5.4 Results

In this section we compare predictions of dispersion and attenuation by the models with frequency-independent coefficients discussed above. The material properties of the solid frame in the example are those of Rock from Table 4.1. The pores are fully saturated with water and gas (Table 3.2). It has been shown in Chapters 3 and 4 that White's model is in agreement with the exact solution for this type of material properties, therefore it is used here for reference.

In Figures 5.1–5.3, the real and imaginary parts of the wavenumbers are plotted for different models: model 1 (equation 5.11), model 2 (equation 5.12), model 3 (equation 5.13), and model 4 (equation 5.34, the root corresponding to the fast P-wave is considered). The results are plotted for a fixed periodic cell $L = 0.1$ m, for saturations $s = 10\%$ (Figure 5.1), $s = 50\%$ (Figure 5.2) and $s = 90\%$ (Figure 5.3). As one can observe in all figures, the models obtained in the previous section (model 4) predicts dispersion and attenuation only at low frequencies, and the predictions deviate from the predictions of White's model at higher frequencies. For all models, the predictions are more accurate at high gas saturations. For

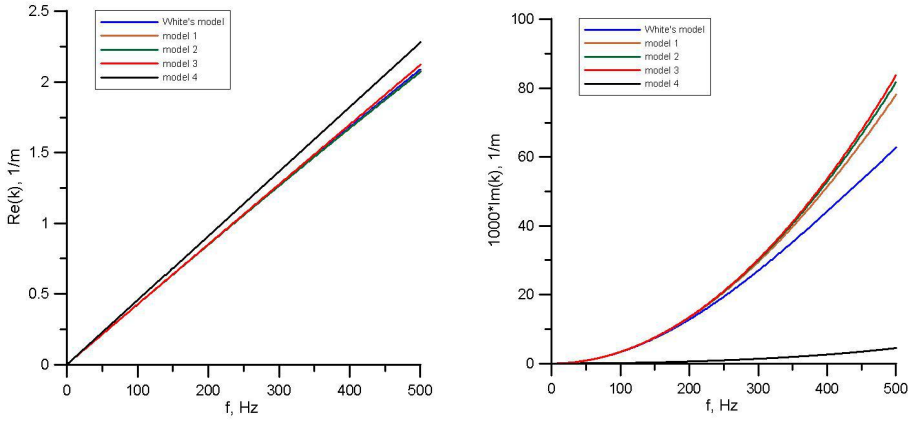

(a) (b)

FIGURE 5.2: Real (a) and imaginary (b) parts of the wavenumber predicted by different models L=0.1 m, gas saturation 50%.

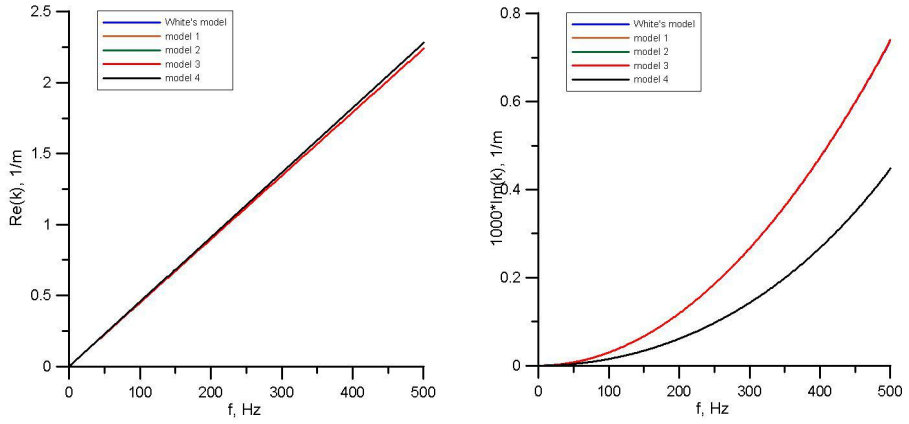

(a) (b)

FIGURE 5.3: Real (a) and imaginary (b) parts of the wavenumber predicted by different models L=0.1m, gas saturation 90%. On the rightmost panel all lines for models 1–3 and White's model coincide.

saturation $s = 90\%$ (Figure 5.3), all lines corresponding to models 1–3 coincide; they are also very close to each other in Figure 5.2, for saturation $s = 50\%$.

5.5 Conclusions

The method of asymptotic expansions with multiple spatial scales was applied to wave propagation in a poroelastic composite with a periodically repeated unit cell that consists of two layers with different properties, each layer governed by

Biot's equations. The results show that this model underestimates attenuation; its performance is getting worse at higher frequencies. One should note that the method of asymptotic expansions is formally only correct when the physical constants are of the same order, which is not always the case for poroelastic constants in media with heterogeneities, especially when heterogeneities occur in saturating fluid properties. That is why models obtained directly from White's model provide more accurate predictions of attenuation. These models are also viscoelastic models, like the model of White, but incorporate higher-order derivatives to account for the presence of heterogeneities. They can be used at sufficiently low frequencies for thinly layered poroelastic composites, where the model of White is also applicable. The advantages of models with coefficients that do not depend on frequency is the possibility to use them for efficient time-domain computations.

5.A Effective coefficients

The expressions for the matrices $\boldsymbol{\alpha}_1$, $\boldsymbol{\alpha}_2$ and $\boldsymbol{\alpha}_3$ from equation (5.33) are given in this appendix. The expression for $\boldsymbol{\alpha}_1$ reads

$$\boldsymbol{\alpha}_1 = -\mathbf{c}_1 \left(\mathbf{P}_0^{-1}\mathbf{E}_0\right)^2 + \mathbf{c}_2\mathbf{P}_0^{-1}\mathbf{E}_0 + \mathbf{c}_3, \tag{5.36}$$

where

$$\mathbf{c}_1 = \tfrac{1}{12}\left(\mathbf{P}_1 - \mathbf{P}_2\right)\left(s(s^3 - s^2)\mathbf{E}_1^{-1}\mathbf{P}_1 + s(-s^3 + 3s^2 - 3s + 1)\mathbf{E}_2^{-1}\mathbf{P}_2\right), \tag{5.37}$$

$$\mathbf{c}_2 = \tfrac{s(\mathbf{P}_1-\mathbf{P}_2)}{12}\left((2s^2-4s+2)\mathbf{D}(\mathbf{E}_1-\mathbf{E}_2)+(2s^2-3s+1)\mathbf{I}\right)+$$

$$\tfrac{\mathbf{E}_1-\mathbf{E}_2}{12s^2}\left[((9s^3-3s^5-6s^2)\mathbf{D}\mathbf{E}_1+(s^6-9s^5+2s^4+6s^3)\mathbf{I})\mathbf{D}\mathbf{P}_1-\mathbf{D}((2s^4-s^5-s^3)\mathbf{P}_1\right.$$

$$-(6s^4-6s^3)\mathbf{P}_2)\mathbf{D}(\mathbf{E}_1-\mathbf{E}_2)-(s^6-s^5)(\mathbf{D}\mathbf{E}_2-\mathbf{I})\mathbf{E}_1^{-1}\mathbf{P}_1$$

$$-\mathbf{D}((3s^5-12s^3+6s^2+9s-6)\mathbf{E}_1-3s(s-1)(s^3+3s^2-s-3)\mathbf{E}_2)\mathbf{D}\mathbf{E}_1\mathbf{E}_2^{-1}\mathbf{P}_2$$

$$+\mathbf{D}\mathbf{E}_2\mathbf{D}((18s^3-6s^5-12s^4)\mathbf{P}_2+3s^2(s^3+2s^2-3s)\mathbf{P}_1)+$$

$$((s^6+11s^5+3s^4-7s^3-8s^2)\mathbf{I}+6s^2(s^3-3s+2)\mathbf{D}\mathbf{E}_1)\mathbf{D}\mathbf{P}_2+$$

$$((13s^2-s^5-3s^4-5s^3+6s-10)s\mathbf{D}\mathbf{E}_1+s^2(s-s^4-s^3-3s^2+4)\mathbf{I})\mathbf{E}_2^{-1}\mathbf{P}_2$$

$$\left.+(s(6s^2-s^4-2s^3-2s-1)\mathbf{D}\mathbf{E}_1+s^2(3s-s^3-3s^2+1)\mathbf{I})\mathbf{E}_2^{-1}\mathbf{P}_2\mathbf{D}(\mathbf{E}_1-\mathbf{E}_2)\right], \tag{5.38}$$

$$\mathbf{c}_3 = \tfrac{\mathbf{E}_1-\mathbf{E}_2}{12s}\left[((2s^4+3s^3-s^2-4s)\mathbf{I}+\mathbf{D}\left(\mathbf{E}_1(19s^4+10s^3-24s^2-15s+10)+\right.\right.$$

$$\mathbf{E}_2(12s^2-19s^4-10s^3+17s)+\mathbf{D}\mathbf{E}_1\mathbf{D}(\tfrac{2}{s}(13s^5-s^4-28s^3+4s^2+15s-3)\mathbf{E}_1+$$

$$(2s^3-26s^4+53s^2-8s-21)\mathbf{E}_2)+\mathbf{D}\mathbf{E}_2\mathbf{D}((26s^4+28s^3-32s^2-22s)\mathbf{E}_2+$$

$$(35s^2-26s^4-28s^3+28s-9)\mathbf{E}_1)+3\mathbf{D}\left((\tfrac{1}{s}(3s^5-s^4-11s^3+9s^2+4s-4)\mathbf{E}_1\right.$$

$$-(3s^4+5s^3-13s^2-s+6)\mathbf{E}_2)\mathbf{D}\mathbf{E}_1+((s(3s^3+7s^2-7s-3)\mathbf{E}_2-$$

$$\left.\left.-\ (s-1)(3s^3+4s^2-5s-2)\mathbf{E}_1)\mathbf{D}\mathbf{E}_2\right)\mathbf{D}(\mathbf{E}_1-\mathbf{E}_2)\right]. \tag{5.39}$$

In equations (5.37)–(5.39),

$$\mathbf{D} = s(s\mathbf{E}_2+(1-s)\mathbf{E}_1)^{-1}, \quad \mathbf{I} \quad \text{is an identity matrix.} \tag{5.40}$$

The expression for $\boldsymbol{\alpha}_2$ is

$$\boldsymbol{\alpha}_2 = \mathbf{c}_1\left(\mathbf{P}_0^{-1}\mathbf{E}_0\mathbf{P}_0^{-1}\mathbf{B}_0+\mathbf{P}_0^{-1}\mathbf{B}_0\mathbf{P}_0^{-1}\mathbf{E}_0\right)-\mathbf{c}_2\mathbf{P}_0^{-1}\mathbf{B}_0+\mathbf{c}_4-\mathbf{c}_5\mathbf{P}_0^{-1}\mathbf{E}_0, \tag{5.41}$$

where

$$\mathbf{c}_4 = \tfrac{s(\mathbf{B}_1-\mathbf{B}_2)}{12}\left((2s^2-4s+2)\mathbf{D}(\mathbf{E}_1-\mathbf{E}_2)+(2s^2-3s+1)\mathbf{I}\right)+$$

$$\tfrac{\mathbf{E}_1-\mathbf{E}_2}{12}\left[(s+4-s^4-s^3-3s^2)\mathbf{I}+\tfrac{1}{s}(13s^2+6s-10-s^5-3s^4-5s^3)\mathbf{D}\mathbf{E}_1\right.$$

$$+(s^4+11s^3+3s^2-7s-8)\mathbf{D}\mathbf{E}_2-\tfrac{3}{s^2}(s^5-4s^3+2s^2+3s-2)\mathbf{D}\mathbf{E}_1\mathbf{D}\mathbf{E}_1+$$

$$+(6s^3-18s+12)\mathbf{D}\mathbf{E}_1\mathbf{D}\mathbf{E}_2+\tfrac{3}{s}(s-1)(s^3+3s^2-s-3)\mathbf{D}\mathbf{E}_2\mathbf{D}\mathbf{E}_1-$$

$$-6s(s^2+2s-3)\mathbf{D}\mathbf{E}_2\mathbf{D}\mathbf{E}_2)\mathbf{E}_2^{-1}\mathbf{B}_2+((3s+1-s^3-3s^2)\mathbf{I}+$$

$$+6s(s-1)\mathbf{D}\mathbf{E}_2+\tfrac{1}{s}(6s^2-2s-1-s^4-2s^3)\mathbf{D}\mathbf{E}_1)\mathbf{E}_2^{-1}\mathbf{B}_2\mathbf{D}(\mathbf{E}_1-\mathbf{E}_2)+$$

$$+((s^4-s^3)\mathbf{I}+s(s^3-9s^2+2s+6)\mathbf{D}\mathbf{E}_1+(9s-3s^3-6)\mathbf{D}\mathbf{E}_1\mathbf{D}\mathbf{E}_1+$$

$$+(s^3-s^4)\mathbf{D}\mathbf{E}_2+(3s^3+6s^2-9s)\mathbf{D}\mathbf{E}_2\mathbf{D}\mathbf{E}_1)\mathbf{E}_1^{-1}\mathbf{B}_1+$$

$$\left.+\,s(s^2-2s+1)\mathbf{D}\mathbf{E}_1\mathbf{E}_1^{-1}\mathbf{B}_1\mathbf{D}(\mathbf{E}_1-\mathbf{E}_2)\right].$$

$$\mathbf{c}_5 = \tfrac{1}{12}\left(\mathbf{P}_1-\mathbf{P}_2\right)s((s^3-s^2)\mathbf{E}_1^{-1}\mathbf{B}_1+(3s^2-s^3-3s+1)\mathbf{E}_2^{-1}\mathbf{B}_2)+$$

$$+\tfrac{1}{12}\left(\mathbf{B}_1-\mathbf{B}_2\right)s((s^3-s^2)\mathbf{E}_1^{-1}\mathbf{P}_1+(3s^2-s^3-3s+1)\mathbf{E}_2^{-1}\mathbf{P}_2). \tag{5.42}$$

The expression for $\boldsymbol{\alpha}_3$ is

$$\boldsymbol{\alpha}_3 = -\mathbf{c}_6+\mathbf{c}_5\mathbf{B}_0^{-1}\mathbf{E}_0-\mathbf{c}_1(\mathbf{P}_0^{-1}\mathbf{B}_0)^2, \tag{5.43}$$

where

$$\mathbf{c}_6 = \frac{1}{12}\left(\mathbf{B}_1-\mathbf{B}_2\right)s((s^3-s^2)\mathbf{E}_1^{-1}\mathbf{B}_1+(3s^2-s^3-3s+1)\mathbf{E}_2^{-1}\mathbf{B}_2). \tag{5.44}$$

Chapter 6

An effective anisotropic poroelastic model for elastic wave propagation in finely layered media

In this chapter, a new effective poroelastic model for finely layered media is presented and its performance is evaluated focusing on the angle-dependent attenuation behavior. To enable this, an exact solution is obtained for the response of a periodically layered medium to a surface point load using Floquet's theory. This solution is compared to that of the new model and the equivalent viscoelastic VTI medium available from existing literature. It is observed that the qP-wave dispersion and attenuation is predicted with high accuracy by the new effective poroelastic model. For the qS-wave, the effective poroelastic model provides a perceptibly better prediction of the attenuation, resulting in closer to the exact waveforms. The qS-wave attenuation is underestimated by the effective viscoelastic model, while for the qP-wave the model gives accurate predictions in all cases except for highly permeable weak-frame media.

This chapter was submitted for publication as a journal paper to *Geophysics*. Note that minor changes have been introduced to make the text consistent with the other chapters of this thesis.

6.1 Introduction

Horizontally layered models are commonly used for the analysis of wave propagation in reservoir rocks and sediments. This is a compromise between a relatively accurate representation of heterogeneities in rocks and simplicity of computations. Assuming lateral homogeneity of a reservoir is reasonable because the variations in rock properties in the direction normal to the layering are typical for most reservoir rocks and sediments. Layered models allow to study the effects of local inhomogeneities at the macroscopic scale. The layers can represent mesoscopic-scale heterogeneities when their thicknesses are much larger than the typical pore and grain sizes, but smaller than the wavelength of a propagating wave. Mesoscopic heterogeneities are known to cause strong dispersion and attenuation of seismic waves due to the sub-wavelength scale wave-induced fluid flow (Müller et al., 2010). The attenuation is particularly strong when a medium is saturated with different fluids with a large contrast in compressibility (White et al., 1975, Carcione and Picotti, 2006).

The commonly used equations for description of wave propagation in fluid-saturated media are Biot's equations of poroelasticity (Biot, 1962). This theory predicts one shear and two compressional waves in a macroscopically homogeneous medium. It is widely accepted that Biot's theory underestimates observed attenuation and dispersion of elastic waves (Johnston et al., 1979; Winkler, 1985; Gist, 1994). One of the reasons is a violation of the assumption of uniform saturation with a single fluid. Inhomogeneities in solid-frame properties also cause attenuation. Many models for wave propagation in heterogeneous porous media were developed to address this effect. Each model proposes an attenuation mechanism which is based on certain assumptions. These assumptions are related, among other things, to the scale of the heterogeneities and their distributions, and the frequency range of interest. Depending on the scale of observations, different models are used to study wave attenuation and dispersion. Attenuation due to dissipation at the pore scale is described by a squirt-flow mechanism (O'Connell and Budiansky, 1977; Mavko and Nur, 1979; Palmer and Traviola, 1980; Dvorkin and Nur, 1993). Differences in fluid saturation between thin compliant pores and larger stiffer ones, the presence of thin cracks, different shape and orientation of the pores, as well as distribution of immiscible fluids in a pore cause attenuation and dispersion due to local or squirt flow. This mechanism usually plays a role at ultrasonic frequencies. At seismic frequencies another attenuation mechanism

caused by the subwavelength-scale fluid flow due to the presence of mesoscopic-scale heterogeneities plays a role. This mechanism is not captured by Biot's theory which accounts for a global (wavelength-scale) flow attenuation mechanism. Since gas, oil and water are often present in rocks and sediments as mesoscopic-scale patches, multiple models are being developed that describe attenuation of seismic waves in such heterogeneous media.

One of the pioneering works on seismic attenuation caused by the wave-induced fluid flow is the work of White et al. (1975), in which a periodically layered porous medium was considered and a frequency-dependent plane-wave modulus was derived for normal wave incidence. Similar but differently derived moduli were reported in other publications: e.g., Norris (1993), Brajanovski and Gurevich (2005) and Vogelaar and Smeulders (2007). Some other models of effective P-wave moduli make use of a frequency-dependent branching function that connects the low- and high-frequency limits (e.g., Johnson, 2001). This approach was used by Krzikalla and Müller (2011), who introduced an effective vertical transverse isotropic (VTI) medium to describe propagation of qP- and qS-waves at different angles. In their model, the low- and high-frequency elastic moduli from poroelastic Backus averaging by Gelinsky and Shapiro (1997) are connected by a frequency-dependent function — the effective P-wave modulus of White et al. (1975) for periodic layering and normal incidence. For a randomly layered medium with a small fluctuation of parameters, the frequency-dependent function can be derived from Gelinsky et al. (1998). With the approach used by Krzikalla and Müller (2011), any model where a plane-wave modulus for P-wave propagation normal to the layering is derived can be extended for arbitrary angle of incidence. Another approach to compute the frequency-dependent coefficients of the effective VTI medium numerically was proposed by Carcione et al. (2011). The resulting effective medium in both approaches is governed by the equations of a viscoelastic VTI medium and has five complex-valued frequency-dependent stiffnesses. This means that the fluid-to-solid relative motion is not explicitly present in the model. Instead, the information about attenuation caused by the interaction of the fluid and solid phases at the subwavelength-scale is included in the frequency dependence of the effective stiffnesses. Furthermore, this effective model does not predict a slow P-wave on a macroscopic scale, as predicted by Biot's theory. On the one hand, this is advantageous from the computational point of view as the presence of the slow wave requires a very fine meshing in 3-D numerical simulations. On the other hand, the Biot's global flow mechanism — macroscopic attenuation due to

viscous forces between fluid and solid phases — is not captured in the equations of viscoelasticity, which may be disadvantageous even in the seismic frequency range (Kudarova et al., 2013, this thesis, Chapter 3).

In this chapter, we combine the effective constants from the poroelastic Backus averaging (Gelinsky and Shapiro, 1997) and the method proposed by Krzikalla and Müller (2011). We use the effective P-wave moduli introduced in Chapter 3. This results in the effective stiffnesses of an effective poroelastic VTI medium governed by Biot's equations. This effective medium accounts for the macroscopic (Biot's global-flow) attenuation via the effective inertia and viscous terms used in Biot's equations, and for the mesoscopic (sub-wavelength scale) attenuation via the frequency-dependence of the effective stiffnesses. We consider wave propagation in a 2-D half-space, subject to a point-source at the surface. Solutions to this problem are obtained for the effective viscoelastic model mentioned above and for the newly derived poroelastic model. As a reference, an exact analytical solution is obtained with the use of Floquet's theory (Floquet, 1883). The responses predicted by all three solutions are compared.

The chapter is structured as follows. First, Biot's equations are briefly reviewed, and the exact analytical solution for a periodically layered medium is formulated using Floquet's theory. Secondly, the equations for the effective viscoelastic model are presented. Then, the effective poroelastic model is introduced. The numerical examples follow, and the discussion of the results and conclusions finalize the chapter.

6.2 Theoretical models

In this section, we present the equations of Biot's theory, followed by the equations of the effective viscoelastic model and the derivation of the effective poroelastic model. The exact solution for a periodically layered medium governed by Biot's equations is given in Appendix 6.A.

6.2.1 Biot's theory

Biot's equations of motion read (Biot, 1962)

$$\begin{aligned} \tau_{ij,j} &= \rho\ddot{u}_i + \rho_f\ddot{w}_i, \\ -p_{,i} &= \rho_f\ddot{u}_i + \frac{\alpha_{ij}\rho_f}{\phi}\ddot{w}_j + \eta r_{ij}\dot{w}_j. \end{aligned} \tag{6.1}$$

Throughout this chapter, comma in the subscript denotes a spatial derivative, an overdot denotes a time derivative, and repeated indices are summed over. The following notations are used: ρ_f, ρ_s are fluid and solid grain densities, respectively; ϕ is porosity, and the total density $\rho = (1-\phi)\rho_s + \phi\rho_f$; $\alpha_{ij} = \alpha_\infty\delta_{ij}$, where α_∞ is the tortuosity, δ_{ij} is the Kronecker delta, and η is the fluid viscosity; τ_{ij} are the elements of the total stress tensor, p is the fluid pressure, and u and w are the displacements of the solid phase and the relative fluid-to-solid displacement multiplied by ϕ, respectively. Tensor $\mathbf{r} = \mathbf{k_0^{-1}}$, where the elements of $\mathbf{k_0}$ are the permeabilities k_{ij}, and for the isotropic case $k_{ij} = k_0\delta_{ij}$. The high-frequency correction to Biot's viscous damping factor is commonly adopted to account for dynamic effects, resulting in the dynamic permeability $\hat{k}_0 = k_0(\sqrt{1 + \mathrm{i}\omega M/(2\omega_B)} + \mathrm{i}\omega/\omega_B)^{-1}$ [and consequently, temporal convolution in (6.1)], where M is the parameter that depends on the pore geometry, permeability and porosity; throughout the chapter, we assume $M = 1$ (Johnson et al., 1987). The real part of the square root is taken greater than zero. Biot's critical frequency $\omega_B = \phi\eta/(k_0\alpha_\infty\rho_f)$ separates the regimes where inertial and viscous forces dominate.

Throughout the chapter, a hat above a quantity stands for frequency dependence and a tilde stands for frequency-wavenumber dependence. The Fourier transform is applied for transforming to the frequency-wavenumber domain:

$$\tilde{f}(k_x, z, \omega) = \int_{-\infty}^{\infty}\int_{-\infty}^{\infty} \exp(-\mathrm{i}\omega t)\exp(\mathrm{i}k_x x) f(x, z, t)\, dt\, dx. \tag{6.2}$$

The inverse Fourier transform is formulated in a following way:

$$f(x, z, t) = \frac{1}{2\pi^2}\int_0^{\infty} \mathrm{Re}\left(\int_{-\infty}^{\infty} \tilde{f}(k_x, z, \omega)\exp(\mathrm{i}\omega t)\exp(-\mathrm{i}k_x x)\, dk_x\right) d\omega. \tag{6.3}$$

Only positive frequencies are considered, as the negative frequency components do not provide information independent of the positive components (Wapenaar and

Berkhout, 1989). We study propagation of the plane waves in the $x-z$ plane, where x is the horizontal direction, and z is the vertical direction.

The stress-strain relations for an isotropic medium read

$$\begin{aligned}
\tau_{xx} &= E_1 u_{x,x} + (E_1 - 2\mu) u_{z,z} + E_2 (w_{x,x} + w_{z,z}), \\
\tau_{zz} &= (E_1 - 2\mu) u_{x,x} + E_1 u_{z,z} + E_2 (w_{x,x} + w_{z,z}), \\
\tau_{xz} &= \mu (u_{x,z} + u_{z,x}), \\
-p &= E_2 (u_{x,x} + u_{z,z}) + E_3 (w_{x,x} + w_{z,z}),
\end{aligned} \tag{6.4}$$

where the coefficients are defined as follows (Biot, 1962):

$$\begin{aligned}
&E_1 = P + 2Q + R, \quad E_2 = (Q+R)/\phi, \quad E_3 = R/\phi^2, \\
&P = \frac{\phi K_m + (1-\phi) K_f \left(1 - \phi - K_m/K_s\right)}{\phi + K_f \left(1 - \phi - K_m/K_s\right)/K_s} + \frac{4}{3}\mu, \\
&Q = \frac{\phi K_f \left(1 - \phi - K_m/K_s\right)}{\phi + K_f \left(1 - \phi - K_m/K_s\right)/K_s}, \\
&R = \frac{\phi^2 K_f}{\phi + K_f \left(1 - \phi - K_m/K_s\right)/K_s}.
\end{aligned} \tag{6.5}$$

In the above equations, K_s, K_f and K_m are the bulk moduli of the solid grains, fluid and the drained frame, respectively; μ is the shear modulus of the drained frame.

In the frequency-wavenumber domain, we look for plane-wave solutions of the equations (6.1) in the form

$$\tilde{\mathbf{u}} = (\tilde{U}_x, \tilde{U}_z, \tilde{W}_x, \tilde{W}_z)^{\mathrm{T}} \exp(-\mathrm{i} k_z z). \tag{6.6}$$

In the isotropic case, the P- and S-wave motions are decoupled. The corresponding dispersion relations are obtained by introducing the displacement potentials $[\tilde{\phi}_s,\ \tilde{\psi}_s,\ \tilde{\phi}_f,\ \tilde{\psi}_f] = [\tilde{\Phi}_s,\ \tilde{\Psi}_s,\ \tilde{\Phi}_f,\ \tilde{\Psi}_f] \exp(-\mathrm{i} k_z z)$, where

$$\begin{aligned}
&\tilde{u}_x = -\mathrm{i} k_x \tilde{\phi}_s - \tilde{\psi}_{s,z}, \quad \tilde{w}_x = -\mathrm{i} k_x \tilde{\phi}_f - \tilde{\psi}_{f,z}, \\
&\tilde{u}_z = \tilde{\phi}_{s,z} - \mathrm{i} k_x \tilde{\psi}_s, \quad \tilde{w}_z = \tilde{\phi}_{f,z} - \mathrm{i} k_x \tilde{\psi}_f.
\end{aligned} \tag{6.7}$$

Substitution of these relations into (6.1) leads to the dispersion equation

$$\left\{(E_1E_3 - E_2^2)s^4 - (\rho E_3 + \hat{m}E_1 - 2\rho_f E_2)s^2 + \rho\hat{m} - \rho_f^2\right\}\left\{\mu\hat{m}s^2 - \rho\hat{m} + \rho_f^2\right\} = 0. \tag{6.8}$$

In equation (6.8), $s = \sqrt{k_x^2 + k_z^2}/\omega$ denotes slowness. The operator $\hat{m} = \rho_f\alpha_\infty/\phi + \hat{b}/(\mathrm{i}\omega\phi^2)$, where $\hat{b} = b_0\sqrt{1 + \mathrm{i}\omega/(2\omega_B)}$ is the dynamic viscous factor (the real part of the square root is positive), and $b_0 = \eta\phi^2/k_0$. The first term between curly brackets in (6.8) is a dispersion equation for P-waves and the second one for S-waves.

6.2.2 Effective viscoelastic VTI model

We first introduce the equations for the effective viscoelastic model, and then the additional parameters are defined to obtain the equations of motion for the effective poroelastic model, given in the next section. The effective vertical transversely isotropic (VTI) model for wave propagation in layered media at arbitrary angle was presented by Krzikalla and Müller (2011). This effective model makes use of the poroelastic Backus averaging (Gelinsky and Shapiro, 1997) and the effective plane-wave modulus obtained for a periodic 1-D medium (White et al., 1975). The resulting equations in the effective medium are equations of elasticity with frequency-dependent coefficients. Throughout the chapter, we refer to this model as the viscoelastic model.

The analysis of dispersion and attenuation predicted by this model for media with inhomogeneities in frame properties was carried out by Krzikalla and Müller (2011). In the current chapter, we present the space-time domain responses of the effective medium to a surface point load. We discuss examples with inhomogeneities both in solid frame and fluid properties. The equations used in this analysis are outlined below.

The equations of motion for the effective VTI viscoelastic model read

$$\begin{aligned} -\mathrm{i}k_x\tilde{\tau}_{xx} + \tilde{\tau}_{xz,z} &= -\omega^2\rho\tilde{u}_x, \\ -\mathrm{i}k_x\tilde{\tau}_{xz} + \tilde{\tau}_{zz,z} &= -\omega^2\rho\tilde{u}_z, \end{aligned} \tag{6.9}$$

where ρ is the density of the homogenized medium obtained by averaging over the layers 1 and 2 of the periodic cell: $\rho = \langle\rho(z)\rangle$. Throughout the chapter, the

angular brackets denote averaging over the layers in the periodic cell

$$\langle f \rangle = \frac{1}{L} \int_L f(z) dz. \tag{6.10}$$

The stress-strain relations for the effective viscoelastic VTI model read

$$\begin{aligned} \tilde{\tau}_{xx} &= -\mathrm{i}k_x \hat{A} \tilde{u}_x + \hat{F} \tilde{u}_{z,z}, \\ \tilde{\tau}_{xz} &= \hat{D}(\tilde{u}_{x,z} - \mathrm{i}k_x \tilde{u}_z), \\ \tilde{\tau}_{zz} &= -\mathrm{i}k_x \hat{F} \tilde{u}_x + \hat{C} \tilde{u}_{z,z}. \end{aligned} \tag{6.11}$$

In the effective medium, the stiffnesses in the above equations are frequency dependent. The expressions for the effective stiffnesses $\hat{A}$, $\hat{F}$, $\hat{C}$ and $\hat{D}$ were obtained by Gelinsky and Shapiro (1997) in two limiting cases of relaxed and unrelaxed pore pressures (the expressions are given in Appendix 6.C). These limits are referred to as quasi-static and no-flow limits, respectively. It is assumed that the fluid flow is independent of the loading direction (i.e., direction of wave propagation), and a single relaxation function connects the relaxed and unrelaxed limits of the effective stiffnesses. This function is based on a frequency-dependent modulus $\hat{K}(\omega)$, derived originally by White et al. (1975). The expression for $\hat{K}(\omega)$ is given in Appendix 6.C. The normalized relaxation function reads

$$\hat{R}(\omega) = \frac{\hat{K}(\omega) - C^u}{C^r - C^u}, \tag{6.12}$$

where the superscripts r and u refer to the relaxed and unrelaxed limits, respectively. The effective stiffnesses then read

$$\left\{\hat{A}, \hat{C}, \hat{F}, \hat{D}\right\} = \{A, C, F, D\}^u - \hat{R}(\omega)(\{A, C, F, D\}^u - \{A, C, F, D\}^r). \tag{6.13}$$

It follows from (6.13) that $\hat{C} = \hat{K}(\omega)$. Since the shear modulus does not depend on the fluid pressure, it is the same in the relaxed and the unrelaxed cases, and the effective shear modulus $\hat{D}$ does not depend on frequency:

$$\hat{D} = D = D^u = D^r = \left\langle \frac{1}{\mu} \right\rangle^{-1}. \tag{6.14}$$

To obtain the dispersion equations of the effective viscoelastic VTI model, we look for the solution of (6.9) in the frequency-wavenumber domain in the form

$$(\tilde{u}_x, \tilde{u}_z) = (\tilde{U}_x, \tilde{U}_z) \exp(\mathrm{i}k_z z). \tag{6.15}$$

Substituting this into the equation of motion (6.9) and taking into account (6.11), provides the following solutions of the dispersion equation:

$$\begin{aligned}
&k_{1z}^{\pm} = \pm\sqrt{\frac{\varepsilon_1 + \sqrt{\varepsilon_2}}{2D\hat{C}}}, \quad k_{2z}^{\pm} = \pm\sqrt{\frac{\varepsilon_1 - \sqrt{\varepsilon_2}}{2D\hat{C}}},\\
&\varepsilon_1 = \rho(\hat{C} + D) - (\hat{A}\hat{C} - 2D\hat{F} - \hat{F}^2)k_x^2,\\
&\varepsilon_2 = (\hat{A}^2\hat{C}^2 - 4(\hat{A}\hat{C} + \hat{F})D - 2\hat{F}^2(\hat{A}\hat{C} - 2D^2) + \hat{F}^3(4D + \hat{F}))k_x^4 +\\
&\quad +2\rho(\hat{F}(D + \hat{C})(\hat{F} + 2D) + \hat{C}D(2D + \hat{A}) - \hat{A}\hat{C}^2)k_x^2 + \rho^2(\hat{C} - D)^2.
\end{aligned} \tag{6.16}$$

The pairs of the wavenumbers $k_{1z,2z}^{\pm}$ correspond to up- and downgoing quasi-P (qP) and quasi-S (qS) waves. The amplitude ratios $\tilde{U}_z/\tilde{U}_x$ read:

$$\left(\frac{\tilde{U}_z}{\tilde{U}_x}\right)_{1,2}^{\pm} = \frac{\rho\omega^2 - \hat{A}k_x^2 - D\left(k_{1z,2z}^{\pm}\right)^2}{(\hat{F} + D)k_x k_{1z,2z}^{\pm}}. \tag{6.17}$$

6.2.3 Effective poroelastic VTI model

In this section, we introduce the effective poroelastic model based on the poroelastic Backus averaging (Gelinsky and Shapiro, 1997) and the effective plane-wave moduli obtained for P-wave propagation at normal incidence in a periodically layered porous medium (Kudarova et al., 2013; this thesis, Chapter 3). These effective moduli result from employing the boundary conditions at the interfaces of the periodic cell, different from those used in White's model (White et al., 1975). The no-flow condition is replaced with the pressure continuity condition, allowing fluid flow at the macroscopic scale. As a result, two additional plane-wave moduli are derived to describe the effective medium with Biot's equations. These effective moduli are used to define the effective stiffnesses $\hat{B}_6$, $\hat{B}_7$, $\hat{B}_8$ (notation used as in Gelinsky and Shapiro, 1997) required to describe the effective poroelastic VTI model. Apart from the effective stiffnesses, the effective densities have to be defined. We use the results obtained by Molotkov and Bakulin (1999), who

showed that the effective medium representing a stack of Biot layers is a generalized transversely isotropic Biot medium. In this poroelastic medium, the densities and the viscous terms in Biot's equations are defined differently in the x and z directions. The equations of motion read

$$\begin{aligned}
-\mathrm{i}k_x\tilde{\tau}_{xx} + \tilde{\tau}_{xz,z} &= -\omega^2\hat{\rho}_x\tilde{u}_x - \omega^2\hat{\rho}_{fx}\tilde{w}_x,\\
-\mathrm{i}k_x\tilde{\tau}_{xz} + \tilde{\tau}_{zz,z} &= -\omega^2\rho_z\tilde{u}_z - \omega^2\rho_{fz}\tilde{w}_z,\\
\mathrm{i}k_x\tilde{p} &= -\omega^2\hat{\rho}_{fx}\tilde{u}_x - \omega^2\hat{m}_x\tilde{w}_x,\\
-\tilde{p}_{,z} &= -\omega^2\rho_{fz}\tilde{u}_z - \omega^2\hat{m}_z\tilde{w}_z,
\end{aligned} \tag{6.18}$$

where the coefficients on the right-hand side read (Molotkov and Bakulin, 1999):

$$\begin{aligned}
&\hat{\rho}_{fx} = \frac{s_1\rho_{f1}\hat{m}_2 + s_2\rho_{f2}\hat{m}_1}{s_1\hat{m}_2 + s_2\hat{m}_1}, \quad \hat{m}_x = \left\langle \frac{1}{\hat{m}} \right\rangle^{-1},\\
&\hat{\rho}_x = \langle\rho\rangle - \frac{s_1 s_2(\rho_{f1} - \rho_{f2})^2}{s_1\hat{m}_2 + s_2\hat{m}_1},\\
&\rho_z = \langle\rho\rangle, \quad \rho_{fz} = \langle\rho_f\rangle, \quad \hat{m}_z = \langle\hat{m}\rangle.
\end{aligned} \tag{6.19}$$

The indices 1 and 2 in equations (6.19) refer to the layers 1 and 2. The volume fractions of the layers are $s_1 = l_1/L$, $s_2 = l_2/L$.

The stress-strain relations read

$$\begin{aligned}
\tilde{\tau}_{xx} &= -\mathrm{i}k_x\hat{A}\tilde{u}_x + \hat{F}\tilde{u}_{z,z} + \hat{B}_6(-\mathrm{i}k_x\tilde{w}_x + \tilde{w}_{z,z}),\\
\tilde{\tau}_{zz} &= -\mathrm{i}k_x\hat{F}\tilde{u}_x + \hat{C}\tilde{u}_{z,z} + \hat{B}_7(-\mathrm{i}k_x\tilde{w}_x + \tilde{w}_{z,z}),\\
\tilde{\tau}_{xz} &= D(\tilde{u}_{x,z} - \mathrm{i}k_x\tilde{u}_z),\\
-\tilde{p} &= -\mathrm{i}k_x\hat{B}_6\tilde{u}_x + \hat{B}_7\tilde{u}_{z,z} + \hat{B}_8(-\mathrm{i}k_x\tilde{w}_x + \tilde{w}_{z,z}).
\end{aligned} \tag{6.20}$$

The frequency-dependent stiffnesses in (6.20) are defined in the same way as in the effective viscoelastic model, but the frequency dependence is incorporated via the effective plane-wave moduli obtained with the method proposed by Kudarova et al., 2013 (this thesis, Chapter 3).

These effective moduli are obtained from the solution of the 1-D problem for the periodic cell consisting of two isotropic layers (see Figure 3.1) where harmonic stress and pressure are applied to the outer edges of the cell normal to the layering.

The layers are governed by Biot's equations (6.1) (with z-dependent field variables u_z, w_z, τ_{zz} and p). The problem is solved in the frequency domain. In each layer the displacements u_z and w_z are found as up- and down-going plane waves (a fast and a slow P-wave), resulting in eight unknown amplitudes. These amplitudes are found from the following boundary conditions: continuity of the intergranular stress σ_{zz}, pore pressure p, displacements u_z and w_z at the interface between the layers, and continuity of the total stress τ_{zz} and pressure p at the outer edges of the cell. The strains $u_{z,z}$ and $w_{z,z}$ are found as the difference between the displacements at the outer edges of the unit cell, divided by the cell width. This gives us the coefficients of the frequency-dependent symmetric compliance matrix $\hat{\alpha}_{ij}$:

$$\begin{aligned} \hat{u}_{z,z} &= \hat{\alpha}_{11}\hat{\tau}_{zz} + \hat{\alpha}_{12}\hat{p}, \\ \hat{w}_{z,z} &= \hat{\alpha}_{12}\hat{\tau}_{zz} + \hat{\alpha}_{22}\hat{p}. \end{aligned} \tag{6.21}$$

They are equated to the coefficients of the compliance matrix obtained from Biot's stress-strain relations (6.4) (for the 1-D case, with $k_x = 0$):

$$\begin{aligned} \hat{u}_{z,z} &= \tfrac{1}{\hat{\Delta}}\left(\hat{E}_3\hat{\tau}_{zz} + \hat{E}_2\hat{p}\right), \\ \hat{w}_{z,z} &= \tfrac{1}{\hat{\Delta}}\left(-\hat{E}_2\hat{\tau}_{zz} - \hat{E}_1\hat{p}\right), \qquad \hat{\Delta} = \hat{E}_1\hat{E}_3 - \hat{E}_2^2. \end{aligned} \tag{6.22}$$

Then, the frequency-dependent elastic parameters $\hat{E}_1$, $\hat{E}_2$, $\hat{E}_3$ are found, describing attenuation and dispersion due to wave-induced mesoscopic fluid flow in 1-D periodically layered medium:

$$\hat{E}_1 = \frac{\hat{\alpha}_{22}}{\hat{\alpha}_{11}\hat{\alpha}_{22} - \hat{\alpha}_{12}^2}, \quad \hat{E}_2 = -\frac{\hat{\alpha}_{12}}{\hat{\alpha}_{11}\hat{\alpha}_{22} - \hat{\alpha}_{12}^2}, \quad \hat{E}_3 = \frac{\hat{\alpha}_{11}}{\hat{\alpha}_{11}\hat{\alpha}_{22} - \hat{\alpha}_{12}^2}. \tag{6.23}$$

The coefficients α_{ij} are computed numerically by solving a system of eight by eight linear algebraic equations corresponding to eight boundary conditions in the cell problem (for more details, see Chapter 3).

Following Krzikalla and Müller (2011), we introduce a branching function

$$\hat{R}_1(\omega) = \frac{\hat{E}_1(\omega) - C^u}{C^r - C^u}. \tag{6.24}$$

to obtain the frequency-dependent effective moduli $\hat{A}$, $\hat{C}$ and $\hat{F}$:

$$\left\{\hat{A}, \hat{C}, \hat{F}\right\} = \{A, C, F\}^u - \hat{R}_1(\omega)(\{A, C, F\}^u - \{A, C, F\}^r). \tag{6.25}$$

As discussed above, the modulus $\hat{D}$ is not frequency dependent, and is defined in equation (6.14). Note that $\hat{R}_1(\omega)$ is equivalent to $\hat{R}(\omega)$ (equation (6.12)) when the frequency is much lower than Biot's critical frequency ω_B. The effective plane-wave modulus $\hat{E}_1$ is an extension of White's frequency-dependent modulus $\hat{K}(\omega)$ to higher frequencies, first proposed by Vogelaar and Smeulders (2007). Further generalization was proposed by Kudarova et al., 2013 (this thesis, Chapter 3), where the no-flow boundary conditions at the outer edges of the unit cell were replaced by the pressure continuity condition, allowing the global flow to take place. This results in additional effective moduli $\hat{E}_2$ and $\hat{E}_3$ used to describe the effective Biot medium.

By comparing the expressions for τ_{zz} and p in equations (6.4) (with incorporated frequency-dependent coefficients $\hat{E}_1$, $\hat{E}_2$ and $\hat{E}_3$ introduced above) and (6.20), we can find out how the other moduli of the effective poroelastic VTI model should be chosen. First, it can be observed that

$$\hat{B}_7 = \hat{E}_2, \quad \hat{B}_8 = \hat{E}_3. \tag{6.26}$$

Next, the effective coefficient $\hat{B}_6$ should be obtained. In the particular case when the shear modulus is constant throughout the layers, there is no anisotropy in the stiffness matrix of the effective poroelastic medium, and $\hat{B}_6 = \hat{B}_7 = \hat{E}_2$. Anisotropy remains in the viscous and inertia terms, according to their definition in (6.19). In the general case, complying with the method used by Krzikalla and Müller (2011), the frequency-dependence of $\hat{B}_6$ is specified using a second normalized relaxation function:

$$\hat{R}_2(\omega) = \frac{\hat{E}_2 - B_7^u}{B_7^r - B_7^u}. \tag{6.27}$$

The final expression for the effective modulus $\hat{B}_6$ then reads

$$\hat{B}_6 = B_6^u - \hat{R}_2(\omega)(B_6^u - B_6^r). \tag{6.28}$$

Now, all effective constants have been determined. For clarity, we underline that the effective poroelastic model incorporates both the mesoscopic and the macroscopic attenuation mechanisms; the former is captured by the effective stiffnesses in equation (6.20), while the latter comes in through the effective terms defined in equation (6.19).

To obtain the dispersion equation of the effective poroelastic VTI model, we look for the solution of equations (6.20) in the form

$$\{\tilde{u}_x, \tilde{u}_z, \tilde{w}_x, \tilde{w}_z\} = \left\{\tilde{U}_x, \tilde{U}_z, \tilde{W}_x, \tilde{W}_z\right\} \exp(-\mathrm{i}k_z z). \tag{6.29}$$

Substitution of (6.29) into stress-strain relations (6.20) and the equations of motion (6.18) gives the dispersion relation $\det(\mathbf{M}) = 0$ with solutions $k_z(k_x, \omega)$, where $\mathbf{M}$ is a matrix with coefficients given as:

$$\mathbf{M} = \begin{bmatrix} \hat{A}k_x^2 + Dk_z^2 - \omega^2\hat{\rho}_x & (D+\hat{F})k_xk_z & \hat{B}_6k_x^2 - \omega^2\hat{\rho}_{fx} & \hat{B}_6k_xk_z \\ (\hat{F}+D)k_xk_z & \hat{C}k_z^2 + Dk_x^2 - \omega^2\rho_z & \hat{B}_7k_xk_z & \hat{B}_7k_z^2 - \omega^2\rho_{fz} \\ -\hat{B}_6k_x^2 + \omega^2\hat{\rho}_{fx} & -\hat{B}_7k_xk_z & -\hat{B}_8k_x^2 + \hat{m}_x\omega^2 & -\hat{B}_8k_xk_z \\ -\hat{B}_6k_xk_z & -\hat{B}_7k_z^2 + \omega^2\rho_{fz} & -\hat{B}_8k_xk_z & -\hat{B}_8k_z^2 + \hat{m}_z\omega^2 \end{bmatrix}. \tag{6.30}$$

The equation $\det(\mathbf{M}) = 0$ provides the dispersion relation:

$$c_1k_z^6 + c_2k_z^4 + c_3k_z^2 + c_4 = 0. \tag{6.31}$$

Explicit expressions for the coefficients c_i are not presented here for the sake of brevity; they can be expressed in terms of the elements of the matrix $\mathbf{M}$. The solution of (6.31) is

$$\begin{aligned} k_{1z}^{\pm} &= \pm\sqrt{\tfrac{a}{6c_1} - \tfrac{2}{3}\tfrac{3c_1c_3 - c_2^2}{c_1 a} - \tfrac{c_2}{3c_1}}, \\ k_{2z}^{\pm} &= \pm\sqrt{-(1-\mathrm{i}\sqrt{3})\tfrac{a}{12c_1} + 2(1+\mathrm{i}\sqrt{3})\tfrac{3c_1c_3 - c_2^2}{6c_1 a} - \tfrac{c_2}{3c_1}}, \\ k_{3z}^{\pm} &= \pm\sqrt{-(1+\mathrm{i}\sqrt{3})\tfrac{a}{12c_1} + 2(1-\mathrm{i}\sqrt{3})\tfrac{3c_1c_3 - c_2^2}{6c_1 a} - \tfrac{c_2}{3c_1}}, \end{aligned} \tag{6.32}$$

where

$$\begin{aligned} a = \Big(&12\sqrt{3(27c_1^2c_4^2 - 18c_1c_2c_3c_4 + 4c_1c_3^3 + 4c_2^3c_4 - c_2^2c_3^2)}c_1 - \\ &-108c_4c_1^2 + 36c_1c_2c_3 - 8c_2^3\Big)^{1/3}. \end{aligned} \tag{6.33}$$

These vertical components of the wavenumbers correspond to the up- and down-going fast qP-waves, the slow qP-waves and the qS-waves.

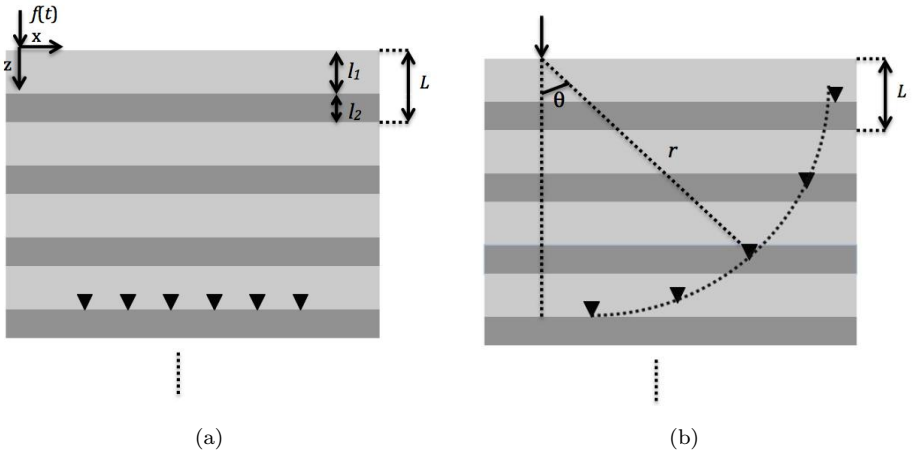

(a) (b)

FIGURE 6.1: Point-force source at the top of the layered half-space and receivers on a horizontal line below the source (a) and on an arc (b).

6.3 Results

In this section, we compare the space-time domain responses of three half-spaces subject to a surface point-source (vertical stress component) and evaluate the performance of the effective models for media with different properties. The first half-space consists of periodically alternating layers, where each layer is governed by Biot's equation. The exact analytical solution presented in Appendix 6.A is used to obtain the response in the frequency-wavenumber domain. The response in the space-time domain is obtained with the use of the inverse Fourier transform (6.3). The second half-space is a homogeneous viscoelastic VTI medium governed by the equations of the effective viscoelastic VTI model outlined above, originally introduced by Krzikalla and Müller (2011). The third half-space is a homogeneous VTI poroelastic medium governed by the equations of the effective poroelastic VTI model introduced in this chapter.

6.3.1 Configuration

We consider a periodically layered half-space with the normal stress at the surface applied at some reference point $x = 0$. The receivers are located on one horizontal line (Fig. 6.1(a)), and on the arc of a circle with the radius r (Fig. 6.1(b)). The latter configuration is instrumental to highlight angle-dependent effects. The sets of the material parameters are given in Tables 6.1 (solid frame properties) and

Parameter	Notation	Units	Rock 1	Rock 2	Sandstone	Medium sand	Coarse sand
Density of solid grains	ρ_s	kg/m^3	2650	2650	2650	2650	2650
Bulk modulus of solid grains	K_s	GPa	40	40	40	36	36
Bulk modulus of frame	K_m	GPa	12.7	4.3	1.37	0.108	0.217
Porosity	ϕ	–	0.15	0.17	0.36	0.4	0.35
Permeability	k_0	m^2	10^{-13}	$2 \cdot 10^{-13}]$	$1.6 \cdot 10^{-12}$	10^{-11}	10^{-10}
Shear modulus	μ	GPa	20.3	8.8	0.82	0.05	0.1
Tortuosity	α_∞	–	1	1	2.8	1.25	1.25
Biot cr. freq. (water)	$\frac{\omega_B}{2\pi}$	kHz	1500	850	80.3	5.1	0.445
Biot cr. feq. (CO_2)	$\frac{\omega_B}{2\pi}$	kHz	445	252	23.9	9.5	0.8
Biot cr. feq. (gas)	$\frac{\omega_B}{2\pi}$	kHz	107	60	5.7	2.3	0.2

TABLE 6.1: Sets of material properties chosen for numerical examples.

Parameter	Notation	Units	Water	Gas	CO_2
Density	ρ_f	kg/m^3	1000	140	505
Bulk modulus	K_f	GPa	2.25	0.056	0.025
Viscosity	η	Pa $\cdot$ s	0.001	0.00022	0.00015

TABLE 6.2: Mechanical properties of the sample pore fluids: water and gas.

6.2 (saturating fluids properties). The examples with rocks and water- and gas-saturated coarse sand were used by Gelinsky and Shapiro (1997). The properties of the coarse and medium sands originate from Turgut and Yamamoto (1990). The examples with alternating layers of a brine-saturated mudstone and CO_2-saturated sandstone were introduced by Carcione et al. (2011).

The boundary conditions at the top interface $z = 0$ read

$$\tau_{zz} = f(t)\delta(x), \quad \tau_{xz} = 0, \quad p = 0. \tag{6.34}$$

For the effective VTI viscoelastic model, only the first two boundary conditions apply, because the fluid pressure is not present in the equations of the viscoelastic model. For the function $f(t)$, a Ricker wavelet is used:

$$f(t) = f_0 \left(1 - 2\pi^2 f_R^2 (t - t_0)^2\right) \exp\left(-\pi^2 f_R^2 (t - t_0)^2\right). \tag{6.35}$$

In the above equation, f_0 is a constant scaling coefficient with the dimension of stress (Pa), f_R is the central frequency of the wavelet and t_0 is an arbitrary time shift chosen such that the dominant part of the wavelet lies within the positive domain $t > 0$; only the components that are infinitely small are left in the domain $t < 0$. In the examples, we compare the vertical components of the solid displacements u_z.

6.3.2 Numerical examples

First, we look at the response of a medium consisting of alternating water-saturated Rocks 1 and 2. The receivers are located on a horizontal line at a vertical distance $z = 400$ m from the source, and the layer thicknesses are $l_1 = l_2 = 0.2$ m. The wavelet parameters are $f_R = 50$ Hz, $f_0 = 10^9$ Pa, $t_0 = 0.022$ s. Since there is a variation in the shear modulus of the layers, the effective viscoelastic medium is a VTI medium (not isotropic), as well as the effective poroelastic medium. The exact solution describes the original layered medium. Time-domain responses are shown in Figure 6.2. In all the plots, the dashed black line corresponds to the solution predicted by the effective viscoelastic model, the solid black line corresponds to the exact analytical solution, and the solid grey line corresponds to the effective poroelastic model. In Figure 6.2 all three lines coincide; both effective models are in agreement with the exact solution for both the qP- and qS-waves, as well as for the head wave that can be distinguished.

The second example is a medium consisting of sandstone layers with alternating water and CO_2 saturations, the thicknesses of the layers are the same as in the previous example. This configuration was also considered by Carcione et al. (2011). The shear modulus is constant throughout the layers, which means that the effective viscoelastic medium is isotropic (the effective elastic coefficients $\hat{A} = \hat{C} = \hat{F} + 2D$), resulting in decoupling between P- and S-waves motions. In this particular case, the qS-wave velocity in the effective viscoelastic model is equal to the S-wave velocity $v = \sqrt{\mu/\rho}$, where μ is a real-valued shear modulus, and ρ is a real-valued effective density. Hence, the effective viscoelastic model does not predict any S-wave attenuation. However, the effective poroelastic model is not isotropic because of the anisotropy in the effective density terms (eq. (6.18)). Therefore, the qS-wave is attenuated in the effective poroelastic model and the exact solution. To observe this effect, the central frequency of the wavelet in this example is increased to 200 Hz, and $t_0 = 0.0055$ s. The qP-wave waveforms are shown in Figure 6.3 and the qS-wave ones in Figure 6.4. The traces for the qS-wave are shifted in time by $-(t_n - \Delta t_n + 0.01n)$ s, where $n = 2, .., 6$ is the trace number (the numbering in the direction of increasing offset), t_n is the actual arrival time of the qS-wave in the n_{th} trace and Δt_n is the difference between the arrival time of the qS-wave in the n_{th} trace and the first trace. The interval between the arrival times is then $t = 0.01$ s. This is done just for visualization purposes. It can be observed that the qP-waveforms are all in agreement (all lines coincide), but the

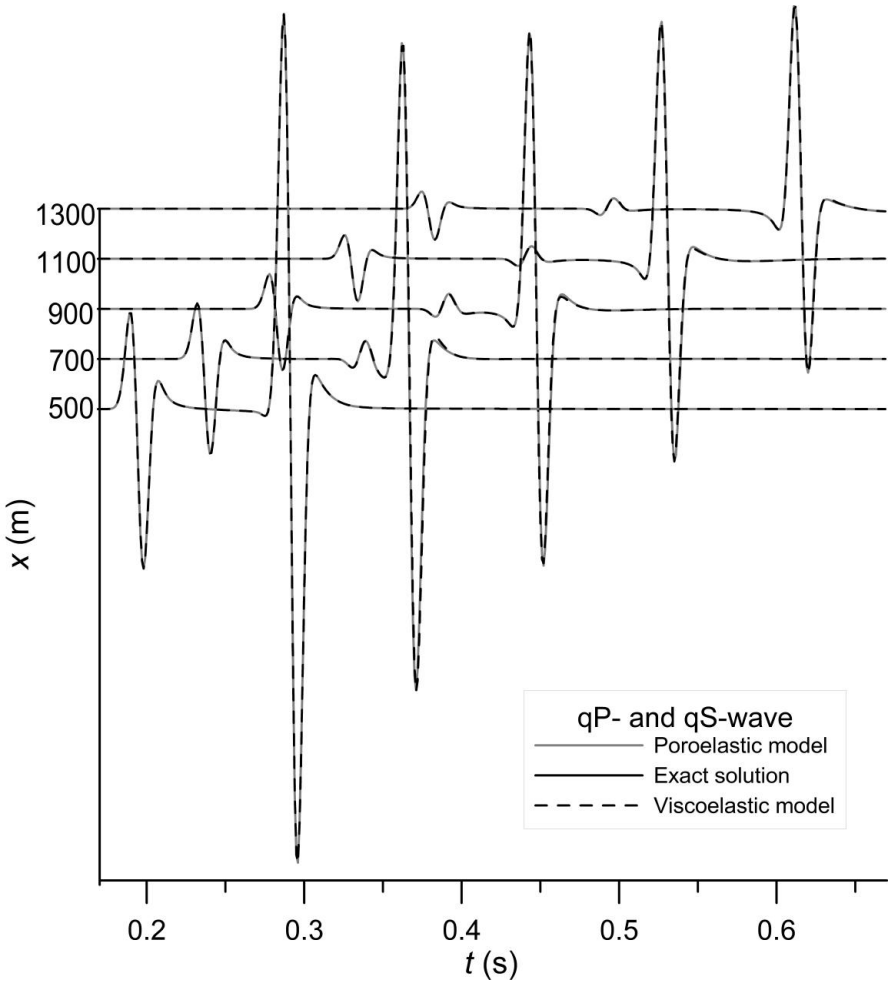

FIGURE 6.2: Time-domain response at a depth $z = 400$ m for different x. The medium consists of water-saturated alternating layers of Rock 1 and Rock 2, $l_1 = l_2 = 0.2$ m,$f_R = 50$ Hz. All three lines coincide.

qS-wave attenuation is underestimated by the effective models; with the effective viscoelastic model, it is underestimated to a greater extent, whereas the difference between the predictions by the effective poroelastic model and the exact solution is smaller.

In the effective poroelastic model, Biot's global flow mechanism causes qS-wave attenuation captured by the viscous terms in equations (6.18). This mechanism is not present in the effective viscoelastic model, which could result in different predictions as shown in Figure 6.4. However, the influence of Biot's global flow mechanism at this frequency range well below Biot's critical frequency (see Table 6.1) is probably small, which is confirmed by the fact that the predictions for the qP-waveforms match for all models. The observed differences in the qS-waveforms are likely to be related to the different description of the mesoscopic-scale attenuation mechanism in the models. In the viscoelastic model, there is no S-wave

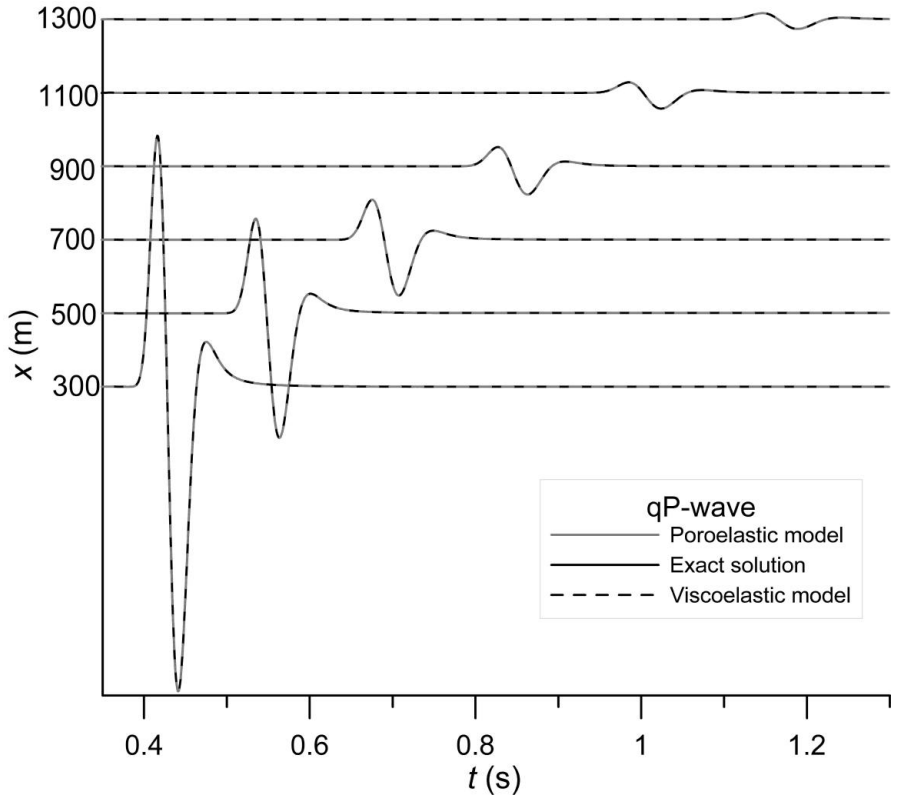

FIGURE 6.3: qP-waveforms at a depth $z = 400$ m for different x. The medium consists of water- and CO_2-saturated sandstone layers, $l_1 = l_2 = 0.2$ m, $f_R = 200$ Hz. All three lines coincide.

attenuation; in the poroelastic model, the mesoscopic-scale attenuation of the qS-wave is captured in the compressional motion, associated with the qS-wave. The difference between the effective poroelastic model qS-waveform and that of the exact solution is probably due to more complicated fluid pressure distribution associated with the qS-wave (Wenzlau et al., 2010), which is not captured by the effective moduli derived for the 1-D cell problem.

It was shown in Chapter 3 that Biot's global flow mechanism is also important for predictions of P-wave attenuation at seismic frequencies for highly permeable weak-frame media. In the next examples, we consider such media to compare the predictions of the three models considered in this chapter for both qP- and qS-waves. First, water-saturated alternating layers of medium sand and coarse sand are considered. The thicknesses of the layers are $l_1 = l_2 = 0.2$ m, and the receivers are located at a depth $z = 400$ m. The central frequency of the wavelet is defined as $f_R = 50$ Hz. For visualization purposes, the traces in Figure 6.5 are shifted in time, in the same way as in the previous example. It also applies to the traces in Figure 6.6, but the interval between the arrival times

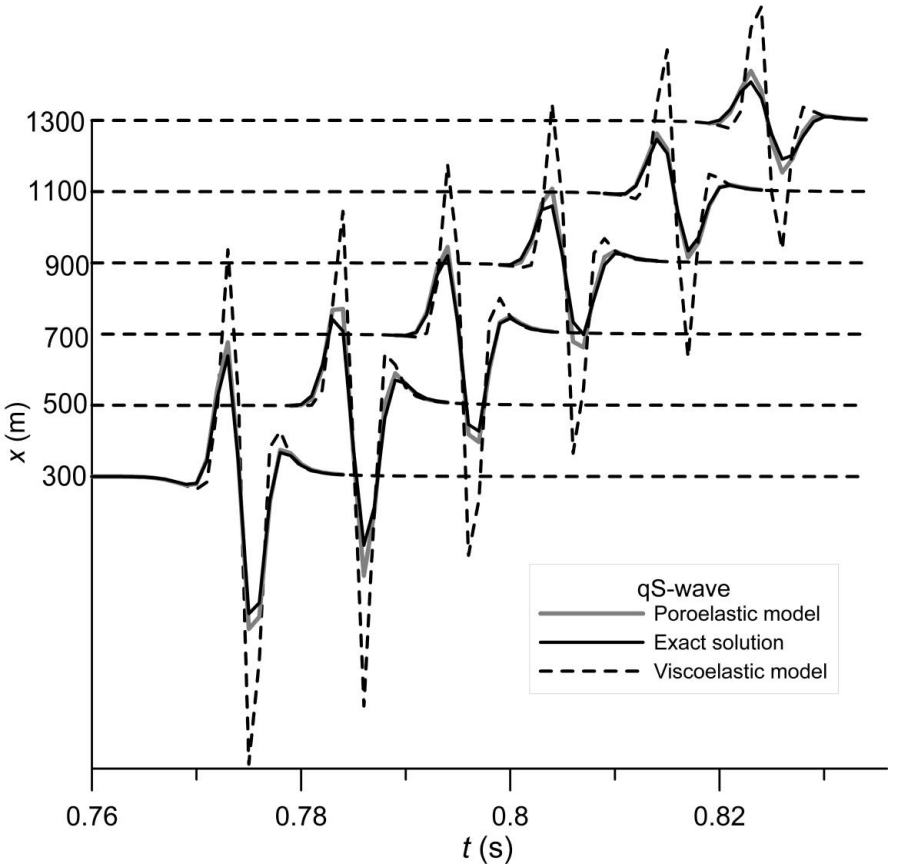

FIGURE 6.4: qS-waveforms at a depth $z = 400$ m for different x. The medium consists of water- and CO_2-saturated sandstone layes, $l_1 = l_2 = 0.2$ m, $f_R = 200$ Hz. The actual arrival times are not shown here, the interval between the arrival times $t = 0.01$ s is chosen for visualization purposes.

is chosen differently: $t = 0.1$ s. It can be observed from the waveforms of the qP- (Figure 6.5) and qS-waves (Figure 6.6) that the effective viscoelastic model underestimates both qP- and qS-wave attenuation. The effective poroelastic model predicts the same qP-waveforms as the exact solution, and its predictions for the qS-wave are closer to the exact solution than the predictions of the effective viscoelastic model. In this example, the effective viscoelastic model is a VTI medium, because there is a variation in the shear moduli of the layers. P- and S-waves motions are coupled, therefore the qS-wave is not lossless. However, Biot's global flow mechanism is still not captured by this model, this is why the model gives inaccurate predictions. Clearly, the attenuation caused by Biot's global flow mechanism is not negligible at low frequencies for highly permeable media. The difference in the qS-waveforms predicted by the effective poroelastic model and the exact solution, which changes with offset, suggests again that the mesoscopic-scale attenuation mechanism incorporated in the model via the effective frequency-dependent elastic moduli derived from the 1-D cell problem fails to predict the

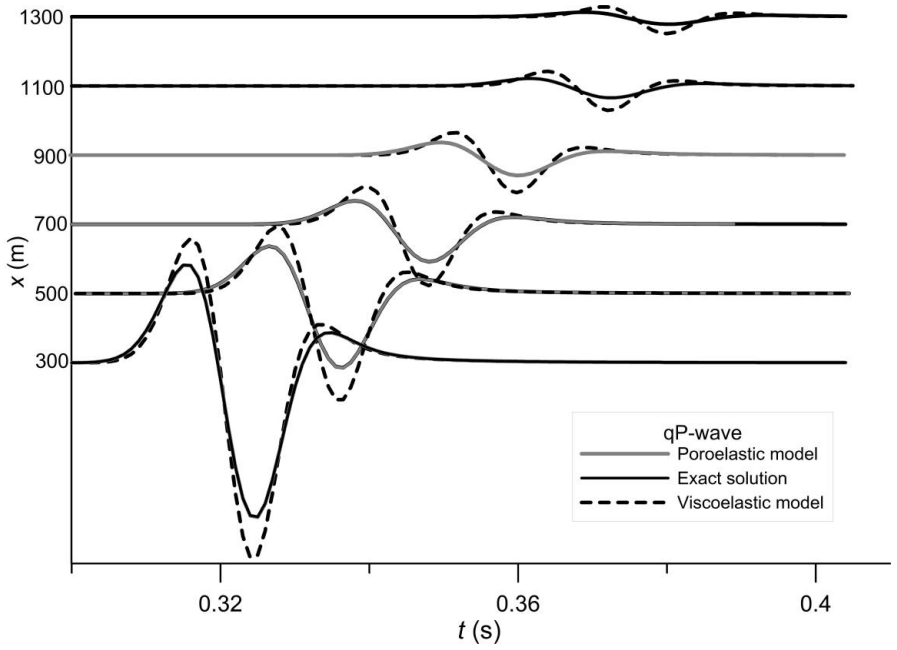

FIGURE 6.5: qP-waveforms at a depth $z = 400$ m for different x. The medium consists of water-saturated medium and coarse sand, $l_1 = l_2 = 0.2$ m, $f_R = 50$ Hz. Grey and black solid lines coincide. The actual arrival times are not shown here, the interval between the arrival times $t = 0.01$ s is chosen for visualization purposes.

qS-wave attenuation with high accuracy.

The attenuation of seismic waves is known to be very pronounced in finely layered porous media with patchy saturation (Carcione and Picotti, 2006). The next example is a finely layered coarse sand saturated with water and gas. The layer thicknesses are $l_1 = 0.09$ m (water-saturated) and $l_2 = 0.01$ m (gas-saturated). The vertical distance from the source to the receivers is $z = 100$ m. The wavelet's central frequency is given by $f_R = 50$ Hz. The time-domain responses for the horizontal line of receivers are depicted in Figures 6.7 (qP-wave) and 6.8 (qS-wave). The horizontal positions of the receivers are chosen differently, compared to those in the previous examples, for visualization purposes (the medium is highly attenuative). In Figure 6.7, each trace is multiplied by the corresponding propagation distance and the traces predicted by the effective viscoelastic model are scaled by a factor 0.1 (for visualization purposes). In Figure 6.8, the traces predicted by the effective viscoelastic model are scaled by a factor 0.5, and the waveforms are shifted in time by $-(t_n - \Delta t_n + 0.04n)$ s, similar to the previous examples, such that the interval between the arrival times is $t = 0.04$ s. Clearly, the effective viscoelastic model vastly underestimates the attenuation, to a much greater extent than in the previous examples, while the effective poroelastic model is in good

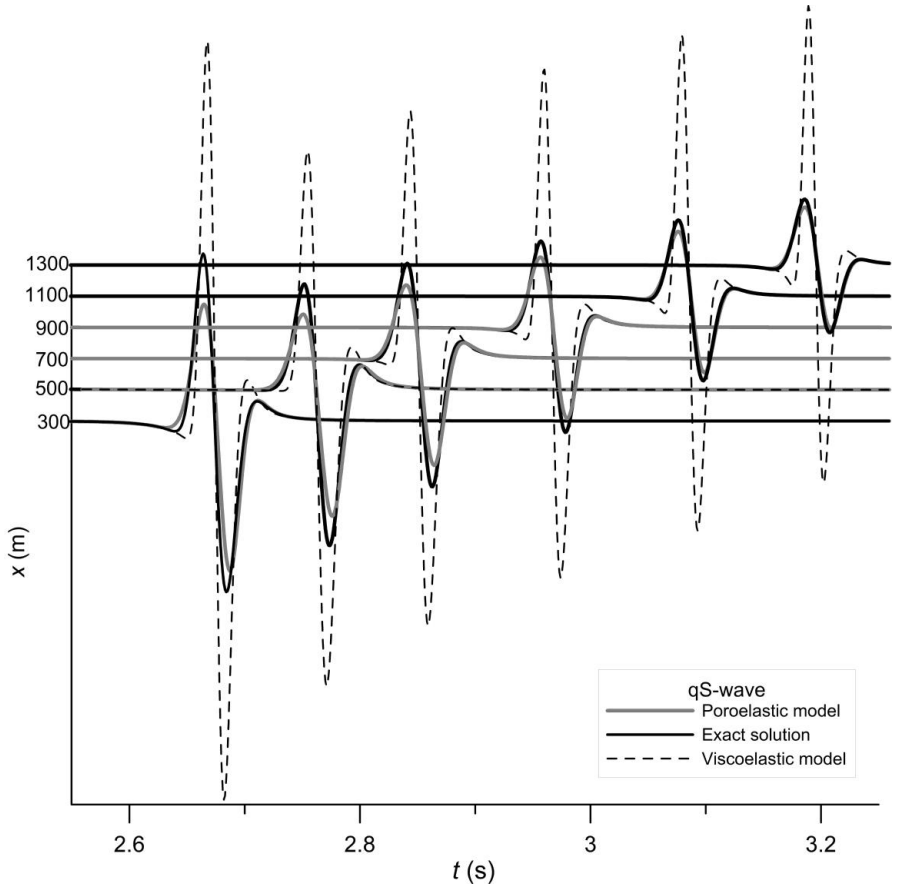

FIGURE 6.6: qS-waveforms at a depth $z = 400$ m for different x. The medium consists of water-saturated medium and coarse sand, $l_1 = l_2 = 0.2$ m, $f_R = 50$ Hz. The actual arrival times are not shown here, the interval between the arrival times $t = 0.1$ s is chosen for visualization purposes.

agreement with the exact solution. The effective viscoelastic model also predicts lower qP-wave velocities than the poroelastic model and the exact solution, as can be seen in Figure 6.7. The waveforms predicted by the effective viscoelastic model are also different, suggesting that the dispersion is not captured properly. It can be observed in the (f, k_x) domain that the effective poroelastic model (Figure 6.9(a)) and the exact solution (Figure 6.9(b)) are in good agreement, while the amplitudes predicted by the effective viscoelastic model (Figure 6.9(c)) are much higher, and the P-wave velocity is lower.

Since highly permeable media are also highly dispersive and attenuative, it is interesting to explore the angle-dependent effects in more detail with the configuration of receivers depicted in Figure 6.1(b). The distance from source to the receivers is $r = 100$ m. The results for this configuration are depicted in Figures 6.10 and 6.11. In these plots, the time-domain reponses are shown for the locations of receivers at different angles θ. The results for the qP-wave are depicted

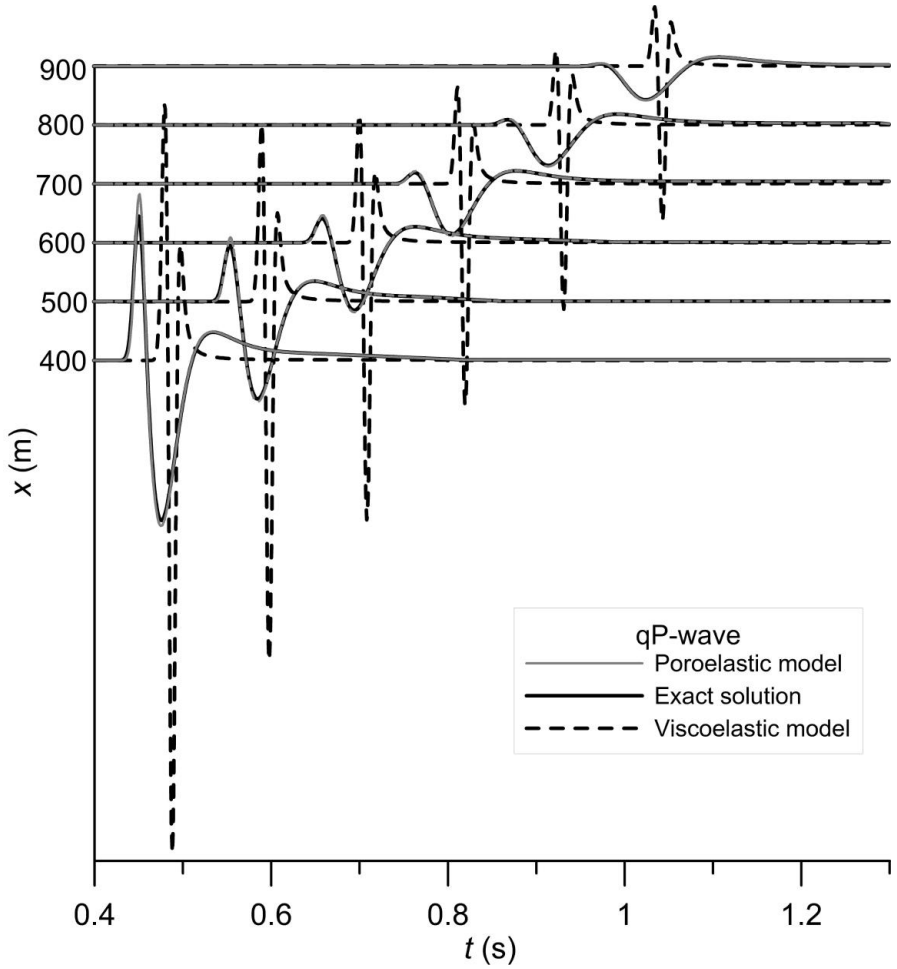

FIGURE 6.7: qP-waveforms at a depth $z = 100$ m for different x. The medium consists of the layers of coarse sand, $l_1 = 0.09$ m (water-saturated), $l_2 = 0.01$ m (gas-saturated), $f_R = 50$ Hz. Each trace is multiplied by the corresponding propagation distance, and the traces predicted by the effective viscoelastic model are scaled by a factor 0.1.

in Figure 6.10. The deviation of the predictions of the effective viscoelastic model from the exact result is visible even at normal incidence; this result is consistent with that obtained in Chapter 3. The effective poroelastic model predicts the same attenuation and dispersion as the exact solution. It can be observed in Figure 6.10 that the effective viscoelastic model does not correctly predict the angle-dependent dispersion of this medium. There is a significant phase shift between the predictions of the viscoelastic and poroelastic solutions, observed by the change in the waveform. The dispersion effects are very pronounced in the effective poroelastic model and the exact solution: with increasing angle, the waveform spreads.

There is again some difference in the predictions of the effective poroelastic model and the exact solution for the qS-wave as can be seen in Figure 6.11. In

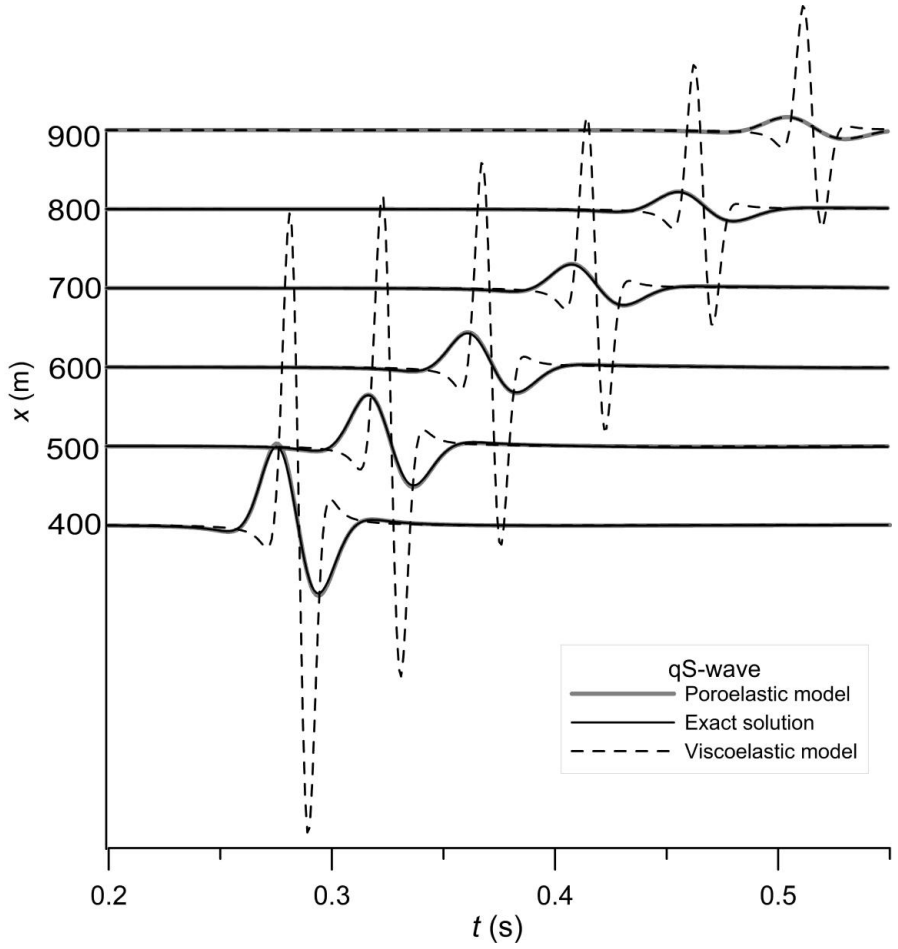

FIGURE 6.8: qS-waveforms at a depth $z = 100$m for different x. The medium consists of the layers of coarse sand, $l_1 = 0.09$ m (water-saturated), $l_2 = 0.01$ m (gas-saturated), $f_R = 50$ Hz. The actual arrival times are not shown here, the interval between the arrival times $t = 0.04$ s is chosen for visualization purposes. The traces predicted by the effective viscoelastic model are scaled by a factor 0.5.

these highly dispersive media, the qS-wave attenuation due to the mesosocopic-scale wave-induced fluid flow is more significant than in the less permeable stiffer rocks. However, the S-wave attenuation and dispersion due to mesosocopic effects is not described by the effective models. Only the effective P-wave modulus is incorporated in the models to describe attenuation due to the mesoscopic wave-induced fluid flow. Still, the effective poroelastic model gives better predictions of the qS-wave attenuation than the viscoelastic model.

In this section we have observed that both qP and qS-waveforms are predicted accurately for Rock 1 and Rock 2 (Figure 6.2), where the influence of Biot's global flow mechanism is negligible, and the mesoscopic-scale attenuation mechanism is captured properly by the effective moduli in both models. The differences in

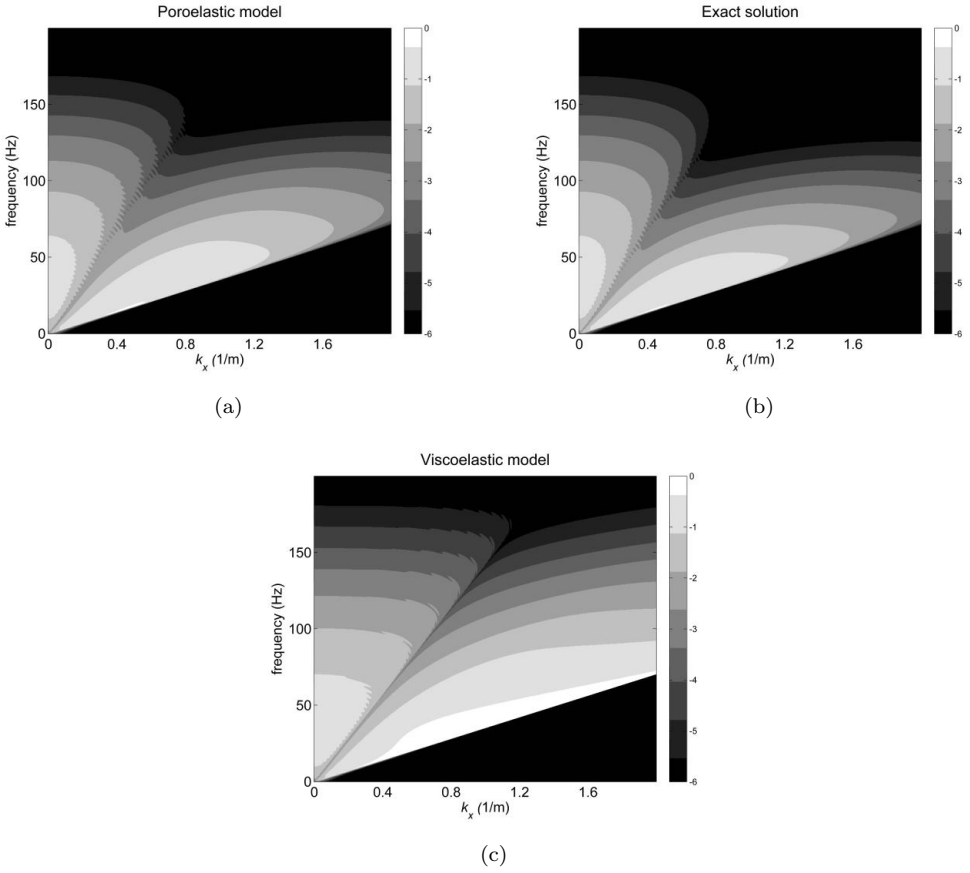

FIGURE 6.9: Logarithm of the amplitude spectrum in the (f, k_x)-domain for the vertical component of solid particle displacement at a depth $z = 100$ m. Water- and gas-saturated coarse sand.

qS-waveforms are more pronounced with increasing the frequency and for softer sandstones (Figure 6.4). Biot's global flow mechanism becomes non-negligible for unconsolidated sands (Figures 6.5–6.11), resulting in underestimation of both qP- and qS-wave attenuation by the effective viscoelastic model; the poroelastic model however predicts the proper qP-wave attenuation for such materials, while the qS-wave attenuation has higher accuracy than that predicted by the viscoelastic model.

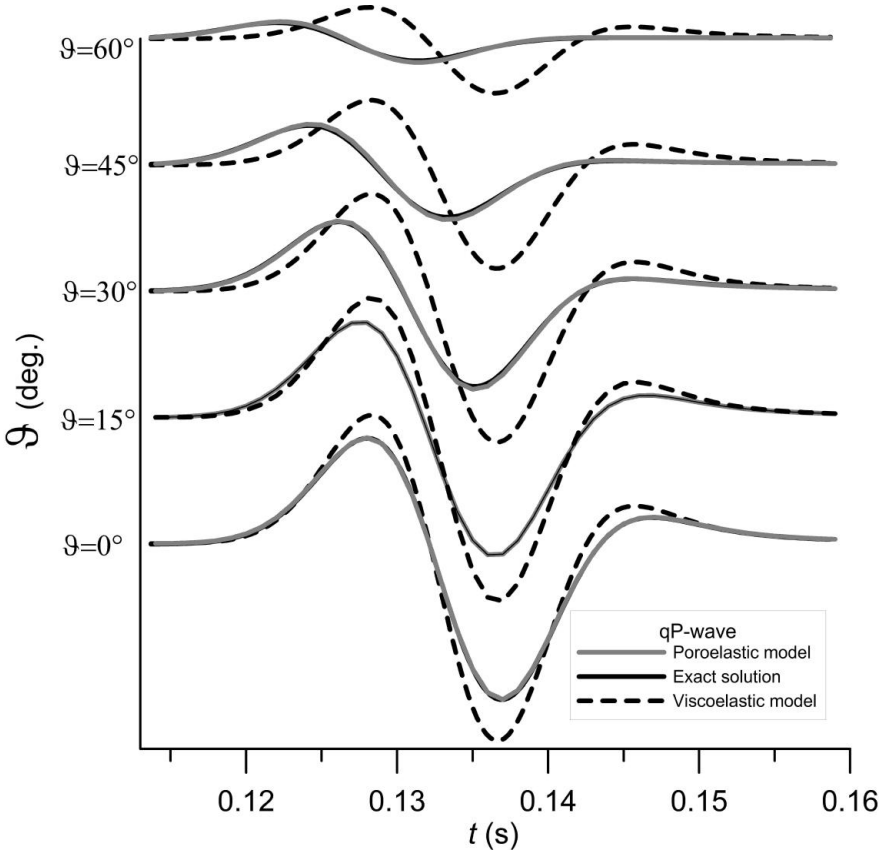

FIGURE 6.10: qP-waveforms at a distance $r = 100$ m from the source at different angles. The medium consists of the layers of coarse sand, $l_1 = 0.09$ m (water-saturated), $l_2 = 0.01$ m (gas-saturated), $f_R = 50$ Hz. Grey and black solid lines coincide.

6.4 Discussion

The effective models discussed in this paper are based on the assumption that the direction of fluid flow is always perpendicular to the layering: the frequency-dependent functions in both effective models describe the attenuation due to inter-layer flow at normal incidence. It was shown in this study that this assumption is reasonable for qP-waveforms: the predictions by the effective poroelastic model are in good agreement with the predictions by the exact solution. Predictions by the effective viscoelastic model are in agreement with the exact solution only in situations where Biot's global flow mechanism is not significant.

The exact solution is readily available for periodically layered media. One may question the justification of the development of effective models for such configurations. However, it is much easier to work with effective homogenized equations giving simpler expressions. The model of White et al. (1975) is an example; many publications report on studies with this model already for decades.

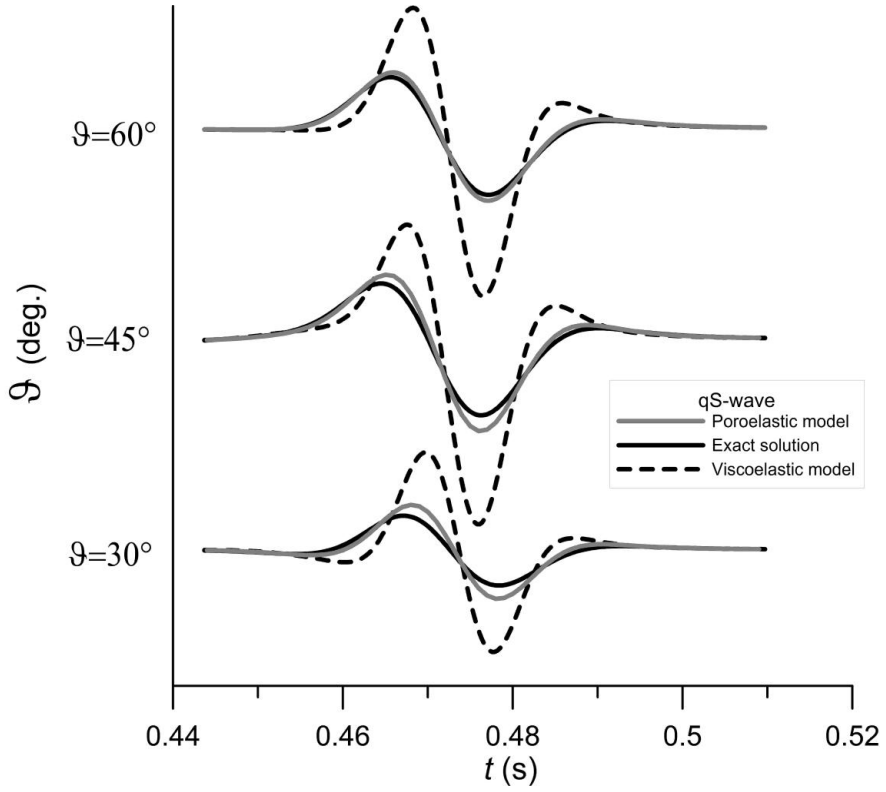

FIGURE 6.11: qS-waveforms at a distance $r = 100$ m from the source at different angles. The medium consists of the layers of coarse sand, $l_1 = 0.09$ cm (water-saturated), $l_2 = 0.01$ m (gas-saturated), $f_R = 50$ Hz.

The effective models for periodic structures can in many cases be extended to the non-periodic case to handle more complicated geometries. The exact analytical solution available for periodically distributed inclusions validates the methods used to obtain the effective models. Although only 2-D numerical examples were shown, the models discussed in this paper can be used to solve problems in 3-D, and can be extended to the situation of non-periodic layering when different frequency-dependent relaxation functions are used (derived for a non-periodic case).

Viscoelastic models are often advantageous over the poroelastic ones because they require less parameters and are more computationally efficient. However, poroelastic models are required for predictions of frequency dependent attenuation in highly permeable media such as shallow marine sediments with inhomogeneous frame and partial saturation, and unconsolidated sand reservoirs.

6.5 Conclusions

Finely layered porous media can be highly dispersive and attenuative, for example due to the variations in the properties of saturating fluids, the presence of soft layers and fractures. In previous work, an effective anisotropic viscoelastic model was proposed for wave propagation in such layered porous media. In this paper, a new effective poroelastic model is proposed. In this new model, the attenuation of seismic waves at mesoscopic scale is described by three frequency-dependent relaxation functions, which were computed for P-waves at normal incidence. The extension to the angle-dependent propagation is provided by the use of poroelastic Backus averaging. Both effective models, the viscoelastic and the poroelastic one, are validated with the exact analytical solution obtained with the use of Floquet's theory applied to Biot's equations with periodically varying coefficients. The effective models predict different qP-wave attenuation and dispersion for soft unconsolidated layers. This is explained by the fact that Biot's global flow attenuation mechanism is not included in the effective viscoelastic model. The examples show that the effective poroelastic model predicts the qP-waveform with high accuracy.

There is a major difference in the predictions of qS-wave attenuation by the effective viscoelastic model and the newly introduced poroelastic model. The effective viscoelastic model predicts mesoscopic attenuation of qS-waves due to the coupling between P- and S-wave motions. The effective medium is isotropic when the shear modulus is constant; then, there is no coupling between P- and S-wave motions. In this case, the S-wave in the effective viscoelastic model is lossless. However, the effective poroelastic model predicts mesoscopic S-wave attenuation even for constant shear modulus; in addition, there is attenuation due to Biot's global flow. The numerical examples show that this results in perceptible differences between the waveforms predicted by the effective viscoelastic and poroelastic models, and that the predictions by the effective poroelastic model are much closer to the exact result.

We conclude that the method used for extension of the attenuation and dispersion caused by the inter-layer flow in 1-D to the arbitrary angle of incidence provides a very good match between the resulting effective model and the exact solution, especially for the qP-wave. The effective poroelastic VTI model, introduced in this paper, is advantageous when soft unconsolidated layers are present. It is also applicable at a broader frequency range than the effective viscoelastic model.

6.A Analytical solution for periodically layered porous medium

The solution of the first-order differential equations with periodic coefficients can be obtained using Floquet's theorem (Floquet, 1883). This theory is extensively used in numerous applications in different disciplines. In particular, it has been applied to elastic composites by Braga and Hermann (1992), and to a 1-D poroelastic composite by Kudarova et al. (2013) (this thesis, Chapter 3). In this section, we apply the method to a 2-D poroelastic composite to obtain an analytical solution that will be used to validate the effective models. The procedure is outlined below.

We consider a periodically layered medium consisting of alternating layers 1 and 2, with the thicknesses l_1 and l_2, and the period $L = l_1 + l_2$ (see Figure 6.1(a)). Each layer is described by Biot's equations of poroelasticity (6.1), and each layer is isotropic. The equations of motion (6.1) and stress-strain relations (6.4) in the frequency-wavenumber domain can be written in the matrix notation:

$$\frac{\partial \tilde{\mathbf{f}}}{\partial z} = \mathrm{i}\tilde{\mathbf{N}}\tilde{\mathbf{f}}, \tag{6.36}$$

where $\tilde{\mathbf{N}}$ is a matrix given in Appendix 6.B; $\tilde{\mathbf{f}} = [\tilde{v}_z, \tilde{\xi}_z, \tilde{\sigma}_{xz}, \tilde{\sigma}_{zz}, \tilde{p}, \tilde{v}_x]$ is a vector containing field variables: $\tilde{v}_z$ and $\tilde{v}_x$ are the z- and x-components of the solid particle velocity, respectively; $\tilde{\xi}_z = (1-\phi)\tilde{v}_z + \phi\tilde{v}_z^f$, where $\tilde{v}_z^f$ is a vertical component of the fluid particle velocity; $\tilde{\sigma}_{xz} = -\tilde{\tau}_{xz}$ and $\tilde{\sigma}_{zz} = -\tilde{\tau}_{zz} - \tilde{p}$ are intergranular stresses.

The elements of the matrix $\tilde{\mathbf{N}}$ are periodic functions of the vertical coordinate z (with the period L) and depend on frequency ω and horizontal slowness s_x. According to Floquet (Floquet, 1883), the solution of (6.36) can be found in the form

$$\tilde{\mathbf{f}} = \tilde{\mathbf{X}}(z)\tilde{\mathbf{c}}, \quad \tilde{\mathbf{X}} = \tilde{\mathbf{F}}(z)\exp(\mathrm{i}\tilde{\mathbf{A}}z) \tag{6.37}$$

where $\tilde{\mathbf{c}}$ is a vector containing six constants to be defined by the boundary conditions, and matrix $\tilde{\mathbf{F}}(z)$ is a periodic matrix, $\tilde{\mathbf{F}}(z) = \tilde{\mathbf{F}}(z+L)$; matrix $\tilde{\mathbf{A}}$ is constant with respect to z. In order to find the matrices $\tilde{\mathbf{F}}$ and $\tilde{\mathbf{A}}$, let us consider the solution of (6.36) within one period L that consists of two layers and is referred to as a periodic cell.

For a stack of layers, the solution of (6.36) can be expressed via the propagator matrix $\tilde{\mathbf{P}}(z)$: $\tilde{\mathbf{f}}(z) = \tilde{\mathbf{P}}(z)\tilde{\mathbf{f}}(z_0)$, where z_0 is the vertical coordinate of the top interface. It follows from this expression that $\tilde{\mathbf{P}}(z_0) = \mathbf{I}$, where $\mathbf{I}$ is the identity matrix. Using Floquet's solution (6.37) at $z = z_0$, one finds $\tilde{\mathbf{f}}(z_0) = \tilde{\mathbf{F}}(z_0)\exp(\mathrm{i}\tilde{\mathbf{A}}z_0)\tilde{\mathbf{f}}(z_0)$, and consequently, $\tilde{\mathbf{F}}(z_0)\exp(\mathrm{i}\tilde{\mathbf{A}}z_0) = \mathbf{I}$. From this relation and the periodicity of $\tilde{\mathbf{F}}(z)$, it follows that

$$\tilde{\mathbf{f}}(z_0 + L) = \tilde{\mathbf{F}}(z_0)\exp(\mathrm{i}\tilde{\mathbf{A}}z_0)\exp(\mathrm{i}\tilde{\mathbf{A}}L)\tilde{\mathbf{f}}(z_0) = \exp(\mathrm{i}\tilde{\mathbf{A}}L)\tilde{\mathbf{f}}(z_0). \tag{6.38}$$

On the other hand, $\tilde{\mathbf{f}}(z_0 + L) = \tilde{\mathbf{P}}(z_0 + L)\tilde{\mathbf{f}}(z_0)$. Hence, $\tilde{\mathbf{P}}(z_0 + L) = \exp(\mathrm{i}\tilde{\mathbf{A}}L)$.

Let us now consider the solution for the two layers of the periodic cell with the coordinates $z_0 \le z \le z_0 + l_1$ for layer 1 and $z_0 + l_1 \le z \le z_0 + L$ for layer 2. In each of the layers 1 and 2, the solution of (6.36) is

$$\begin{aligned} &\tilde{\mathbf{f}}_k(z) = \tilde{\mathbf{M}}_k(z)\tilde{\mathbf{f}}_k(z_k), \quad k = 1, 2, \\ &\tilde{\mathbf{M}}_k(z) = \exp(\mathrm{i}\tilde{\mathbf{N}}_k z), \quad \tilde{\mathbf{M}}_k(z_k) = \mathbf{I}, \end{aligned} \tag{6.39}$$

where z_k is the vertical coordinate of the top interface of the layer k. Summation convention does not apply here. Following this solution, $\tilde{\mathbf{f}}(z_0 + l_1) = \tilde{\mathbf{M}}_1(l_1)\tilde{\mathbf{f}}(z_0)$, and $\tilde{\mathbf{f}}(z_0 + L) = \tilde{\mathbf{M}}_2(l_2)\tilde{\mathbf{f}}(z_0 + l_1) = \tilde{\mathbf{M}}_2(l_2)\tilde{\mathbf{M}}_1(l_1)\tilde{\mathbf{f}}(z_0)$. Hence,

$$\tilde{\mathbf{P}}(z_0 + L) = \exp(\mathrm{i}\tilde{\mathbf{A}}L) = \exp(\mathrm{i}\tilde{\mathbf{N}}_2 l_2)\exp(\mathrm{i}\tilde{\mathbf{N}}_1 l_1). \tag{6.40}$$

Matrix $\tilde{\mathbf{A}}$ is now defined via the relation of the matrix exponentials in (6.40). The eigenvalues of the matrix $\tilde{\mathbf{A}}$ are the so-called Floquet wavenumbers that govern the wave propagation in periodic media. The first step in finding these wavenumbers is to find the matrix exponential $\exp(\mathrm{i}\tilde{\mathbf{N}}_k l_k)$, $k = 1, 2$. In order to compute this matrix, it is convenient to use the eigendecomposition $\tilde{\mathbf{N}}_k = \tilde{\mathbf{L}}_k\tilde{\mathbf{\Lambda}}_k\tilde{\mathbf{L}}_k^{-1}$, where $\tilde{\mathbf{L}}_k$ is a matrix containing the eigenvectors of the matrix $\tilde{\mathbf{N}}_k$, and $\tilde{\mathbf{\Lambda}}_k$ is a diagonal matrix containing its eigenvalues which are the vertical components of the wavenumbers governing wave propagation inside the layer:

$$\begin{aligned} &k_{1z}^{\pm} = \pm\omega\sqrt{\frac{-\hat{d}_1 - \sqrt{\hat{d}_1^2 - 4\hat{d}_0 d_2}}{2d_2} - s_x^2}, \quad k_{2z}^{\pm} = \pm\omega\sqrt{\frac{-\hat{d}_1 + \sqrt{\hat{d}_1^2 - 4\hat{d}_0 d_2}}{2d_2} - s_x^2}, \\ &k_{3z}^{\pm} = \pm\omega\sqrt{\frac{\hat{d}_0}{\mu\hat{\rho}_{22}} - s_x^2}, \end{aligned} \tag{6.41}$$

where $\hat{d}_0 = \hat{\rho}_{11}\hat{\rho}_{22} - \hat{\rho}_{12}^2$, $\hat{d}_1 = -(P\hat{\rho}_{22} + R\hat{\rho}_{11} - 2Q\hat{\rho}_{12})$, $d_2 = PR - Q^2$, the density terms $\hat{\rho}_{ij}$ are defined in Appendix 6.B. The vertical wavenumbers in (6.41) correspond to the up- and downgoing fast and slow P-waves, and S-waves. The elements of the matrices $\tilde{\mathbf{L}}_k$ are not explicitly presented here for the sake of brevity; they are expressed via the elements of the matrices $\tilde{\mathbf{N}}_k$ and can be found using the eigendecomposition. The vertical components of the Floquet wavenumbers k_{iz}^F are expressed via the eigenvalues τ_i of the matrix $\exp(\mathrm{i}\tilde{\mathbf{A}}L)$: $\tau_i = \exp(\mathrm{i}k_{iz}^F L)$.

The next step towards obtaining the solution of (6.36) is to find the periodic matrix $\tilde{\mathbf{F}}(z)$. Without loss of generality, we assume the coordinate of the top interface $z_0 = 0$. Let us define the local coordinate $z_n = z - (n-1)L$, where n is the number of the periodic cell and $0 \le z_n \le L$. Then, the following equalities hold:

$$\tilde{\mathbf{P}}(z) = \tilde{\mathbf{F}}(z)\exp(\mathrm{i}\tilde{\mathbf{A}}z) = \tilde{\mathbf{F}}(z_n)\exp(\mathrm{i}\tilde{\mathbf{A}}z_n)\exp(\mathrm{i}\tilde{\mathbf{A}}L(n-1)) = \tilde{\mathbf{P}}(z_n)\exp(\mathrm{i}\tilde{\mathbf{A}}L(n-1)). \tag{6.42}$$

Right-multiplying (6.42) by $\exp(-\mathrm{i}\tilde{\mathbf{A}}z)$ results in the expression

$$\tilde{\mathbf{F}}(z) = \tilde{\mathbf{P}}(z_n)\exp(-\mathrm{i}\tilde{\mathbf{A}}z_n), \tag{6.43}$$

where the propagator matrix $\tilde{\mathbf{P}}(z_n)$ is defined as

$$\tilde{\mathbf{P}}(z_n) = \begin{cases} \tilde{\mathbf{M}}_1(z_n), & 0 \le z_n \le l_1, \\ \tilde{\mathbf{M}}_2(z_n - l_1)\tilde{\mathbf{M}}_1(l_1), & l_1 \le z_n \le L. \end{cases} \tag{6.44}$$

The matrices $\tilde{\mathbf{F}}$ and $\tilde{\mathbf{A}}$ have been determined in equations(6.40) and (6.43) , and the solution of (6.36) can now be obtained:

$$\tilde{\mathbf{f}}(z) = \tilde{\mathbf{F}}(z)\exp(\mathrm{i}\tilde{\mathbf{A}}z)\tilde{\mathbf{f}}(0) = \tilde{\mathbf{P}}(z_n)\exp(\mathrm{i}\tilde{\mathbf{A}}L(n-1))\tilde{\mathbf{f}}(0). \tag{6.45}$$

The vector $\hat{\mathbf{f}}(0)$ is the solution of Biot's equations related to the top layer:

$$\tilde{\mathbf{f}}(z_0) = \tilde{\mathbf{S}}\begin{bmatrix} A_1 & A_2 & A_3 & A_4 & A_5 & A_6 \end{bmatrix}^{\mathrm{T}}. \tag{6.46}$$

The elements of matrix $\tilde{\mathbf{S}}$ are given in Appendix 6.B. The unknown amplitudes A_i are defined by the boundary conditions. In the examples that follow, we consider the half-space subject to a point-source $\tau_{zz} = f(t)\delta(x)$ at the top interface. In this case, the following six boundary conditions are applied: the stress σ_{zz} is

continuous, $\sigma_{zx} = 0$, fluid pressure $p = 0$ at the top interface $z = 0$ and the radiation condition, which implies the absence of all three up-going Floquet waves.

6.B Matrices of coefficients in the analytical solution

The matrix of coefficients $\tilde{\mathbf{N}}$ in the equations of motion (6.36) reads

$$\tilde{\mathbf{N}} = \omega \begin{bmatrix} \mathbf{0} & \tilde{\mathbf{N}}^a \\ \tilde{\mathbf{N}}^b & \mathbf{0} \end{bmatrix},$$

$$\tilde{\mathbf{N}}^a = \begin{bmatrix} -\frac{R}{d_2} & \phi\frac{Q'}{d_2} & s_x\left(1-\frac{2\mu R}{d_2}\right) \\ .. & \frac{s_x^2\phi^2}{\hat{\rho}_{22}} - \frac{\phi(\phi P-(1-\phi)Q)}{d_2} + \frac{\phi(1-\phi)Q'}{d_2} & s_x\left(1-\phi-\phi\frac{\hat{\rho}_{12}}{\hat{\rho}_{22}}+\frac{2\mu\phi Q'}{d_2}\right) \\ .. & .. & 4\mu s_x^2\left(1-\frac{\mu R}{d_2}\right)+\frac{\hat{\rho}_{12}^2}{\hat{\rho}_{22}}-\hat{\rho}_{11} \end{bmatrix},$$

$$\tilde{\mathbf{N}}^b = \begin{bmatrix} \frac{2\hat{\rho}_{12}(1-\phi)}{\phi} - \frac{\hat{\rho}_{22}(1-\phi)^2}{\phi^2} - \hat{\rho}_{11} & \frac{\hat{\rho}_{22}(1-\phi)}{\phi^2} - \frac{\hat{\rho}_{12}}{\phi} & s_x \\ .. & -\frac{\hat{\rho}_{22}}{\phi^2} & 0 \\ .. & .. & -\frac{1}{\mu} \end{bmatrix}, \tag{6.47}$$

where the dots denote the elements below the diagonal which are equal to the corresponding elements above the diagonal, since matrices $\tilde{\mathbf{N}}^a$ and $\tilde{\mathbf{N}}^b$ are symmetric. In the elements of $\tilde{\mathbf{N}}$, $s_x = k_x/\omega$ is the horizontal slowness, $\hat{\rho}_{12} = -(\alpha_\infty - 1)\phi\rho_f + \mathrm{i}\hat{b}/\omega$, $\hat{\rho}_{11} = (1-\phi)\rho_s - \hat{\rho}_{12}$, and $\hat{\rho}_{22} = \phi\rho_f - \hat{\rho}_{12}$. The damping operator $\hat{b} = b_0\sqrt{1+\mathrm{i}\omega/(2\omega_B)}$, where $b_0 = \eta\phi^2/k_0$. The coefficients $d_2 = PR - Q^2$, $Q' = Q - (1-\phi)R/\phi$.

The elements of the matrix $\tilde{\mathbf{S}}$ from equation (6.46) read $\tilde{S}_{ij} = \tilde{g}_i(k_{jz}^{\pm}, \omega)$, where $k_{jz}^{\pm}$, $j = 1, .., 6$ are the six wavenumbers defined in (6.41). The functions $\tilde{g}_i(k_z, \omega)$,

$i = 1, 6$, read

$$\begin{aligned}
&\tilde{g}_1 = \mathrm{i}\omega, \quad \tilde{g}_2 = \mathrm{i}\omega(1 + \tilde{\beta}_{zf}),\\
&\tilde{g}_3 = -\mathrm{i}(1-\phi)E_3(k_z\tilde{\beta}_{zf} + k_x\tilde{\beta}_{xf}) + \mathrm{i}(\mu k_z - (1-\phi)E_2k_x)\tilde{\beta}_x - \mathrm{i}(E_2k_z + \mu k_x),\\
&\tilde{g}_4 = \mathrm{i}\left((E_1 - 2\mu)k_x - (1-\phi)E_2k_x\right)\left(\tilde{\beta}_x + \mathrm{i}\left(E_2 - (1-\phi)E_3\right)\left(\tilde{\beta}_{xf}k_x + \tilde{\beta}_{zf}k_z\right) + \right.\\
&\left. + \mathrm{i}k_z(E_1 - (1-\phi)E_2\right),\\
&\tilde{g}_5 = \mathrm{i}E_2(k_z + \tilde{\beta}_x k_x) + E_3(k_z\tilde{\beta}_{zf} + k_x\tilde{\beta}_{xf}), \quad \tilde{g}_6 = \mathrm{i}\omega\tilde{\beta}_x.
\end{aligned} \tag{6.48}$$

The coefficients $\tilde{\beta}_{zf}$, $\tilde{\beta}_{xf}$ and $\tilde{\beta}_x$ are the ratios of the amplitudes $\tilde{W}_z$, $\tilde{W}_x$ and $\tilde{U}_x$ from (6.6) to $\tilde{U}_z$, respectively. They read

$$\begin{aligned}
\tilde{\beta}_x &= -\frac{\hat{m}k_xk_z}{\Delta}\left(\omega^2(E_2\rho_f + \hat{m}(\mu - E_1)) + k_z^2(E' - \mu E_3\right),\\
\tilde{\beta}_{zf} &= -\frac{1}{\Delta}\left(\omega^4\hat{m}' - \omega^2\left((\hat{m}\mu\rho_f + \hat{m}'E_2)k_z^2 + \rho_f k_x^2(\rho_f E_2 - \hat{m}E_1)\right) + \right.\\
&\quad \left. + \hat{m}\mu E_2 k_z^4 + (\mu(\hat{m}E_2 - \rho_f E_3) + E'\rho_f)k_z^2k_x^2\right),\\
\Delta &= \hat{m}\omega^4\hat{m}' - \omega^2\left((\hat{m}'E_3 + \hat{m}^2\mu)k_z^2 + \hat{m}(\hat{m}E_1 - \rho_f E_2)k_x^2\right) + \hat{m}k_z^2(\mu E_3 k_z^2 + E'k_x^2),\\
\tilde{\beta}_{xf} &= -\frac{\rho_f}{\hat{m}}\beta_x, \qquad \hat{m}' = \hat{m}\rho - \rho_f^2, \quad E' = E_1E_3 - E_2^2.
\end{aligned} \tag{6.49}$$

6.C Formulas for the effective viscoelastic VTI medium

The formulas for relaxed and unrelaxed elastic coefficients used by Krzikalla and Müller (2011) and used in this chapter were originally derived by Gelinsky and Shapiro (1997). The unrelaxed coefficients read

$$\begin{aligned}
A^u &= \left\langle \frac{4\mu(\lambda^u + \mu)}{P^u} \right\rangle + \left\langle \frac{1}{P^u} \right\rangle^{-1} \left\langle \frac{\lambda^u}{P^u} \right\rangle^2,\\
C^u &= \left\langle \frac{1}{P^u} \right\rangle^{-1}, \qquad F^u = \left\langle \frac{1}{P^u} \right\rangle^{-1} \left\langle \frac{\lambda^u}{P^u} \right\rangle, \qquad D^u = \left\langle \frac{1}{\mu} \right\rangle^{-1},\\
B_6^u &= B_7^u = \left\langle \frac{\frac{1-\phi}{K_s} - \frac{K_m}{K_s^2} + \frac{\phi}{K_f}}{\left(1 - \frac{K_m}{K_s}\right)} \right\rangle^{-1}.
\end{aligned} \tag{6.50}$$

In equations 6.50,

$$\lambda^u = K_m - \frac{2}{3}\mu + \left(1 - \frac{K_m}{K_s}\right)^2 \left(\frac{1-\phi}{K_s} - \frac{K_m}{K_s^2} + \frac{\phi}{K_f}\right)^{-1}, \quad P^u = \lambda^u + 2\mu. \tag{6.51}$$

The unrelaxed limit of B_8 is not defined, because this coefficient is not present in the stress-strain relations, since $\nabla \cdot \mathbf{w} = \mathbf{0}$ (no-flow condition, see Gelinsky and Shapiro (1997)). The relaxed coefficients read

$$\begin{aligned}
A^r &= \left\langle \frac{4\mu(\lambda^r+\mu)}{P^r} \right\rangle + \left\langle \frac{1}{P^r} \right\rangle^{-1} \left\langle \frac{\lambda}{P^r} \right\rangle^2 + \frac{(B_6^r)^2}{B_8^r}, \\
C^r &= \left\langle \frac{1}{P^r} \right\rangle^{-1} + \frac{(B_7^r)^2}{B_8^r}, \qquad F^u = \left\langle \frac{1}{P^r} \right\rangle^{-1} \left\langle \frac{\lambda^r}{P^r} \right\rangle + \frac{B_6^r B_7^r}{B_8^r}, \qquad D^u = \left\langle \frac{1}{\mu} \right\rangle^{-1}, \\
B_6^r &= -B_8^r \left(\left\langle \frac{2\left(1-\frac{K_m}{K_s}\right)\mu}{P^r} \right\rangle + \left\langle \frac{1-\frac{K_m}{K_s}}{P^r} \right\rangle \left\langle \frac{\lambda^r}{P^r} \right\rangle \left\langle \frac{1}{P^r} \right\rangle^{-1} \right), \\
B_7^r &= -B_8^r \left\langle \frac{1-\frac{K_m}{K_s}}{P^r} \right\rangle \left\langle \frac{1}{P^r} \right\rangle^{-1}, \\
B_8^r &= \left(\left\langle \frac{1-\phi}{K_s} - \frac{K_m}{K_s^2} + \frac{\phi}{K_f} \right\rangle + \left\langle \frac{\left(1-\frac{K_m}{K_s}\right)^2}{P^r} \right\rangle - \left\langle \frac{1-\frac{K_m}{K_s}}{P^r} \right\rangle^2 \left\langle \frac{1}{P^r} \right\rangle^{-1} \right)^{-1}.
\end{aligned} \tag{6.52}$$

In equations 6.52,

$$\lambda^r = K_m - \frac{2}{3}\mu, \quad P^r = \lambda^r + 2\mu. \tag{6.53}$$

The frequency-dependent plane-wave modulus that connects the relaxed and unrelaxed regimes (see (6.13)) was derived by White et al. (1975). It is defined by the following relations:

$$\hat{K}(\omega) = \frac{K^*}{1 + 2(R_1 - R_2)^2 \mathrm{i}/(\omega L(Z_1 + Z_2))}, \quad K^* = \left\langle (P^u)^{-1} \right\rangle^{-1}, \tag{6.54}$$

where for each layer 1 and 2

$$\begin{aligned}
R &= \left(1 - \frac{K_m}{K_s}\right)\frac{K_a}{P_u}, \quad K_a = \left(\frac{1-\phi}{K_s} - \frac{K_m}{K_s^2} + \frac{\phi}{K_f}\right)^{-1}, \\
Z &= Z_0 \cot(\frac{1}{2}\alpha_w l), \quad Z_0 = \sqrt{\eta K_e \mathrm{i}/(\omega k_0)} \\
\alpha_w &= \sqrt{-\mathrm{i}\omega\eta/(k_0 K_e)}, \quad K_e = K_a(K_m + \frac{4}{3}\mu)/P^u.
\end{aligned} \tag{6.55}$$

Chapter 7

Conclusions

In this thesis effective models are studied for wave propagation in porous media with mesoscopic-scale heterogeneities. There is an increasing demand in establishing links between subsurface properties, including both reservoir and overburden properties, and seismic attenuation, which has a significant potential as an attribute for subsurface characterization. The presence of mesoscopic-scale heterogeneities (those larger than the pore and grain sizes but smaller than the wavelength) in porous media causes significant frequency-dependent attenuation at seismic frequencies. Effective models are used to link the poroelastic parameters of the subsurface to the observed dispersion and attenuation of seismic waves, introducing some assumptions on the distribution and size of heterogeneities. This approach helps to reduce uncertainty in characterization by limiting the number of unknown parameters by using a homogenized model.

Models for periodically distributed heterogeneities are studied in this thesis. A new model is proposed in Chapter 3 for 1-D wave propagation in a periodically layered poroelastic solid, where each layer is governed by Biot's equations, and heterogeneities can occur in the porous frame and in saturating fluid properties. This study was motivated by the effective viscoelastic model of White et al. (1975) and its extension by Vogelaar and Smeulders (2007), which is also considered in Chapter 3. The simplicity of White's model makes it attractive for numerous applications. One of the important applications is a benchmark solution for more complicated problems. However, the exact solution can be obtained for periodic structures with the use of Floquet's theory. The derivation of the exact solution for a 1-D periodic poroelastic composite is therefore also presented in Chapter 3. Comparison of the predictions of White's model against the predictions of the exact

solution showed that White's model significantly underestimates attenuation for high-permeable media, such as marine sediments. This is because White's model does not account for Biot's global flow attenuation mechanism. The new model proposed in Chapter 3 incorporates Biot's global flow mechanism together with the attenuation due to the presence of mesoscopic heterogeneities, and predicts the same result as the exact solution at the whole frequency range where the model is valid (up to the frequencies where the wavelength is still large compared to the period of the system). The novelty of the model lies in the application of pressure-continuity boundary conditions instead of the no-flow conditions at the outer edges of the elementary cell. The new model is advantageous in geological environments where soft and highly permeable unconsolidated layers are present.

A new poroelastic model for periodically distributed spherical inclusions is proposed in Chapter 4. This model also originates from viscoelastic models by White (1975) and Vogelaar et al. (2010). It is also possible to derive the exact solution with Floquet's theory for this configuration, however it is more demanding than for the layered medium, and is not presented here. The results obtained from the comparison of the models are similar to those obtained for the periodically layered composite: the effective poroelastic model is in agreement with the effective viscoelastic one, but performs better for soft sediments. This result has a practical application for marine soils. Shallow near-surface sediments are often partially saturated, containing free gas bubbles. The proposed model can be used to estimate free gas saturation from seismic reflection data.

In Chapter 5 effective models are proposed that are governed by equations with coefficients that do not depend on frequency, using higher-order terms in the equations of motion. Such models are useful for time-domain analysis, which is advantageous over frequency-domain analysis in nonlinear problems. Although the effective model is a linear model, it can be coupled to a domain with nonlinear behaviour. The absence of coefficients with complicated frequency dependence enables efficient coupling. It is shown that such a model can be derived for a periodically layered porous medium in a simple manner by expanding the dispersion equation of White's model in powers of frequency and reconstructing the equation of motion including higher-order terms from this expansion. The results of such an approximation for low frequencies are presented and are shown to work well for sufficiently low frequencies.

Another approximation is also proposed in Chapter 5, which uses homogenization with the two-scale method of asymptotic expansions. A similar approximation

is well-known for an elastic composite. In Chapter 5, we extend the derivation to a poroelastic composite. The effective matrix coefficients are derived. The model gives a good approximation at lower frequencies, while at higher frequencies the viscoelastic approximation from the dispersion equation of White's model gives better predictions.

The new effective model presented in Chapter 3 is used in Chapter 6 to derive a 2-D vertical transversely isotropic effective poroelastic model for periodically layered media to predict angle-dependent qP- and qS-wave attenuations. The exact solution is obtained for the periodically layered half-space, using Floquet's theory in the frequency-wavenumber domain, similar to the solution for the 1-D case in Chapter 3. The solution is also obtained for the effective viscoelastic model, a model based on White's effective modulus. The time-domain responses predicted by all solutions are compared. Similar to the 1-D case, the effective poroelastic model gives accurate predictions of qP-waveforms for soft sediments whereas the viscoelastic model fails. However, the results for the qS-waveforms differ for all models. Still, the predictions of the effective poroelastic model are closer to the exact solution than those of the effective viscoelastic model. In case of constant shear modulus throughout the layers, the effective viscoelastic model is isotropic, and the P- and S-wave motions are decoupled, with the S-wave being lossless. The effective poroelastic model, however, remains anisotropic, and P-wave motions contribute to the attenuation of qS-wave. Furthermore, the mesoscopic-scale attenuation mechanism incorporated in the model is based solely on the mesoscopic P-wave attenuation mechanism; inclusion of a frequency-dependent shear wave modulus might improve the results. Biot's global flow also influences S-wave attenuation, and for soft sediments, where the effect is important, the differences in qS-wave predictions by the models are even more pronounced, since the viscoelastic model does not incorporate this mechanism. Another important result is the validation of the assumption of the 1-D mesoscopic fluid flow (i.e., normal to the layering) for description of wave propagation in 2-D layered media.

The models proposed in this thesis can be used to study seismic attenuation in media with heterogeneities. They can be instrumental in predicting the dependence between material properties and attenuation in media with heterogeneities, especially in shallow marine sediments with inhomogeneous frame and partial saturation, and in unconsolidated sand reservoirs, where the previously developed viscoelastic models might give inaccurate predictions.

Bibliography

Allard, J.F., Depollier, C., and Lesperance, A., 1986, Observation of the Biot slow-wave in a plastic foam of high flow resistance at acoustical frequencies: Journal of Applied Physics, **59**, 3367–3370.

Amalokwu, K., Best, A.I., Sothcott, J., Chapman, M., Minshull, T., and Li, X.Y., 2014, Water saturation effects on elastic wave attenuation in porous rocks with aligned fractures: Geophysical Journal International, **197**, 943–947.

Andrianov, I.V., Bolshakov, V.I., Danishevskyy, V.V., and Weichert, D., 2008, Higher order asymptotic homogenization and wave propagation in periodic composite materials: Proceedings of the Royal Society A, **464**, 1181–1201.

Auriault, J.L., 1980a, Dynamic behaviour of a porous medium saturated by a Newtonian fluid: International Journal of Engineering Science, **18**, 775–785.

———, 1980b, Heterogeneous medium. Is an equivalent macroscopic description possible?: International Journal of Engineering Science, **27**, 785–795.

———, 2002, Upscaling heterogeneous media by asymptotic expansions: Journal of Engineering Mechanics, **128**, 817–822.

Auriault, J.L., Borne, L., and Chambon, R., 1985, Dynamics of porous saturated media, checking of the generalized law of Darcy: Journal of the Acoustical Society of America, **77**, 1641–1650.

Bakhvalov, N.S. and Panasenko, G.P., 1989, Homogenization: averaging processes in periodic media: Dordrecht: Kluwer.

Benssousan, A., Lions, J.L., and Papanicoulau, G., 1978, Asymptotic analysis for periodic structures: Amsterdam: North-Holland.

Berryman, J.G., 1980, Confirmation of Bit's theory: Applied Physics Letters, **37**, 382–384.

———, 1986, Elastic wave attenuation in rocks containing fluids: Applied Physics Letters, **49**, 552–554.

———, 2005, Comparison of upscaling methods in poroelasticity and its generalizations: Journal of Engineering Mechanics, **131**, 928–936.

Biot, M.A., 1956a, Theory of propagation of elastic waves in a fluid-saturated porous solid. I. Low-frequency range: Journal of the Acoustical Society of America, **28**, 168–178.

———, 1956b, Theory of propagation of elastic waves in a fluid-saturated porous solid. II. Higher frequency range: Journal of the Acoustical Society of America, **28**, 179–191.

———, 1962, Mechanics of deformation and acoustic propagation in porous media: Journal of Applied Physics, **33**, 1482–1498.

Biot, M.A. and Willis, D.G., 1957, The elastic coefficents of the theory of consolidation: Journal of Applied Mechanics, **24**, 594–601.

Bonnet, G., 1987, Basic singular solutions for a poroelastic medium in the dynamic range: Journal of the Acoustical Society of America, **82**, 1758–1762.

Bowen, R., 1976, Theory of mixtures, Continuum physics Vol. III: A. Eringen, ed., Academic, New York.

Bowen, R.M., 1980, Incompressible porous media models by use of the theory of mixtures: International Journal of Engineering Science, **18**, 1129–1148.

———, 1982, Compressible porous media models by use of the theory of mixtures: International Journal of Engineering Science, **20**, 697–735.

Braga, A.B. and Hermann, G., 1992, Floquet waves in anisotropic layered composites: Journal of the Acoustical Society of America, **91**, 1211–1227.

Brajanovski, M. and Gurevich, B., 2005, A model for P-wave attenuation and dispersion in a porous medium permeated by aligned fractures: Geophysical Journal International, **163**, 372–384.

Brown, R.J.S., 1980, Connection between formation factor for electrical resistivity and fluid-solid coupling factor in Bit's equations for acoustic waves in fluid-filled porous media: Geophysics, **45**, 1269–1275.

Burridge, R. and Keller, J.B., 1981, Poroelasticity equations derived from microstructure: Journal of the Acoustical Society of America, **70**, 1140–1146.

Capdeville, Y., Guillot, L., and Marigo, J.J., 2010a, 1-D non-periodic homogenization for seismic wave equation: Geophysical Journal International, **181**, 897–910.

———, 2010b, 2-D non-periodic homogenization to upscale elastic media for P-SV waves: Geophysical Journal International, **182**, 903–922.

Carcione, J.M., 2007, Wave fields in real media: wave propagation in anisotropic, anelastic, porous and electromagnetic media: Elsevier Science Ltd, Amsterdam.

Carcione, J.M., Helle, H.B., and Pham, N.H., 2003, White's model for wave propagation in partially saturated rocks: comparison with poroelastic numerical experiments: Geophysics, **68**, 1389–1398.

Carcione, J.M., Morency, C., and Santos, J.E., 2010, Computational poroelasticity — A review.: Geophysics, **75**, A229–A243.

Carcione, J.M. and Picotti, S., 2006, P-wave seismic attenuation by slow-wave diffusion: Effects of inhomogeneous rock properties: Geophysics, **71**, O1–O8.

Carcione, J.M., Santos, J.E., and Picotti, S., 2011, Anisotropic poroelasticity and wave-induced fluid flow: harmonic finite-element simulations: Geophysical Journal International, **186**, 1245–1254.

Chen, W. and Fish, J., 2001, A dispersive model for wave propagation in periodic heterogeneous media based on homogenization with multiple spatial and temporal scales: Journal of Applied Mechanics, **68**, 153–161.

Chotiros, N.P., 1995, Biot model of sound propagation in water-saturated sand: Journal of the Acoustical Society of America, **97**, 199–214.

Cryer, C.W., 1963, A comparison of the three-dimensional consolidation theories of Biot and Terzaghi: The Quarterly Journal of Mechanics and Applied Mathematics, **16**, 401–412.

de Boer, R., 2000, Theory of porous media: Highlights in historical development and current state: Springer.

de Boer, R., Ehlers, W., and Liu, Z., 1993, One-dimensional transient wave propagation in fluid-saturated incompressible porous media: Archive of Applied Mechanics, **63**, 59–72.

Deng, J., Qu, S., Wang, S., Zhu, S., and Wang, X., 2012, P-wave attenuation and dispersion in a porous medium permeated by aligned fractures - a new poroelastic approach: Journal of Geophysics and Engineering, **9**, 115–126.

Deresiewicz, H. and Skalak, R., 1963, On uniqueness in dynamic poroelasticity: Bulletin of the Seismological Society of America, **53**, 783–788.

Diebels, S. and Ehlers, W., 1996, Dynamic analysis of a fully saturated porous medium accounting for geometrical and material non-linearities: International Journal for Numerical Methods in Engineering, **39**, 81–97.

Dutta, N.C. and Ode, H., 1979a, Attenuation and dispersion of compressional waves in fluid-filled porous rocks with partial gas saturation (White model)-part I: Biot theory: Geophysics, **44**, 1777–1788.

———, 1979b, Attenuation and dispersion of compressional waves in fluid-filled

porous rocks with partial gas saturation (White model)-part II: Rresults: Geophysics, **44**, 1789–1805.

Dutta, N.C. and Seriff, A.J., 1979, On White's model of attenuation in rocks with partial gas saturation: Geophysics, **44**, 1806–1812.

Dvorkin, J. and Nur, A., 1993, Dynamic poroelasticity: A unified model with the squirt and the Biot mechanisms: Geophysics, **58**, 524–533.

Ehlers, W. and Kubik, J., 1994, On finite dynamic equations for fluid- saturated porous media: Acta Mechanica, **105**, 101–117.

Fish, J., Chen, W., and Nagai, G., 2002, Nonlocal dispersive model for wave propagation in heterogeneous media: one-dimensional case: International Journal for Numerical Methods in Engineering, **54**, 331–346.

Floquet, G., 1883, Sur les équations différentielles linéaires à coefficients périodiques: Annales scientifiques de l'École Normale Supérieure, **2**, 47–88.

Frenkel, J., 1944, On the theory of seismic and seismoelectric phenomena in a moist soil: Journal of Physics, **VIII**, 230–241.

Gelinsky, S. and Shapiro, S., 1997, Poroelastic Backus averaging for anisotropic layered fluid- and gas-saturated sediments: Geophysics, **62**, 1867–1878.

Gelinsky, S., Shapiro, S.A., Müller, T., and Gurevich, B., 1998, Dynamic poroelasticity of thinly layered structures: International Journal of Solids and Structures, **35**, 4739–4751.

Gist, G.A., 1994, Interpreting laboratory velocity measurements in partially gas-saturated rocks: Geophysics, **59**, 1100–1109.

Gurevich, B. and Schoenberg, M., 1999, Interface conditions for Biot's equations of poroelasticity: Journal of the Acoustical Society of America, **105**, 2585–2589.

Hefner, B.T. and Jackson, D.R., 2010, Dispersion and attenuation due to scattering from heterogeneities of the frame bulk modulus of a poroelastic medium: Journal of the Acoustical Society of America, **127**, 3372–3384.

Jocker, J. and Smeulders, D., 2009, Ultrasonic measurements on poroelastic slabs: Determination of reflection and transmission coefficients and processing for Biot input parameters: Ultrasonics, **49**, 319–330.

Johnson, D.L., 1980, Equivalence between the fourth sound in liquid He ii at low temperatures and Bit slow wave in consolidated porous media: Applied Physics Letters, **37**, 1065–1067.

———, 2001, Theory of frequency dependent acoustics in patchy-saturated porous media: Journal of the Acoustical Society of America, **110**, 682–694.

Johnson, D.L., Koplik, J., and Dashen, R., 1987, Theory of dynamic permeability

and tortuosity in fluid-saturated porous media: Journal of Fluid Mechanics, **176**, 379–402.

Johnston, D.H., Toksöz, M.N., and Timur, A., 1979, Attenuation of seismic waves in dry and saturated rocks: mechanisms: Geopysics, **44**, 691–711.

Kelder, O. and Smeulders, D.M.J., 1997, Observation of the Biot slow wave in water-saturated Nivelsteiner sandstone: Geophysics, **62**, 1794–1796.

Kliments, T. and McCann, C., 1988, Why is the Biot slow compressional wave not observed in real rocks: Geophysics, **53**, 1605–1609.

Krzikalla, F. and Müller, T., 2011, Anisotropic P-SV-wave dispersion and attenuation due to inter-layer flow in thinly layered porous rocks: Geophysics, **76**, WA135–WA145.

Kudarova, A.M., van Dalen, K.N., and Drijkoningen, G.G., 2013, Effective poroelastic model for one-dimensional wave propagation in periodically layered media: Geophysical Journal International, **195**, 1337–1350.

Lee, M.W. and Collett, T.S., 2009, Unique problems associated with seismic analysis of partially gas-saturated unconsolidated sediments: Marine and Petroleum Geology, **26**, 775–781.

Levy, T., 1979, Propagation of waves in a fluid-saturated porous elastic solid: International Journal of Engineering Science, **17**, 1005–1014.

Liu, Z., Bluhm, J., and de Boer, R., 1998, Inhomogeneous plane waves, mechanical energy flux, and energy dissipation in a two-phase porous medium: Journal of Applied Mathematics and Mechanics (ZAMM), **78**, 617–625.

Mavko, G. and Nur, A., 1979, Wave propagation in partially saturated rocks: Geophysics, **44**, 161–178.

Mei, C.C. and Auriault, J.L., 1989, Mechanics of heterogeneous porous media with several spatial scales: Proceedings of the Royal Society A, **426**, 391–423.

Molotkov, L.A. and Bakulin, A.V., 1999, Effective models of stratified media containing porous Biot layers: Journal of Mathematical Sciences, **96**, 3371–3385.

Morgan, E.C., M, V., I, L., Baise, L.G., Longva, O., and McAdoo, B., 2012, Estimation of free gas saturation from seismic reflection surveys by the genetic algorithm inversion of a P-wave attenuation model: Geophysics, **77**, R175–R187.

Müller, T.M. and Gurevich, B., 2005, Wave-induced fluid flow in random porous media: Attenuation and dispersion of elastic waves: Journal of the Acoustical Society of America, **117**, 2732–2741.

Müller, T.M., Gurevich, B., and Lebedev, M., 2010, Seismic wave attenuation and dispersion resulting from wave-induced flow in porous rocks — A review:

Geophysics, **75**, A147–A164.

Nagy, P.B., Adler, L., and Bommer, B.P., 1990, Slow-wave propagation in air-filled porous materials and natural rocks: Applied Physics Letters, **56**, 2504–2506.

Nakagawa, S., Kneafsey, T.J., Daley, T.M., Freifeld, B.M., and Rees, E.V., 2013, Laboratory seismic monitoring of supercritical CO2 flooding in sandstone cores using the Split Hopkinson Resonant Bar technique with concurrent x-ray Computed Tomography imaging: Geophysical Prospecting, **61**, 254–269.

Nikolaevskiy, V.N., 2005, Biot–Frenkel poromechanics in Russia (Review): Journal of Engineering Mechanics, **131**, 888–897.

Norris, A., 1993, Low-frequency dispersion and attenuation in partially saturated rocks: Journal of the Acoustical Society of America, **94**, 359–370.

O'Connell, R.J. and Budiansky, B., 1977, Visco-elastic properties of fluid-saturated cracked solids: Journal of Geophysical Research, **82**, 5719–5735.

Palmer, I.D. and Traviola, M.L., 1980, Attenuation by squirt flow in undersaturated gas sands: Geophysics, **45**, 1780–1792.

Picotti, S., Carcione, J.M., G., D.G., Rossi, and Santos, J.E., 2012, Seismic modeling to monitor CO_2 geological storage: The Atzbach-Schwanenstadt gas field: Journal of Geophysical Research, **117**, B06103.

Plona, T.J., 1980, Observation of a second bulk compressional wave in porous medium at ultrasonic frequencies: Applied Physics Letters, **36**, 259–261.

Pride, S.R., Berryman, J.G., and Harris, J.M., 2004, Seismic attenuation due to wave-induced flow: Journal of Geophysical Research, **109**, BO1201.

Pride, S.R., Gangi, A.F., and Morgan, F.D., 1992, Deriving the equations of motion for porous isotropic media: Journal of the Acoustical Society of America, **92**, 3278–3290.

Pride, S.R. and Garambois, S., 2005, Electroseismic wave theory of Frenkel and more recent developments: Journal of Engineering Mechanics, **131**, 898–907.

Pride, S.R., Harris, J.M., Johnson, D.L., Mateeva, A., Nihei, K.T., Nowack, R.L., Rector, J.R., Spetzler, H., Wu, R., Yamomoto, T., Berryman, J.G., and Fehler, M., 2003, Permeability dependence of seismic amplitudes.: The Leading Edge, **22**, 518–525.

Pride, S.R., Tromeur, E., and Berryman, J.G., 2002, Biot slow-wave effects in stratified rock: Geophysics, **67**, 271–281.

Qi, Q., Müller, T.M., and Rubino, J.G., 2014, Seismic attenuation: effects of interfacial impedance on wave-induced pressure diffusion: Geophysical Journal International, **199**, 1677–1681.

Quintal, B., 2012, Frequency-dependent attenuation as a potential indicator of oil saturation: Journal of Applied Geohysics, **82**, 119–128.

Quintal, B., Schmalholz1, S.M., and Podladchikov, Y.Y., 2009, Low-frequency reflections from a thin layer with high attenuation caused by interlayer flow: Geophysics, **74**, N15–N23.

Quintal, B., Steeb, H., Freshener, M., and Schmalholtz, S.M., 2011, Quasistatic finite element modeling of seismic attenuation and dispersion due to waveinduced fluid flow in poroelastic media: Journal of Geophysical Research, **116**, B01201.

Rasolofosaon, P.N.J., 1988, Importance of interface hydraulic condition on the generation of second bulk compressional wave in porous media: Applied Physics Letters, **52**, 780–782.

Rubino, J.G. and Holliger, K., 2012, Seismic attenuation and velocity dispersion in heterogeneous partially saturated porous rocks: Geophysical Journal International, **188**, 1088–1102.

Rubino, J.G., Monachesi, L.B., Müller, T.M., Guarracino, L., and Holliger, K., 2013, Seismic wave attenuation and dispersion due to wave-induced fluid flow in rocks with strong permeability fluctuations: Journal of the Acoustical Society of America, **134**, 4742–4751.

Rubino, J.G., Ravazzoli, C.L., and Santos, J.E., 2006, Reflection and transmission of waves in composite porous media: A quantification of energy conversions involving slow waves: Journal of the Acoustical Society of America, **120**, 2425–2436.

———, 2009, Equivalent viscoelastic solids for heterogeneous fluid-saturated porous rocks: Geophysics, **74**, N1–N13.

Rubino, J.G. and Velis, D.R., 2011, Seismic characterization of thin beds containing patchy carbon dioxide-brine distributions: A study based on numerical simulations: Geophysics, **76**, R57–R67.

Rubino, J.G., Velis, D.R., and Sacchi, M.D., 2011, Numerical analysis of wave-induced fluid flow effects on seismic data: Application to monitoring of CO_2 storage at the sleipner field: Journal of Geophysical Research, **116**, B03306.

Sahay, P.N., 2008, On the Biot slow S-wave: Geophysics, **73**, N19–N33.

Sanchez-Palencia, E., 1980, Non-homogeneous media and vibration theory: Springer, Berlin.

Schanz, M., 2009, Poroelastodynamics: linear models, analytical solutions, and numerical methods: Applied Mechanics Reviews, **62**, 030803.

Schanz, M. and Diebels, S., 2003, A comparative study of Biot's theory and the

linear theory of porous media for wave propagation problems: Acta Mechanica, **161**, 213–235.

Schoemaker, F.C., 2011, Electrokinetic conversion: PhD thesis, Delft University of Technology.

Sidler, R., Rubino, J.G., and Holliger, K., 2013, Quantitative comparison between simulations of seismic wave propagation in heterogeneous poro-elastic media and equivalent visco-elastic solids for marine-type environments: Geophysical Journal International, **193**, 463–474.

Smeulders, D.M.J., 2005, Experimental evidence for slow compressional waves: Journal of Engineering Mechanics, **131**, 908–917.

Sommerfeld, A., 1949, Partial differential equations in physics: Academin Press, New York.

Toms, J., Müller, T.M., Ciz, R., and Gurevich, B., 2006, Comparative review of theoretical models for elastic wave attenuation and dispersion in partially saturated rocks: Soil Dynamics and Earthquake Engineering, **26**, 548–565.

Truesdell, C. and Toupin, R., 1960, The classical field theories, Handbuch der Physik Vol. III/1: S. Flügge, ed., Springer-Verlag, Berlin.

Turgut, A. and Yamamoto, T., 1990, Measurements of acoustic wave velocities and attenuation in marine sediments: Journal of the Acoustical Society of America, **87**, 2349–2358.

van Dalen, K.N., 2013, Multi-component acoustic characterization of porous media: Springer.

Vardoulakis, I. and Beskos, D.E., 1986, Dynamic behavior of nearly saturated porous media: Mechanics of Materials, **5**, 87–108.

Vogelaar, B. and Smeulders, D., 2007, Extension of White's layered model to the full frequency range: Geophysical Prospecting, **55**, 685–695.

Vogelaar, B., Smeulders, D., and Harris, J., 2010, Exact expression for the effective acoustics of patchy-saturated rocks: Geophysics, **75**, N87–N96.

Wang, Y., Chen, S., Wang, L., and Li, X.Y., 2013, Modeling and analysis of seismic wave dispersion based on the rock physics model: Journal of Geophysics and Engineering, **10**, 054001.

Wapenaar, C.P.A. and Berkhout, A.J., 1989, Elastic wave field extrapolation: redatuming of single- and multi-component seismic data: Elsevier.

Wenzlau, F., Altmann, J.B., and Müller, T.M., 2010, Anisotropic dispersion and attenuation due to wave-induced fluid flow: Quasi-static finite element modeling in poroelastic solids: Journal of Geophysical Research, **115**, B07204.

White, J.E., 1975, Computed seismic speeds and attenuation in rocks with partial gas saturation: Physics of Solid Earth, **40**, 224–232.

White, J.E., Mikhaylova, N.G., and Lyakhovistkiy, F.M., 1975, Low-frequency seismic waves in fluid saturated layered rocks: Physics of Solid Earth, **11**, 654–659.

Williams, K.L., 2001, An effective density fluid model for acoustic propagation in sediments derived from Biot theory: Journal of the Acoustical Society of America, **110**, 2276–2281.

Winkler, K., 1985, Dispersion analysis of velocity and attenuation in Berea sandstone: Journal of Geophysical Research, **90**, 6793–6800.

Wu, K., Xue, Q., and Adler, L., 1990, Reflection and transmission of elastic waves from a fluid-saturated porous solid boundary: Journal of the Acoustical Society of America, **87**, 2376–2383.

Zhang, Y., Xu, Y., Xia, J., Ping, P., and Zhang, S., 2014, Viscoelastic representation of surface waves in patchy saturated poroelastic media: Earthquake Science, **27**, 421–431.

Summary

Studying seismic wave propagation in porous media is instrumental in finding links between subsurface properties and attributes of wave propagation, such as dispersion and attenuation. Seismic waves are sensitive to the presence of mesoscopic-scale heterogeneities in porous media, those larger than the typical pore and grain sizes but smaller than the wavelength. It is widely accepted that Biot's theory which is commonly used to describe wave propagation in poroelastic solids underestimates observed attenuation and dispersion of elastic waves in such heterogeneous media. The attenuation mechanism in Biot's theory is driven by the wavelength-scale fluid-pressure gradients created by a passing wave, which results in relative fluid-to-solid movement accompanied by internal friction due to the viscous forces between the solid and fluid phases. This mechanism does not account for the wave-induced fluid flow between mesoscopic inhomogeneities caused by pressure gradients on the sub-wavelength scale, which is believed to be the main cause of wave attenuation at seismic frequencies. Many effective models were developed to describe wave propagation in a medium containing heterogeneities with an equivalent homogenous medium to account for the presence of mesoscopic-scale heterogeneities. Such effective models are obtained by introducing some assumptions on the distribution and size of heterogeneities. In this thesis, models for porous media with periodically distributed heterogeneities are studied.

A new effective poroelastic model is proposed for one-dimensional wave propagation in layered porous media where layers represent mesoscopic-scale heterogeneities. The novelty lies in the application of the pressure continuity boundary conditions instead of no-flow conditions at the outer edges of the elementary cell which consists of two layers. Effective frequency-dependent Biots elastic moduli are derived which allow to describe the macroscopic behavior with Biots equations of motion, thus incorporating Biots global flow attenuation mechanism at the macroscale, in addition to the mesoscopic wave-induced fluid flow. The model is validated by the exact solution obtained with the use of Floquet's theory and

compared to well-known Whites model where the effective medium is described by the equation of viscoelasticity. A similar model is proposed for periodically distributed spherical heterogeneities. The new models are advantageous where Biots global flow attenuation is significant at seismic frequencies, i.e., in geological environments with soft and highly permeable properties, like shallow marine sediments with inhomogeneous frame, partial saturation, and unconsolidated sand reservoirs.

Effective models with coefficients that do not depend on frequency are also studied in this thesis. Such models are useful for time-domain analysis, which is advantageous over frequency-domain analysis in nonlinear problems. A model is derived for a periodically layered porous medium by expanding the dispersion equation of White's model in powers of frequency and reconstructing an equation of motion including higher-order terms from this expansion. Another higher-order model is derived by homogenization with the two-scale method of asymptotic expansions applied to a periodically layered poroelastic solid.

Finally, the layered model with frequency-dependent coefficients obtained for one-dimensional wave propagation is used to derive the effective elastic moduli for a vertical transversely isotropic porous medium to study offset-dependent attenuation and dispersion. The exact solution is also extended to the two-dimensional case. The predictions of the new model and the exact solution are compared to the predictions of the similar viscoelastic model. It is found that the assumption of the one-dimensional mesoscopic fluid flow for description of wave propagation in two-dimensional layered media results in accurate predictions of the P-wave attenuation. The predictions of the S-wave attenuation are less accurate for highly permeable media, though still better than those of viscoelastic model. The study also confirms the result obtained for the one-dimensional case that the poroelastic model is advantageous over the viscoelastic one for soft and unconsolidated media.

Samenvatting

Samenvatting in het Nederlands

Aknowledgments

Curriculum Vitae

27 April 1988	Born in Leningrad, Soviet Union
September 2005 - June 2009	Bachelor of Science (*with honors*) Saint Petersburg State Polytechnic University Faculty of Physics and Mechanics Section of Mechanics and Control Processes
September 2009 - May 2011	Master of Science (*with honors*) Saint Petersburg State Polytechnic University Faculty of Physics and Mechanics Section of Theoretical Mechanics
2009 - 2011	Researcher Institute for Problems in Mechanical Engineering Russian Academy of Science Laboratory of Discrete Methods in Mechanics
June 2011 - June 2015	Ph.D. Research Delft University of Technology Faculty of Civil Engineering and Geosciences Department of Geoscience & Engineering Section of Applied Geophysics and Petrophysics
June 2015 -	Research Geophysicist at Shell Global Solutions

Journal publications by the author

- **A.M. Kudarova**, K.N. van Dalen, G.G. Drijkoningen. An effective anisotropic poroelastic model for elastic wave propagation in finely layered media. Under review in *Geophysics*.
- A. V. Metrikine, **A.M. Kudarova**, J.S. Hoving, R. van Vliet. On the minimization of wave reflection at the interface of a discrete system and a dispersively similar continuum. *Journal of Sound and Vibration* 346, pp. 191–199, 2015.
- I.E. Berinskii, A.M. Krivtsov, **A.M. Kudarova**. Bending stiffness of a graphene sheet. *Physical Mesomechanics* 17 (4), pp. 356–364 2014.
- **A.M. Kudarova**, K.N. van Dalen, G.G. Drijkoningen. Effective poroelastic model for one-dimensional wave propagation in periodically layered media. *Geophysical Journal International* 195 (2), pp. 1337–1350, 2013.

Conference publications by the author

- **A.M. Kudarova**, K.N. van Dalen, G.G. Drijkoningen. Seismic wave propagation in porous media with spherical inclusions: Extension of White's model. *SEG Annual Meeting Technical Abstracts*, pp. 4637–4642, Denver, USA, October 26–31, 2014.
- **A.M. Kudarova**, K.N. van Dalen, G.G. Drijkoningen. Models for seismic wave propagation in periodically layered porous media. *Proceedings of the 5th International Geosciences Student Conference (IGSC 5)*, pp. 192–195, Nizhny Novgorod, Russia, July 28 – August 1, 2014.
- **A.M. Kudarova**, K.N. van Dalen, G.G. Drijkoningen. Upscaling in porous media: consequences of reducing the phase on the dynamic behavior of a homogenized medium. *Proceedings of the 9th International conference on structural dynamics (EURODYN)*, pp. 3455–3460, Porto, Portugal, June 30 – July 2, 2014.
- **A.M. Kudarova**, K.N. van Dalen, G.G. Drijkoningen. Higher-order homogenization for one-dimensional wave propagation in poroelastic composites. *Poromechanics V: Proceedings of the Fifth Biot Conference on Poromechanics*, pp. 1766-1771, Vienna, Austria, July 10–12, 2013.

- **A.M. Kudarova**, A.V. Metrikine. Reflection of plane harmonic waves at a plane interface of a semi-infinite lattice and a semi-infinite continuum. *Proceedings of the 3rd International Conference on Computational Methods in Structural Dynamics and Earthquake Engineering (COMPDYN)*. Corfu, Greece, May 25–28, 2011.

- **A.M. Kudarova**, A.V. Metrikine. On the use of gradient continua for minimizing the wave reflection at a discrete-continuum interface. *Proceedings of the International Summer School-Conference Advanced Problems in Mechanics (APM)*, pp. 375–382, July 1–5, St. Petersburg, Russia, 2010.

- **A.M. Kudarova**, A.M. Krivtsov. Description of equivalent elastic continuum for graphene lattice. *Proceedings of the International Summer School-Conference Advanced Problems in Mechanics (APM)*, pp. 375–382, July 1–5, St. Petersburg, Russia, 2010.

- I.E. Berinskiy, A.M. Krivtsov, **A.M. Kudarova**. Two-parameter many-body interaction model for description of elastic properties of graphene. *Achievements in Continuum Mechanics: Proceedings of the All-Russian conference, devoted to the 70th anniversary of academician V.A. Levin*, pp. 67–82, Vladivostok, Russia, September 29 – October 5, 2009 (*In Russian*).

- I.E. Berinskiy, A.M. Krivtsov, **A.M. Kudarova**. Determination of macroscopic characteristics for graphene layer using angle-depending atomic interactions. *Proceedings of the International Summer School-Conference Advanced Problems in Mechanics (APM)*, pp. 122–132, St. Petersburg, Russia, July 6–10, 2008.

- **A.M. Kudarova**. Modeling of graphene crystal lattice. *Proceedings of the International Summer School-Conference Advanced Problems in Mechanics (APM)*, pp. 388–393, St. Petersburg, Russia, July 6–10, 2008.

- E.A. Podolskaya, **A.M. Kudarova**. Simple models for description of non-close packed crystal structures. *Proceedings of the 22nd International Conference Mathematical Modeling in Mechanics of Solids and Constructions. Methods of Boundary and Finite Elements (BEM-FEM)*, pp. 258–262, St. Petersburg, Russia, September 24–27, 2007. (*In Russian*).